Transforming Growth Factor-β3 signaling during palatogenesis

by

Jamie E. Lane

A dissertation submitted in partial fulfillment
of the requirements for the degree of
Doctor of Philosophy
(Cellular and Molecular Biology)
in the University of Michigan
2014

Doctoral Committee:

  Professor Vesa M. Kaartinen, Chair
  Assistant Professor Benjamin Allen
  Professor Yuji Mishina
  Associate Professor Deneen Wellik

DEDICATION

This thesis is dedicated to my family, friends and mentors along the way.

<div align="center">

4/20/2001

5/31/2006

1/11/2008

9/30/2009

12/27/2010

</div>

iii

Table of Contents

List of figures

List of Tables

Chapter 1

Introduction

1-1.   Health Significance

Cleft palate is a common human birth defect occurring in about one out of every 2500

babies (Tolarova and Cervenka, 1998). The causes of clefting are varied and are due to

combinations of environmental and genetic factors [reviewed by(Dixon et al., 2011)]. In order to

learn how to prevent or develop improved treatment strategies, it is necessary to understand the

basic development and signaling mechanisms in the formation of the palate (palatogenesis).

1-2. Early Facial Development

The forming mouse face is made up of facial processes (E9.5) that are derived from

pharyngeal arches and the frontonasal process, surround the primitive mouth (stomodeum) and

form the nose, upper and lower jaw, lip, part of the eye and part of the ear. Pharyngeal arches

are composed of the mesoderm-derived core and ectoderm-derived lining, and they are filled

with highly migratory ecto-mesenchymal cells derived from the cranial neural crest (CNC).

During the late neurulation stage (~E8.0), CNC cells start to form at the dorsal ridges of the

fusing neural tube as a result of instructive signals coming from the neuroectoderm, adjacent

ectoderm and underlying mesenchyme. Subsequently, they undergo epithelial to mesenchymal

transition, delaminate and migrate ventro-laterally to populate pharyngeal arches and other

1

developing head structures (beginning at E8.5) (Figure 1-1). Most of the skeletal structures and connective tissue of the head are derived from the CNC, which is quite exceptional, since in the trunk region of the body, the skeletal structures are derived from the mesoderm.

The rapid growth of pharyngeal arches is caused by massive migration and simultaneous proliferation of CNC-derived cells. The growing first pharyngeal arch branches into two sets of processes: paired maxillary and mandibular processes. Bilateral mandibular processes (arches) continue to grow until they fuse in the midline forming the lower jaw (E10). While the maxillary processes continue to grow towards the middle of the developing face, the frontonasal process undergoes morphological changes to form the nose and forehead. The frontonasal process develops two ectodermal thickenings (nasal placodes), which invaginate to form two separate horse-shoe like structures around the nasal pits, which are then subdivided into medial and lateral nasal processes. The maxillary process and medial nasal processes fuse (E10.5) in an anterior-posterior manner and soon after fuse with the lateral nasal process forming two nostrils of the developing nose (E12.5). These two sets of fused processes are joined in the center by fusion of the intermaxillary prominence, which is the tissue from the frontonasal prominence that separates the newly formed nostrils, which results in formation of the primary palate, upper jaw and upper lip (Figure 1-2)((Alappat et al., 2005) and (Ray and Niswander, 2012)). (The processes described above are similar in human, see Table 1-1 and Figure 1-3.) At a slightly later point in development (E13), paired outgrowths of palatal shelves become visible from the maxillary process that ultimately gives rise to the secondary palate.
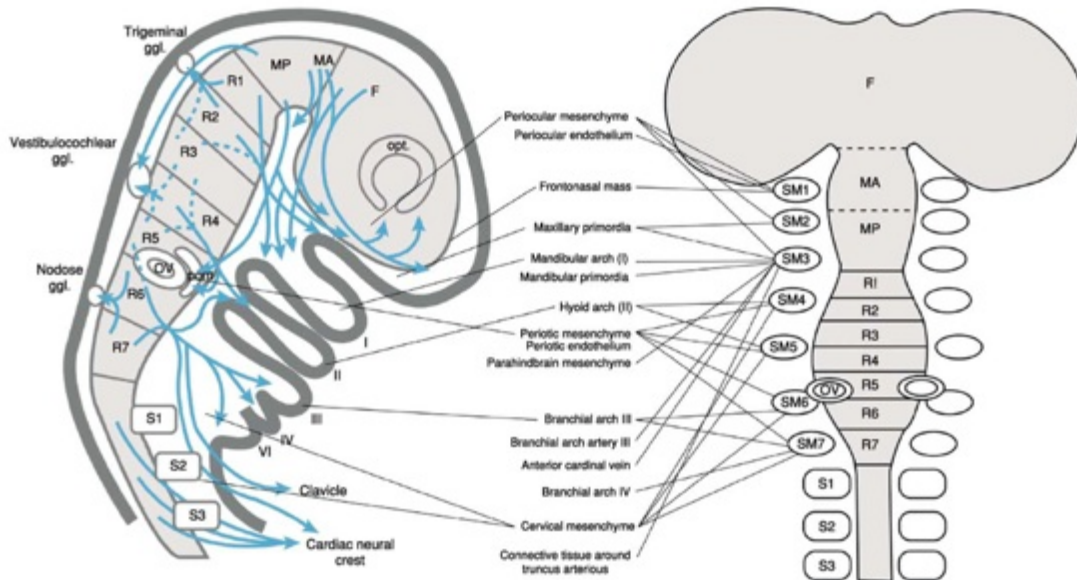
Figure 1-1. Cranial neural crest cells migrate to different regions of the developing face (Dudas and Kaartinen, 2005).

Lateral and dorsal (left and right) views illustrate the migration of cranial neural crest cells that populate regions of the developing face. The cells delaminate from the dorsal ridges of the forming neural tube and migrate ventro-laterally to populate the developing facial primordia and pharyngeal arches (labeled I-IV and VI). Blue arrows indicate the origin and direction of migration of the cranial neural crest cells that populate different areas of the developing face including the frontonasal process, the maxillary processes and pharyngeal arch 1, which gives rise to the mandibular processes. F, Forebrain; ggl.,ganglion; MA, anterior midbrain; MP, posterior midbrain; opt., optic vesicle; OV, otic vesicle; pom, periotic mesenchyme; R1 to R7, rhombomeres 1 to 7; S1 to S3, somites 1 to 3; SM1 to SM7, somitomeres 1 to 7.
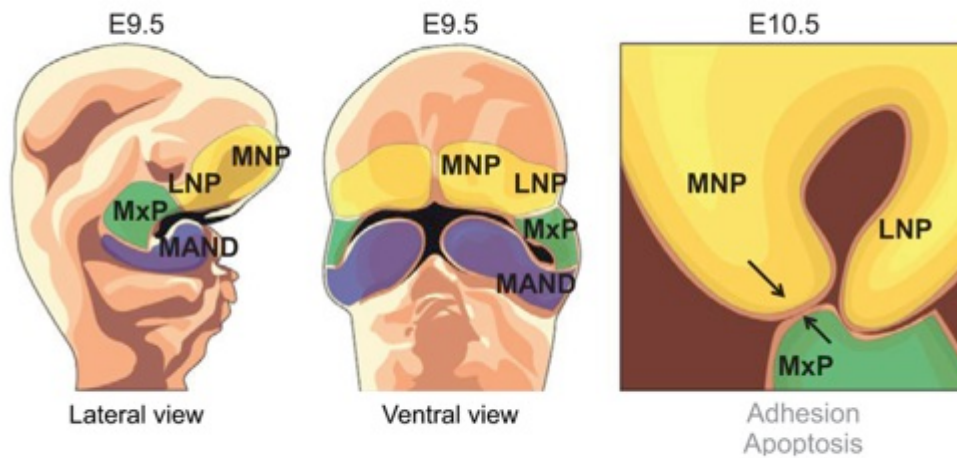
Figure 1-2. Facial Processes in mouse development at E9.5-10.5. (Ray and Niswander, 2012).

(A. lateral view and B. ventral view) At E9.5 the growing first pharyngeal arch gives rise to the paired mandibular (MAND purple) and maxillary processes (MxP green). At this time, the frontonasal prominence (yellow) gives rise to the medial nasal process (MNP) and the lateral nasal process (LNP). c. One day later at E10.5, the MxP and MNP fuse (arrows)(on each side of the fusing processes) and form an invagination and soon after fuse to the LNP forming two nostrils of the developing nose.

Table 1-1 Structures contributing to formation of the human face

Prominence	Structures Formed
Frontonasal	Forehead, bridge of nose, medial and lateral nasal prominences
Maxillary (paired)	Cheeks, lateral portion of upper lip
Medial nasal (paired)	Philtrum of upper lip, crest and tip of nose
Lateral nasal (paired)	Alae of nose
Mandibular (paired)	Lower lip
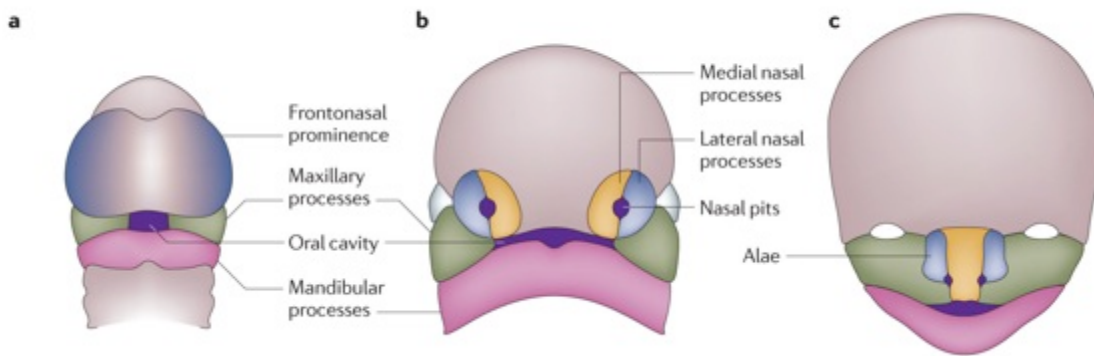
Figure 1-3. Development of the face in humans. (Dixon et al., 2011)

Schematic diagrams of the human developing face. a. During the fourth week of development the primitive mouth (purple) is surrounded by the frontonasal prominence (blue), the maxillary (green) and mandibular processes (pink). b. During the fifth week of development, the frontonasal prominence has given rise to the medial and lateral nasal processes that have gone through fusion to give rise to the developing nose. c. By the end of the sixth week of development the medial nasal processes have fused to form the upper lip and the mandibular processes have fused forming the lower jaw.

Palatogenesis

The secondary palate consists of a bony anterior and muscular soft palate in the posterior. It separates the oral-nasal cavity and allows for efficient feeding, speech and breathing. In humans this process occurs during gestational weeks 8-12 and in mice between embryonic days E12-E15. The palate is composed of many separate structures coming together to form the complete palate: the primary palate, the secondary palate and the nasal septum (in the anterior). The anterior secondary palate is an area beginning after the incisor foramen and before the appearance of the eyes when going through the frontal plane. Palatogenesis begins with the growth of the two palatal shelves (of the secondary palate) from the maxillary processes of the first pharyngeal arch (Ferguson, 1988). They are composed mostly of cranial neural crest derived mesenchyme (Ito et al., 2003), layered by a layer of cuboidal epithelium and then covered in flattened cells known as periderm (a transient cell layer that covers all embryonic epithelium prior to the differentiation of the epithelial layer below). The bilateral palatal shelves grow vertically down along the sides of the tongue, then they rapidly elevate to a horizontal position (within hours in mice) and the two palatal shelves approach each other. Prior to the adherence of the two palatal shelves, the periderm is removed (reviewed in (Dudas et al., 2007)). At this point, the epithelium covering the tips of the palatal shelves that are going to fuse, are known as the medial edge epithelium (MEE). The MEE on each shelf then meet and form the midline epithelial seam (MES). In the anterior nasal side of the secondary palate, the nasal septum fuses with the palatal shelves (Figure 1-4). Once the adherence has taken place, the MES is removed allowing for palatal mesenchymal confluence. Following this time point, the primary palate fuses with the secondary palate.

6

Figure 1-4. Secondary palate formation. (Lane and Kaartinen, 2014)

Schematic representation of palatal growth and fusion. Palatal shelves (PS) can be first seen as outgrowths of the maxillary processes of the first pharyngeal arch (E11.5). Then they grow vertically down along the sides of the tongue (T; E13.0), rapidly elevate (E14.0), form a contact with each other and with the nasal septum (NS) in the anterior palate (P) (E15.0), and eventually fuse (E16.0).

1-4. Control and patterning of the secondary palate

Many studies have shown that gene expression patterns and gene functions are remarkably different in the developing anterior and posterior palate, which give rise to the hard- and soft palate, respectively (Figure 1-5). The anterior–posterior (AP) boundary in the developing palate is on the level of the most posterior ruga. Rugae are ridges on the hard palate that facilitate the movement of food backwards toward the pharynx.

Anterior palate development: It has been demonstrated that Sonic Hedgehog (Shh), an important morphogen, plays a crucial organizing role in development and growth of the anterior secondary palate.(Lan and Jiang, 2009; Rice et al., 2004) *Shh* is expressed in periodic stripes on the oral side of the developing palate; these stripes correspond to future palatal rugae (transverse ridges on the hard palate) (Baek et al., 2011; Economou et al., 2012). Abrogation of *Shh* in the palatal epithelium (by *K14-Cre*) or its receptor *Smoothened* (*Smo*) in the palatal mesenchyme (using *Osr2-Cre*) results in cleft palate and reduced expression of a number of genes relevant for palatal shelf growth, e.g., *Fgf10*, *Bmp2*, *Msx1*, and *Osr2*(Lan and Jiang, 2009). Interestingly, mesenchymal *Fgf10* expression is also needed for appropriate epithelial SHH signaling via epithelial Fgfr2b activation, (Rice et al., 2004) thus an Fgf10-Shh signaling axis provides an important regulatory feedback loop between palatal epithelium and mesenchyme to control palatal anterior growth and patterning (Rice et al., 2004). Similarly, *Bmp4* in the palatal mesenchyme is required both for *Shox2*, which is needed for anterior palatal growth (mesenchymal cell proliferation), (Hilliard et al., 2005; Li et al., 2011) and for *Shh* expression in the palatal epithelium (Zhang et al., 2002). This provides another signaling loop between the epithelium and mesenchyme to control anterior growth of the secondary palate (Zhang et al., 2002). Zhou et al. recently demonstrated that deletion of the paired-box gene-9 (*Pax9*)

transcription factor in the palatal mesenchyme resulted in cleft palate that was caused by defective palatal shelf growth and elevation (Zhou et al.,

2013). In *Pax9* mutants, *Shh* expression in the palatal epithelium, and *Bmp4*, *Fgf10*, *Msx1*, and *Osr2* expression in the palatal mesenchyme were dramatically reduced. The authors further showed that a novel knock-in allele, expressing *Osr2* in the *Pax9* locus (*Pax9^{Osr2KI}*) was able to rescue the posterior, but not the anterior fusion defects in *Pax9*mutants. Consistent with the lack of anterior phenotypic restoration, the expression levels of many key genes,

e.g., *Bmp4*, *Msx1*, *and Shh* were not rescued. The authors concluded that Pax9 acts upstream or parallel to Osr2 and controls several different pathways including Shh, Fgf10, and Bmp4 during development of the anterior palate.

Oro-nasal patterning of the anterior secondary palate: As outlined above, *Shh* is specifically expressed in the oral palatal epithelium, while Shh receptors (*Ptch* and *Smo*) and downstream effectors (*Msx1*, *Osr1,* and *Osr2*) display a graded expression in the adjacent mesenchyme along the oro-nasal axis(Han et al., 2009; Lan et al., 2004). In contrast, the distal-less homeobox-5 (*Dlx5*) and *Fgf7* genes are specifically expressed in the nasal mesenchyme of the palatal shelf, and the authors suggested that the Dlx5-regulated Fgf7 signaling is critically important in negatively regulating the mesenchymal Shh signaling and palatal oro-nasal patterning(Han et al., 2009) (Figure 1-5).

Posterior palate development: The posterior muscular palate (soft palate) functions during swallowing and speech. In addition to neural crest-derived mesenchymal cells, the posterior palate mesenchyme is populated by myogenic cells derived from the cranial paraxial mesoderm (Zhang et al., 1999). The importance of muscle function to palatogenesis was recently demonstrated by Rot-Nikcevic et al., who showed that mouse embryos lacking striated

muscles display cleft palate (Rot-Nikcevic et al., 2006). Compared to the molecular control of

the anterior palate development, much less is known about signaling processes governing the

growth and patterning of the posterior secondary palate. The transcription

factors *Tbx22* and *Meox2* are specifically expressed in the posterior palate,

while *Barx1* and *Mn1* are expressed along the entire AP axis, although the expression of these

genes is stronger in the posterior than in the anterior mesenchyme,(Bush et al., 2002; Li and

Ding, 2007; Liu et al., 2008) and concordant with the posterior expression domain, mice

deficient in *Tbx22* suffer from a submucous cleft palate(Pauws et al., 2009). Zhou et al. recently

showed that unlike previously thought, *Bmp4* is expressed both in the anterior and posterior

palatal mesenchyme, and its expression is dependent on *Pax9* but not on *Msx1* in the posterior

palate (Zhou et al., 2013). Moreover, their results implied that both *Osr2* expression in the

posterior palatal mesenchyme and *Shh* expression in the posterior palatal epithelium (in the

developing sensory papilla) is regulated by Pax9 (Zhou et al., 2013).

1-5. Signaling pathways controlling palatal epithelial differentiation and midline seam
disappearance

        Along with palatal shelf growth, there is growth of maxillary and mandibular processes.

This allows the tongue to slide down and forward, which is required for palatal shelf elevation

and reorientation (Ferguson, 1987). Pioneering studies of Walker and Fraser and their recent

detailed refinement and complementation by Yu and Ornitz showed that mechanisms of the

anterior and posterior palatal shelf elevation are different (Fraser et al., 1957; Yu and Ornitz,

2011). While the anterior palatal shelves are elevated by a 'flipping-up' mechanism, the

posterior palatal shelves undergo tissue-remodeling movement. Molecular mechanisms controlling these events are still poorly known (Bush and Jiang, 2012).

After elevation, the palatal shelves meet in the midline and become adherent (Ferguson, 1988). This event is tightly controlled, because inappropriate adherence prevents palatal shelf elevation resulting in cleft palate (Ingraham et al., 2006; Richardson et al., 2009). Periderm cells, joined to each other by tight junctions, have an important role in controlling palatal shelf adherence and epithelial differentiation (Vaziri Sani et al., 2005);(Yoshida et al., 2012) . This thin (one cell) layer of flattened cells is thought to function as a protective layer or insulator preventing aberrant adhesions. However, the loss of peridermal cells is required at sites of fusion, e.g., the tips of apposing palatal shelves for appropriate epithelial differentiation and adherence (Yoshida et al., 2012). Recent studies have shown that mouse embryos lacking *Fgf10*, *Jagged2*, *Irf6*, *Ikka (chuk)*, or *Tbx1* show aberrant oral adhesions between the tongue and palatal shelves,(Funato et al., 2012; Humphreys et al., 2012; Ingraham et al., 2006; Richardson et al., 2009) and it has been suggested that Jagged2-Notch and p63-Irf6 signaling regulate maintenance of periderm cells during palatogenesis(Casey et al., 2006; Ingraham et al., 2006; Richardson et al., 2009) (Figure 1-6 (a)).
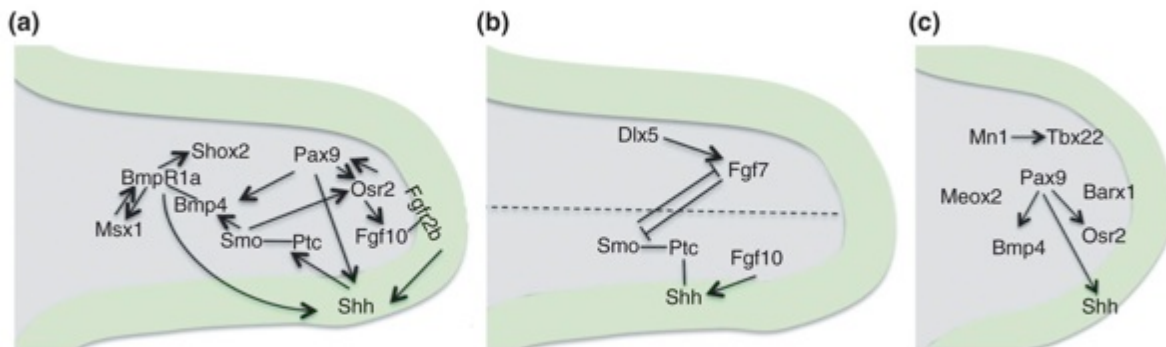
Figure 1-5. Signaling circuits governing palatal shelf growth and patterning (Lane and Kaartinen, 2014).

(a) Epithelial–mesenchymal interactions via Pax9-regulated Shh-Bmp and Shh-Fgf feedback loops control growth and patterning of the anterior palate. (b) Oro-nasal patterning of the anterior secondary palate is regulated via Fgf7-mediated Shh repression. (c) Pax9-regulated expression of *Bmp4* and *Osr2* in the posterior palatal mesenchyme and *Shh* in the posterior palatal epithelium is required for appropriate posterior growth of the secondary palate. In addition, Meox2, Barx1, and Mn1-Tbx22 signaling module regulate posterior palatal growth. Gray, palatal mesenchyme; Green, palatal epithelium.

Once the apposing palatal shelves have adhered, the midline epithelial seam (MES) must be removed to obtain a mesenchymal confluence (Ferguson, 1988). This happens primarily via programmed cell death (apoptosis), although epithelial–mesenchymal transformation and/or migration, could also play some role in MES removal (Dudas et al., 2007; Vaziri Sani et al., 2005; Xu et al., 2006). Nevertheless, it is clear that TGF-β signaling plays a critical role in this process. *Tgfb3* is strongly and specifically expressed in the MEE, (Millan et al., 1991; Pelton et al., 1990) and mice deficient in *Tgfb3* show 100% penetrant cleft palate (Kaartinen et al., 1995; Proetzel et al., 1995). Moreover, palatal epithelial cells deficient for genes encoding TGF-β type I or type II receptors fail to undergo apoptosis resulting in a failure of the MES to disappear (Dudas et al., 2006; Xu et al., 2006). How *Tgfb3* expression is regulated in the MEE is poorly understood. It was recently shown that epithelial-specific *Ctnnb1* (the gene encoding β-catenin) mutants displayed cleft palate and loss of *Tgfb3* expression suggesting that canonical Wnt signaling via β-catenin is required for appropriate MEE-specific *Tgfb3* expression (He et al., 2011). Venza et al. showed that mutations in the *FOXE1* gene result in *Bamforth-Lazarus* syndrome characterized with craniofacial defects including cleft palate (Venza et al., 2011), and that *Tgfb3* is a direct target of Foxe1 (Venza et al., 2011).

It is unclear which genetic components are needed for effective downstream signaling of TGF-β. As outlined above, epithelium-specific deletion of genes encoding TGF-β type I and II receptors resulted in defective palatogenesis (Dudas et al., 2006; Xu et al., 2006). Therefore, epithelium-specific deletion of *Smad4*, which is a critical intracellular TGF-β signal transducer, was expected to result in a similar phenotype. This was not was observed in these loss-of-function mutants (Xu et al., 2008). Xu et al. further demonstrated that simultaneous deletion of *Smad4* and inhibition of p38Mapk resulted in persistent MES in explant cultures suggesting

that both Smad-dependent and Smad-independent TGF-β signaling act redundantly for successful palatal epithelial fusion (Xu et al., 2008). Iwata et al. recently showed that *Irf6* is a direct target of Smad4 in the palatal epithelium, and that overexpression of *Irf6* in the palatal epithelium rescued the palatal defect seen in epithelial-specific *Tgfbr2* mutants (Iwata et al., 2013).   Moreover, they showed that Irf6 is needed to suppress *dNp63*, which is a prerequisite for *p21* (*Cip1*) expression, cell cycle arrest and subsequent MEE loss (Iwata et al., 2013) (Figure 1-6 (b)). Whether the same mechanism is true for *Tgfb3* mutants is unclear.
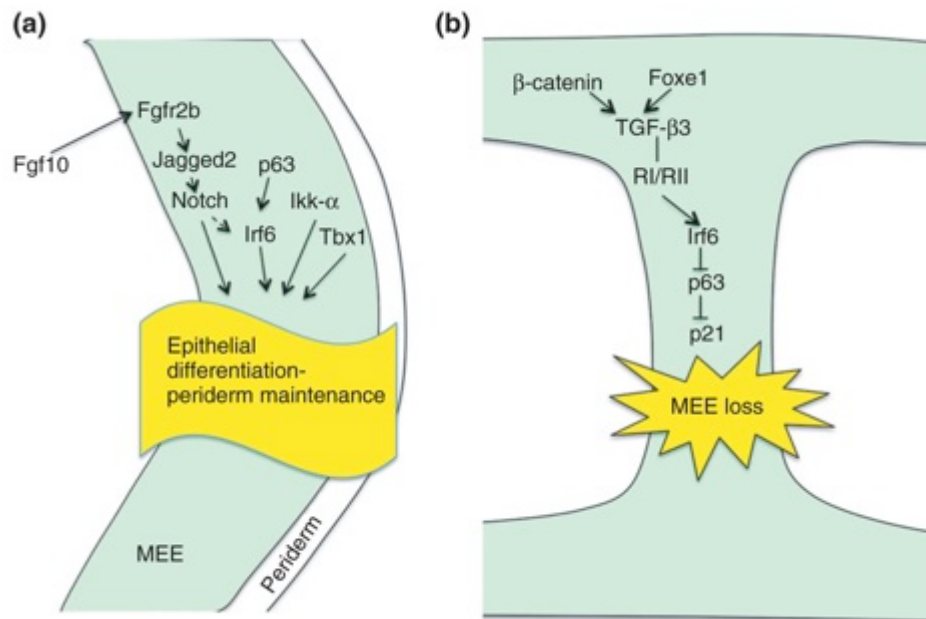
Figure 1-6. Molecular control of palatal epithelial differentiation and disappearance (Lane and Kaartinen, 2014).

a. Molecular control of palatal epithelial (green) differentiation. Fgf-Notch signaling, P63-Irf6 signaling, Tbx1, and Ikk-α regulate differentiation or the prefusion palatal epithelium (green). b. Medial edge epithelial loss is mediated via a signaling cascade involving TGF-β3, Irf6, p63, and p21in the palatal midline epithelial seam (green).

1-6.   Orofacial clefting

Disruptions in any of the signaling pathways that contribute to palatal formation can result in human birth defects. Orofacial fusion defects, such as cleft lip with or without cleft palate (CL/P) and cleft palate only (CP) are common human birth defects (Figure 1-7). CL/P occurs in 1/1000 human births whereas CP occurs in 1/2500 births (Tolarova and Cervenka, 1998). When CL/P and CP are present without any other defects or any known maternal environmental exposures, they are known as nonsyndromic (NSCL/P and NSCP) and occur in 70% of cases. The remaining 30% of cases are syndromic and occur in conjunction with anomalies other than oral clefting. They can be broken down into chromosomal defects, Mendelian syndromes, teratogens and uncategorized syndromes (Schutte and Murray, 1999) (Table 1-2 shows selected syndromes with known genetic cause).

 Syndromic orofacial clefting cases can be associated with an inherited genetic trait. Orofacial cleft phenotypes that are present in multiple family members, particularly in large families are useful for genetic studies. It has been appreciated from the early case history studies that there was a strong genetic component to this abnormality (Schutte and Murray, 1999).

The etiology of cleft lip and cleft palate is often complex. A combination of epidemiological studies, genome-wide association studies and analysis of experimental animal models has started to unravel complex gene-environment interactions that are

A

Upper lip
Hard palate
Soft palate
Uvula

Unilateral
a   b   c   d
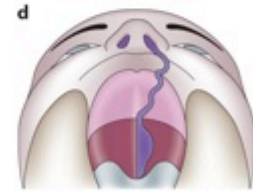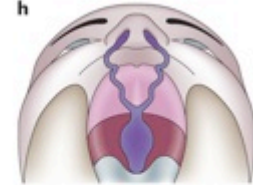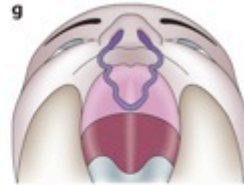
Bilateral
e   f   g   h

B

a Microform CL

b Left unilateral CL

c Left unilateral CL plus CP

d Bilateral CL plus CP

e Van der Woude syndrome:
   bilateral CL plus CP (repaired)
   with lip pits
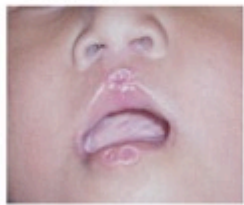
f CPO, soft palate only

g CPO, hard and soft palate

Figure 1-7. Types of orofacial clefts in humans (Dixon et al., 2011).

A. Illustrations of types of cleft lip and/or palate.
(a.-d.) Unilateral clefts. a. Unilateral cleft of the posterior secondary palate. b. Unilateral cleft of the upper lip. c. Unilateral cleft of the hard palate and the upper lip. d. Unilateral cleft of the hard and soft palate and the upper lip. (e-h.) Bilateral clefts. e. Bilateral cleft of the soft palate. f. Bilateral cleft of the upper lip. g. Bilateral cleft of the hard palate and upper lip. h. Bilateral cleft of the hard and soft palate and upper lip. B. Images of patients with varying degrees of cleft with the description of each image. CL, cleft lip; CP, cleft palate; CPO, cleft palate only.

thought to play critical roles in pathogenesis of many of the cleft lip and cleft palate cases. Initial studies have identified several environmental components of clefting, including nutritional status and lifestyle of the expecting mother.   Studies of gene-environment interactions generally examine large populations and look for an increase in single nucleotide polymorphisms (SNPs) along with the presence of maternal risk factors, such as maternal pre-pregnancy obesity (Block et al., 2013), periconsumptional alcohol consumption (Shaw and Lammer, 1999), maternal cigarette smoking during pregnancy (Lieff et al., 1999), environmental tobacco smoke exposure (Wu et al., 2014), folic acid fortification (Hashmi et al., 2005) and intake of anti-epileptic drugs (valproic acid) (Paulson and Paulson, 1981).

Above (Fig. 1-5), I have described molecular mechanisms regulating palatal shelf growth, elevation and fusion (Fig. 1-4). Defects in any of these processes can result in cleft palate. While some of the disease-causing genes, e.g., *IRF6*, have been identified in human genetic studies, most of the mechanistic data we currently have are derived from studies examining genetically manipulated mouse models (see section 1-7).

Table 1-2. Selected CL/P syndromes with known genetic cause(Leslie and Marazita, 2013).

Syndrome	Cleft type observed	Gene	Refs.
Ankyloblepharon-ectodermal dysplasia-clefting	CL/P	TP63	McGrath et al. [2001]
Apert	CP	FGFR2	Wilkie et al. [1995]
Bamforth–Lazarus	CP	FOXE1	Bamforth et al. [1989]
Bartsocas–Papas	CL/P	RIPK4	Kalay et al. [2012], Mitchell et al. [2012]
Branchio-oculo-facial	CL/P	TFAP2A	Milunsky et al. [2008]
Campomelic dysplasia	CP	SOX9	Foster et al. [1994], Wagner et al. [1994]
CHARGE	CP	CHD7	Vissers et al. [2004]
CLP ectodermal dysplasia	CL/P	PVRL1	Suzuki et al. [2000]
Cornelia de Lange	CP	NIPBL	Krantz et al. [2004], Tonkin et al. [2004]
Crouzon	CP	FGFR2	Reardon et al. [1994]
DiGeorge	CP	TBX1	Packham and Brook [2003]
Ectrodactyly-ectodermal dysplasia-clefting	CL/P	TP63	Celli et al. [1999]
Familial gastric cancer and CLP	CL/P	CDH1	Frebourg et al. [2006]
Gorlin	CL/P	PTCH1	Hahn et al. [1996], Johnson et al. [1996]
Holoprosencephaly	CL/P	GLI2	Roessler et al. [2003]
Holoprosencephaly	CL/P	SHH	Roessler et al. [1996]
Holoprosencephaly	CL/P	SIX3	Wallis et al. [1999]
Holoprosencephaly	CL/P	TGIF	Gripp et al. [2000]
Isolated cleft palate	CP	SATB2	FitzPatrick et al. [2003]
Kabuki	CL/P	MLL2, KDM6A	Lederer et al. [2012], Ng et al. [2010a]
Kallmann	CL/P	FGFR1	Dode et al. [2003]
Lethal and Escobar multiple pterygium	CP	CHRNG	Morgan et al. [2006]
Loeys–Dietz	CP	TGFBR1, TGFBR2	Loeys et al. [2005]
Miller	CP	DHODH	Ng et al. [2010b]
Oculofaciocardiodental	CP	BCOR	Ng et al. [2004]
Opitz G/BBB	CL/P	MID1	Quaderi et al. [1997]
Oro-facial-digital	CL/P	GLI3	Johnston et al. [2010]
Oro-facial-digital type 1	CL/P	OFD1	Ferrante et al. [2001]
Otopalatodigital types 1 and 2	CP	FLNA	Robertson et al. [2003]
Pierre Robin	CP	SOX9	Benko et al. [2009]
Popliteal pterygium	CL/P	IRF6	Kondo et al. [2002]
Saethre–Chotzen	CP	TWIST1	el Ghouzzi et al. [1997], Howard et al. [1997]
Stickler type 1	CP	COL2A1	Snead and Yates [1999]
Stickler type 2	CP	COL11A1, COL11A2	Snead and Yates [1999]
Tetra-amelia with CLP	CL/P	WNT3	Niemann et al. [2004]
Tooth agenesis with or without cleft	CL/P	MSX1	van den Boogaard et al. [2000]
Treacher Collins	CP	TCOF1	Group [1996]
Van der Woude	CL/P	IRF6	Kondo et al. [2002]
X-Linked cleft palate and ankyloglossia	CP	TBX22	Braybrook et al. [2001]
Siderius X-linked mental retardation	CL/P	PHF8	Laumonnier et al. [2005]

CL, cleft lip; CP, cleft palate; CL/P, cleft lip with or without cleft palate.

1-7. Mouse as a model system to study palatogenesis

1-7.1. Evolutionary conservation between mouse and human

Conservation in genetics measures the sequence similarity between two species. In general, mammalian genomes between different species are remarkably well conserved; for example, the conservation level between the mouse and human is about 40% (Gregory et al., 2002). This similarity makes it possible to study complex developmental processes, e.g., palatogenesis in the mouse system, when ethical reasons prevent experimentation in humans (Carver and Stubbs, 1997). The mouse as a mammalian model system is convenient because of their small size, short lifespan (1 mouse year is about 30 human years), short reproduction time (18 days), large litter size, sequenced genome, and most importantly because of our ability to manipulate the mouse genome. Altogether more than 300 genes have been implicated in palatal fusion either in humans or in experimental animal models (Gritli-Linde, 2007).

1-7.2. Mouse Embryonic Stem Cells as a method for genomic manipulation

The understanding of the potential of embryonic stem cells in transgenic studies and methodological advances in gene targeting have created a framework for genomic manipulation in experimental animal models. Currently, true embryonic stem cells have mostly been established from mouse embryos; thus the mouse has become one of the most widely used animal models in modern biology.

Mouse embryonic stem cell discovery began as early as the 1950s (many good reviews exist describing specific timelines in the progress (Capecchi, 2005; Evans, 2011). Isolation of a pluripotent population of cells was demonstrated through the use of teratocarcinoma cell lines, where a single cell could give rise to a teratocarcinoma containing differentiated tissues (teeth

and hair), suggested that this population of cells could produce an entire embryo. However, the teratocarcinoma cell could not be transmitted through the germline due to its atypical karyotype (Kleinsmith and Pierce, 1964). The isolated inner cell mass cells from developing mouse blastocysts shared similar characteristics to the teratocarcinoma cells in that they produced differentiated tissues. Yet, they had a normal karyotype and transmitted through the germline (Evans and Kaufman, 1981)(See figure 1-8). Cell lines established from inner cell mass cells are what are currently known as mouse embryonic stem cell lines (Evans and Kaufman, 1981).
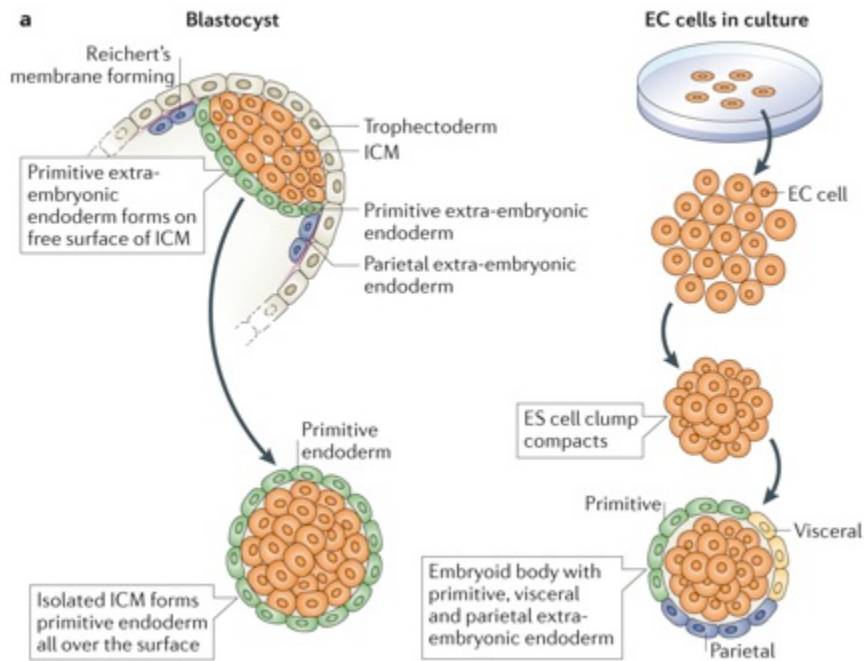
Figure 1-8. Isolated inner cell mass (ICM) is similar to an embryoid body (from embryonal carcinoma) in culture (Evans, 2011).

a. The developing blastocyst contains an interior cell mass that lies within the surrounding trophoectoderm. The inner cell mass (ICM) contains primitive extra-embryonic endoderm that is surrounded by Reichert's membrane, which are parietal extra-embryonic endoderm. When the ICM is isolated from the trophoectoderm, it forms primitive endoderm over its entire surface. b. Embryonal carcinoma (EC) cells in culture form embryoid bodies that contain extra-embryonic endoderm of all types (primitive, visceral and parietal). This shows that EC differentiation is similar to the ICM.

1-7.3. Gene targeting in mouse embryonic stem cells

Gene targeting is a method of incorporating foreign DNA into a specific locus in a cell's genome via homologous recombination (Thomas and Capecchi, 1987). It was first used by Smithies et al, to insert test plasmid DNA into the human beta-globin locus (Smithies et al., 1985), and was subsequently adapted into use in embryonic stem cells by Thomas and Capecchi (Thomas and Capecchi, 1987).

A strategy to target a specific locus in embryonic stem cells was adopted from earlier studies conducted in yeast (Thomas and Capecchi, 1987). A targeting vector was designed that contained foreign DNA flanked by homology arms (sequence similar to those in a target locus). The targeting vector also contained positive and negative selection markers critical for enrichment of correctly targeted clones. A positive selection marker (e.g., neo^r) is (a coding region of a gene) that provides resistance to a cytotoxic antibiotic (e.g., geneticin (G418)), and in a targeting vector it is placed between the homology arms. A negative selection marker (e.g. *DT* or *TK*) is a coding region of a gene producing a toxic product and it is placed outside of the homology region. Therefore, a successful recombination results in formation of clones that survive when the positive selection marker is retained and negative selection marker is lost (Mansour et al., 1988) (Figure 1-9). The embryonic stem cells that contain the correct targeted gene insertion are injected into a pre-implantation mouse blastocyst and transplanted into the uterine horns of a pseudo-pregnant foster-mother. This allows the embryo to develop and be born as a chimeric mouse (Fig. 1-10). This chimeric mouse is bred into the germ-line generating mice that contain a targeted gene modification.
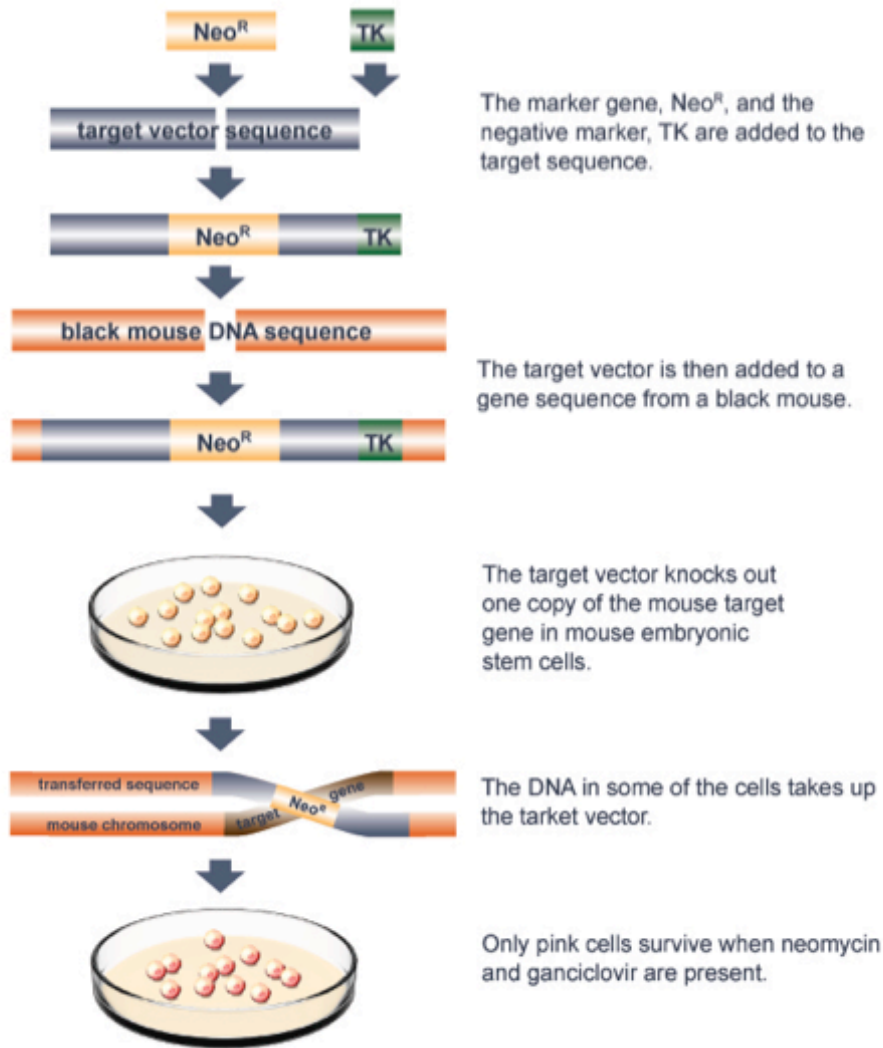
Figure 1-9. Targeted gene deletion through use of homologous recombination in mouse embryonic stem cells. (Nature Education, 2009)

Schematic presentation of gene targeting in mouse embryonic stem cells. A positive (*NeoR*) and a negative selection marker (*TK*) gene is added to the target vector sequence. The target vector homologously recombines with the black mouse DNA sequence, which occurs in mouse embryonic stem cells. Only cells (pink) that include the positive and exclude the negative markers survive with the addition of neomycin and ganciclover.

a ES cells

Rare targeted cell

Targeting vector introduced by electroporation

Positive–negative selection (G418^r/FIAU^r)

Pure population of targeted ES cells

b
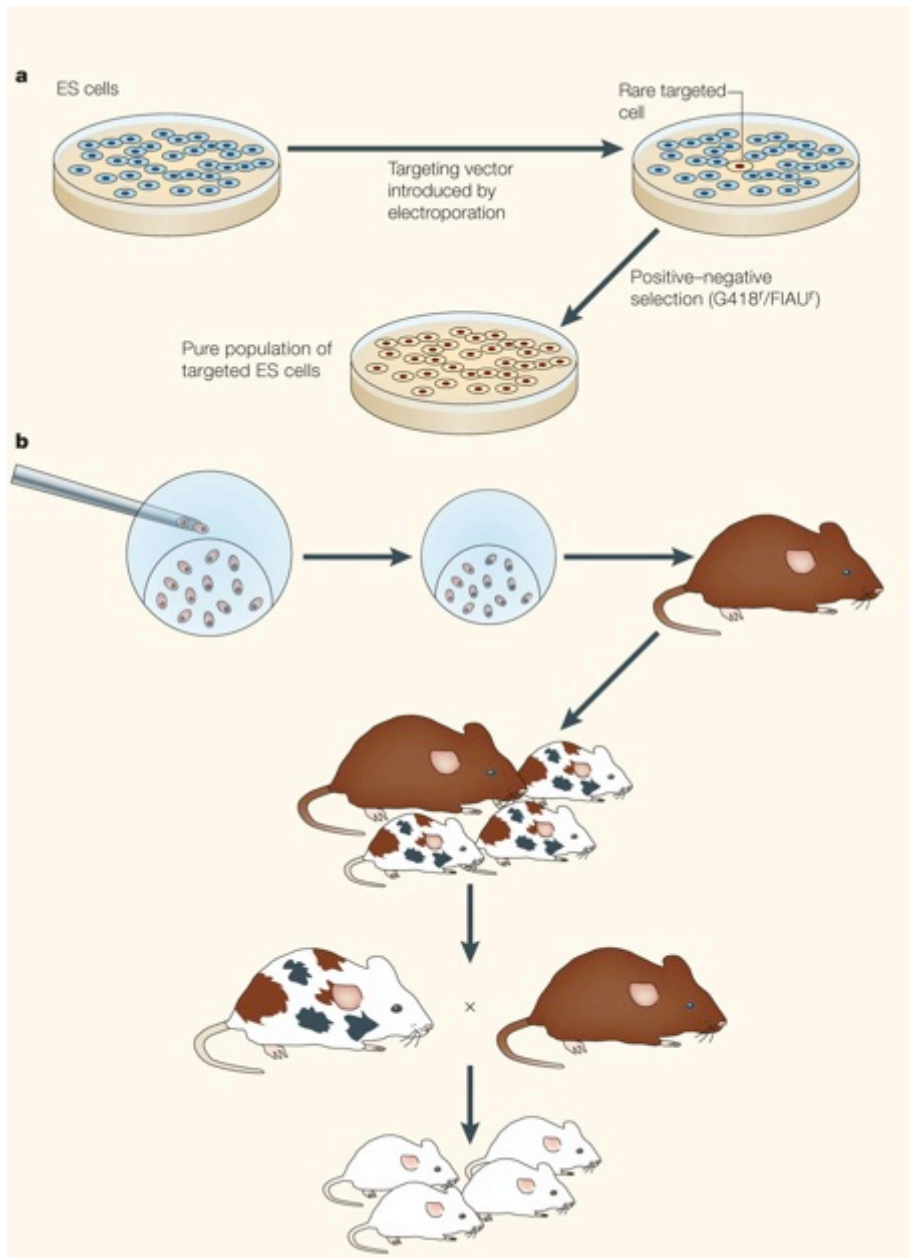
Figure 1-10. Generation of mouse germline chimeras from embryonic stem cells (Capecchi, 2005).

a. An embryonic stem (ES) cell line containing the desired mutation is isolated and enriched for using positive and negative selection markers. b. By injecting the correct ES cells into a recipient blastocyst, embryos are formed that potentially contain the desired mutation. These embryos are then placed in a pseudo-pregnant foster-mother who gives birth to the chimeric mice. To aid in the identification of the desired progeny, the ES cells and the blastocyst are derived from mice with different coat color alleles. The chimeric line can then be bred into a line containing the desired mutation.

1-7.4. Using gene targeting to create a loss-of-function mutation

Gene targeting in the mouse is used to alter a specific gene and study its function. The modifications that are generated through gene targeting can be an addition of sequence (knock-in), point mutation of a sequence or deletion (knock-out). Below I will use a *Tgfb3* knockout study as an example to show how a mouse mutant lacking the known gene has been use to examine palate fusion and pathogenesis of cleft palate. *Tgfb3* is specifically expressed in the midline epithelial seam and when it is removed results in a complete cleft of the secondary palate (Kaartinen et al., 1995; Proetzel et al., 1995). The sequences surrounding the *Tgfb3* gene locus were used to flank the positive selection gene neomycin (neo), which also interrupts exon 6, a crucial exon that is responsible for encoding the mature Tgf-β3 protein (Figure 1-11). The negative selection marker thymidine kinase (*tk*) was included outside of the region of homologous recombination of a correctly inserted recombinant. The targeting vector is electroporated into embryonic stem cells and positive correctly targeted clones were identified. The correct recombinant was then used to generate chimeric mice that were bred into the germ-line generating mice that contain the disrupted exon 6 of *Tgfb3*.
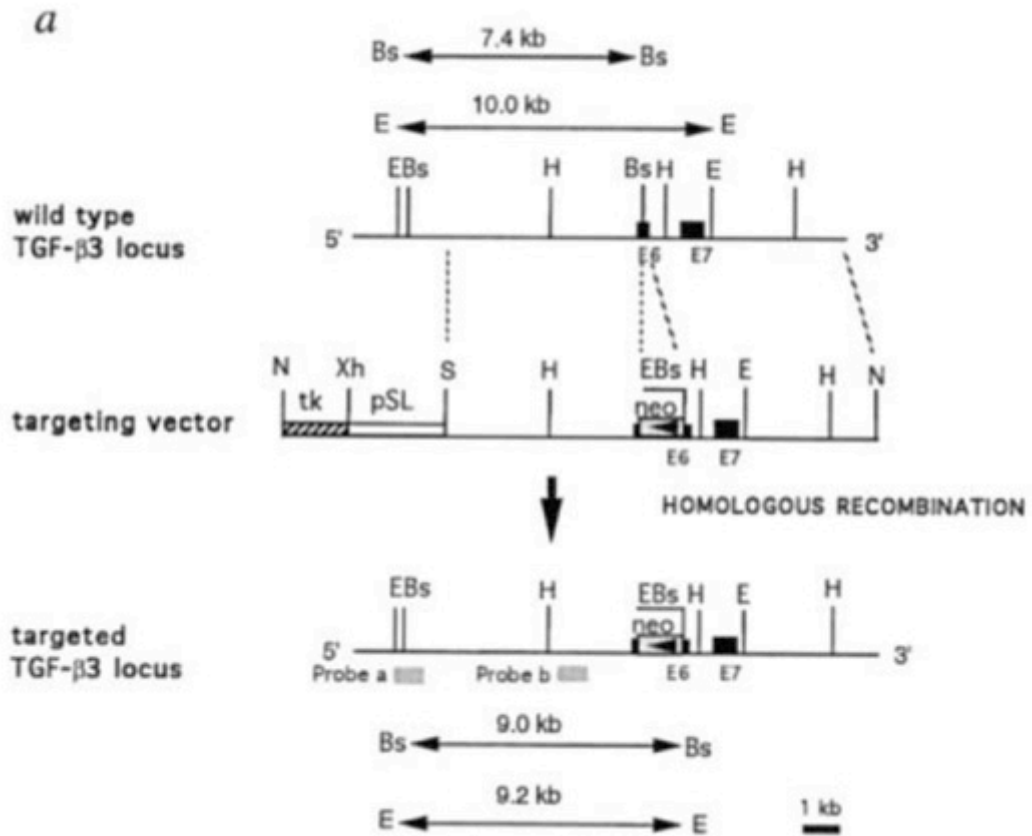
Figure 1-11. Schematic map for disruption of the *Tgfb3* gene (Kaartinen et al., 1995).

The wild-type *Tgfb3* locus is shown and exons 6 and 7 and indicated by black boxes. Exon 6 was disrupted by the insertion of a neo cassette from a targeting vector via homologous recombination. The correct targeting was identified through the use of restriction site digests (E, *EcoRI*; Bs, *Bsu36I*; H, *HindIII*; N, *NotI*; Xh, *XhoI*; S, *SalI*) and the use of internal and external probes for Southern detection (grey shaded boxes) .

The resulting *Tgfb3* mutant animals have a complete cleft of the secondary palate and therefore are not able to suckle milk, which results in death within a day of birth (Kaartinen et al., 1995; Proetzel et al., 1995). This resulting phenotype displays one disadvantage for studying germ-line knockouts due to the lethality that can result when a gene is completely removed. As it may be advantageous to examine loss of a gene at a later time point or in a specific cell type a method to generate conditional knockout animals was developed (see section 1-7.5.).

1-7.5. Conditional gene removal

Soon after introduction of a homologous recombination based technology to manipulate the mouse genome, Klaus Rajewsky and colleagues introduced yet another powerful methodology, which can be used to introduce both temporally and spatially controlled manipulations in the mouse genome(Rajewsky et al., 1996). This so called Cre-*loxP* system allows a gene or locus flanked by the *loxP* sites to be excised in the presence of Cre recombinase. This enzyme from bacteriophage P1 that recognizes so called loxP sequences and catalyzes recombination events (Sauer, 1998). A similar system has been identified in yeast. In this case flippase (*Flp*) recombinase (like *Cre*) recognizes a set of Flp Recombinase Targets (*FRT*, like *loxP*) sequences (Sadowski, 1995)(Table 1-3).

LoxP and *FRT* sites are composed of 34-bp sequences composed of palindromic 5' and 3' ends and core sequences are either 6 (*FRT*) or 8 base pairs (*loxP*), which dictate their directionality(Grainge et al., 2002). If both pairs of sites are inserted in the same orientation, *Cre* drives excision of the flanked sequence, leaving behind a single target site. If the target sites flank the sequence in opposite orientations, then an inversion of the flanked sequence will occur (Figure 1-12).

The conditional removal of a gene is useful to study a gene at a specific time point or within a specific tissue. Similar to the knockout design of *Tgfb3*, a conditional allele was generated that disrupted exon 6, through the use of a targeting vector that contained both positive (*neo*) and negative (*Tk*) selection markers. *LoxP* sites were inserted surrounding exon 6 (floxed) and the neo was flanked with *FRT* sites. Successful gene targeting generates a floxed exon 6 (exon 6 flanked by *loxP* sites), containing *FRT* flanked *neo*^{r} (Figure 1-13). The FRT flanked neo^r sequence that remained in the *Tgfb3* floxed animals was removed through mating with a *Flp* deleter mouse line, that expresses *Flp* recombinase. The resulting progeny that had both the floxed *Tgfb3* and flp recombinase resulted in animals that lacked the neo^r site and contained only the floxed *Tgfb3*. The floxed animals were healthy and bred normally.

The *Tgfb3* allele can be recombined when a mouse is heterozygous either for the *floxed* allele or for the germ-line allele and carries a Cre transgene is crossed with a mouse that contains the homozygous floxed *Tgfb3* gene.

	Recombinase	Target Site

Table 1-3. *Cre-loxP* and *Flp-FRT*. Systems for use in developing conditional gene knockouts are shown. The recombinase drives excision of a gene that is flanked by palindromic sequences that contain a core *LoxP* or *FRT* site (italicized and underlined).

	Recombinase	Target Site
Cre-loxP	Cyclization recombination recombinase (derived from bacteria) (Cre)	34 bp *loxP* sites ATAACTTCGTATA*ATGTATGC*TATACGAAGTTAT
Flp-FRT	Flippase (derived from yeast) (Flp)	Flp recombinase target (*FRT*) sites TTGATGAAAGAA*TACGTT*ATTCTTTCATCAA
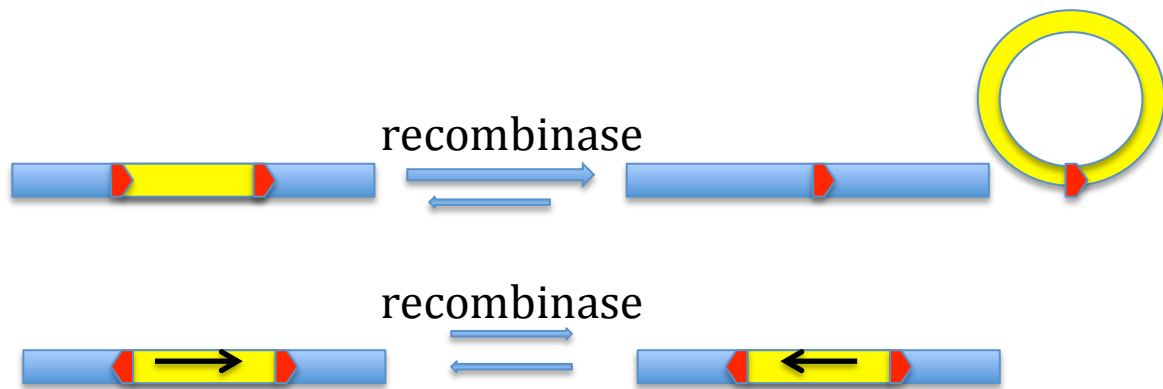
Figure 1-12. Asymmetric gene targeting. Diagram showing asymmetric target sites (loxp, for example). Target sites are labeled as red triangles with the point of the triangle showing the orientation of the core sequence. If the orientation is in the same direction and flanking the area to be recombined (yellow rectangle), then it will excise out that region into a separate plasmid, where if the target sites are in opposite orientations, then the target area will be inverted.
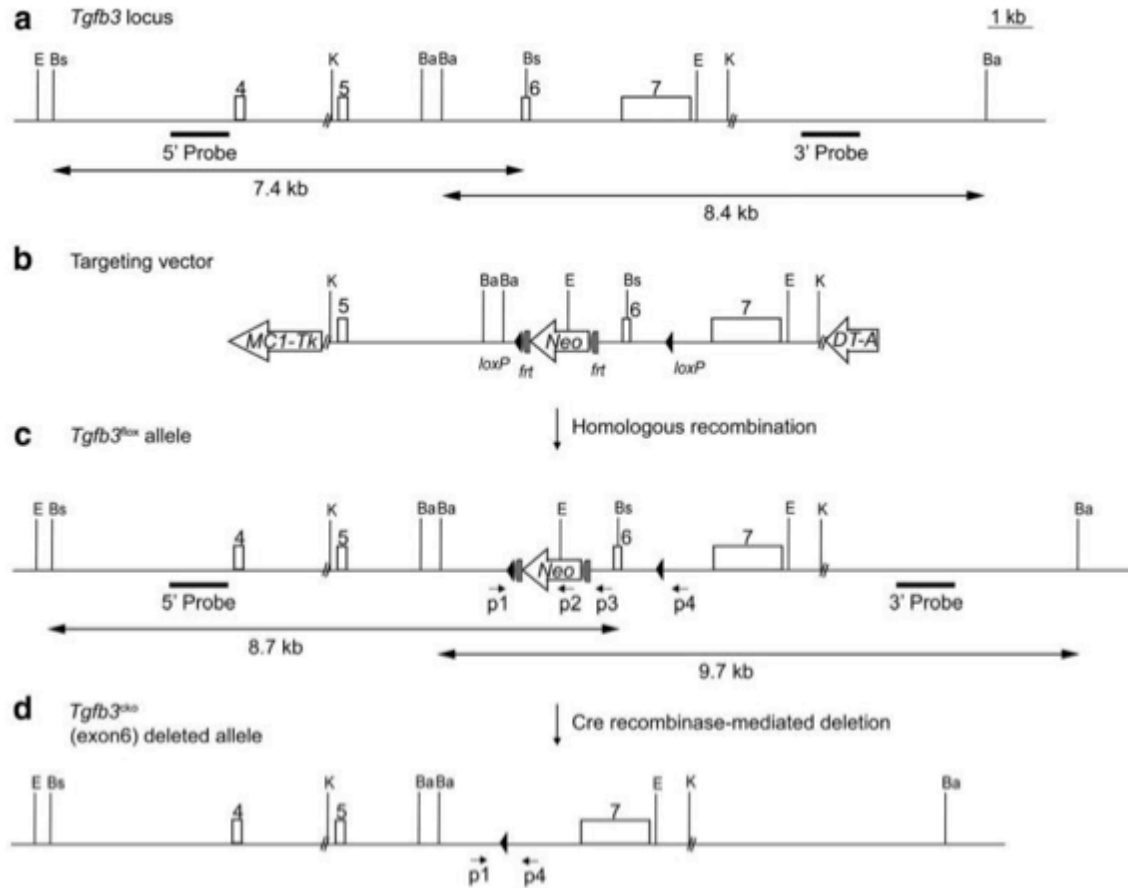
Figure 1-13. Schematic map for generation of the *Tgfb3* floxed allele (Doetschman et al., 2012).

a. The *Tgfb3* wild-type locus showing introns 4-7 (white boxes) and the 3' untranslated region. The black boxes below indicate the probes that were used in Southern blot screening for the correctly targeted mutation. b. The targeting vector is shown with the negative selection gene (*Tk*), a loxP site, followed by FRT flanked *Neo* cassette within intron 6 and another loxP site within intron 7. c. The *Tgfb3*^{flox} allele map is shown along with probes used for Southern analysis (black boxes) and genotyping primers (small black arrows). d. Map showing the *Tgfb3* conditional removal upon Cre-mediated recombination. Primers are indicated below (small black arrows) that were used to identify the removal of Exon 6.

34

1-8. *Cre* driver lines used to study palatogenesis

1-8.1. General use of *Cre* driver lines

As discussed above, in *Cre-loxP* system, Cre drives recombination of a sequence that is flanked by loxP sites allowing a target gene to be removed from a specific tissue. Therefore, the specificity of the system is solely dependent on a *Cre* driver line, i.e., *Cre* needs to be expressed strongly and specifically within the genome for it to be useful for driving recombination in a particular cell type at a particular time.

Cre mouse lines can be generated by using traditional transgenic, or gene knock-in techniques. Traditional transgenic mice are easy and fast to produce. Transgenic constructs are relatively small (<20kb) and often contain few control elements, e.g., a tissue-specific promoter and enhancer. However, due to a random integration and lack of locus control elements, they often fail to mimic endogenous expression patterns. *BAC* transgenics that express *Cre* are useful because they likely contain most of the cis-regulatory elements and thus can overcome positional effects. *BAC* transgenic constructs are large (150-300kb) and are not very sensitive for positional effects. However, generation of BAC transgenic constructs and mice is more demanding than that of traditional transgenics. The most reliable method to generate *Cre* driver lines is to knock in a *Cre* cassette into a desired locus. However, this is relatively time consuming and expensive when compared to transgenic methods based on random integration.

To test and validate novel *Cre* transgenic lines, several different reporter mouse lines have been generated (Novak et al., 2000; Soriano, 1999). Perhaps, the most commonly used line was made by inserting *loxP-STOP-loxP*-reporter cassette into the ubiquitously expressed Rosa26 locus (Soriano, 1999). Once crossed with a Cre driver, the STOP cassette is excised allowing for the *Rosa26* locus to drive reporter (e.g., LacZ, YFP etc) expression wherever and whenever *Cre*

is expressed and active. In order to detect *Cre* expression (both time and location), a tool that is commonly used in the field is the use of a reporter mouse line. Cre time and location of expression can be detected through the use of a reporter mouse, *R26R-LacZ*. Targeted gene deletion was used to insert a neo stop cassette flanked by *loxP* sites, followed by *LacZ*, just downstream of the *Rosa26* locus (Soriano, 1999). The *Rosa26* locus was used because it is constitutively active from the preimplantation stage of embryo development and therefore is on in every cell type of the developing embryo. Once crossed with a *Cre* driver line, the *loxP* sites are excised and allows for the *Rosa26* locus to drive *LacZ* expression wherever and whenever *Cre* is expressed (Fig. 1-14).

1-8.2. Methods of temporal regulation

Cre ER^{T2} transgenic mice allow inducible activation of floxed alleles in adult mice upon administration of tamoxifen. CreER^{T2} is a fusion protein between Cre and a mutant estrogen receptor ligand-binding domain that can be induced in-vivo by the small molecule inducer tamoxifen. Tamoxifen is a synthetic steroid that when it binds CreER^{T2}, the protein is translocated to the nucleus where Cre recombines sequences flanked by the *loxP* sites (Feil et al., 2009).

Another method that allows spatial and temporal regulation is through the use of the tetracycline regulatory system. In the Tet-on system, the tetracycline-responsive transactivator (tTA) contains the *E. coli tet* repressor fused to the transactivation domain of VP16 protein of the Herpes simplex virus along with a tTA dependent promoter that contains an RNA II polymerase promoter fused to *tet* operator sequence. tTA dimers bind the *tet* operator sequence allowing gene transcription. However, in the presence of the inducer doxycycline, tTA undergoes a

conformational change not allowing it to bind the *tet* operator sequence and thus not allowing

gene transcription. In the reverse system, tet-off, there is a sequence change in tTA making it

rtTA, where now the gene is only on in the presence of doxycycline. Again, Cre induced

recombination only takes place in the presence of *loxP* sites that are contained in the mouse or

the embryos within the mouse that is being administered tetracycline.

Both systems allow for temporal regulation of *Cre*. (Figure 1-14 shows the difference

between a global knock-out, a conditional knock-out and a inducible conditional knock-out).
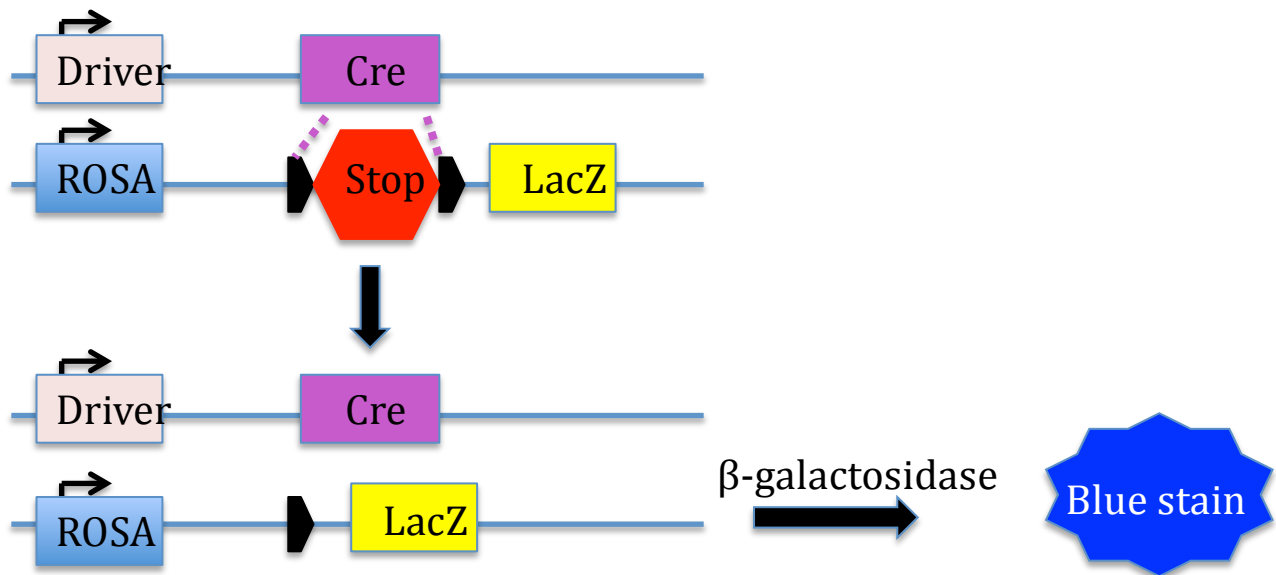
Figure 1-14. R26R-lacZ reporter can be used for lineage tracing.

The ubiquitously expressed Rosa26 locus contains a loxP-STOP-loxP cassette followed by *LacZ* (loxP sites indicated by black triangles). Once crossed with a Cre driver, the STOP sequence is excised and *LacZ* is expressed. *LacZ* expression can be detected by X-gal staining.
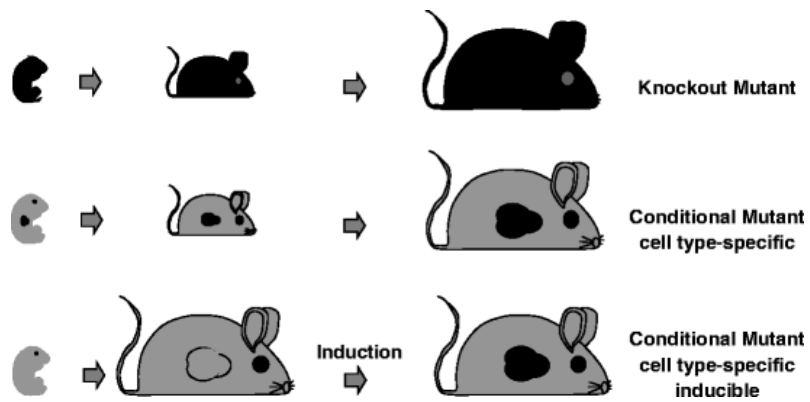
Figure 1-15 Knock –out, conditional knock-out and inducible conditional knock-out mice (Friedel et al., 2011).

a. When a gene is knocked-out, it is removed everywhere (black). b. When a gene is removed conditionally only specific cells have the gene removed (black). c. Cre can be induced temporally removing the gene a specific time and location (black).

1-8.3. Cre drivers used to recombine floxed genes in the palatal mesenchyme

The most commonly used *Cre* driver to delete genes in the CNC including the palatal mesenchyme is *Wnt1-Cre* (Danielian et al., 1998; Rowitch et al., 1998). In *Cre*-positive embryos recombination begins in pre/early migratory neural crest cells at ~E8.5 and continues through E11.5 (Danielian et al., 1998; Rowitch et al., 1998). It recombines in all of the cranial neural crest derived cells, which include the craniofacial neural crest and palatal mesenchyme (Chai et al., 2000). Another line, which recombines in post-migratory palatal mesenchymal cells was recently introduced (Lan et al., 2007). This was achieved by knocking in an IRES-Cre-pA cassette into the 3' untranslated region of the *Osr2* gene. *Osr2-Cre* drives Cre expression at embryonic day 10.5-10.75 within the first pharyngeal arch mesenchyme and later derivatives, which include the palatal mesenchyme (Lan et al., 2007) (Table 1-4).

1-8.4. Cre drivers used to recombine floxed genes in the palatal epithelium

Several different Cre-driver lines have been used to delete floxed genes from the palatal epithelium (Table 1-4). The most widely used driver is *K14-Cre*, which recombines in ectodermal derivatives including oral/palatal ectoderm beginning at E11 (Andl et al., 2004). However, this driver is not expressed in the overlying periderm (Chapter 4). *Pitx2-Cre* driven by the *Pitx2* promoter and first pharyngeal arch enhancer fragments (cis-regulatory elements) drives *Cre* expression in the palatal and dental epithelium beginning at E11.5. However, its expression is mainly in the posterior of the secondary palate (Xiong et al., 2009). *Foxg1-Cre* is expressed around E12.5 in the palatal epithelium (a part of the expressing facial and head ectoderm) and other epithelial structures of the head and in the foregut. However, Cre recombination is highly dependent on a genetic background (Hebert and McConnell, 2000); in addition, it is not known,

whether *Foxg1-Cre* recombines in palatal peridermal cells. *Tgfb3-Cre* was generated through

knock-in of cre into exon1 of *Tgfb3*. Cre positive embryos show specific recombination in the

palatal epithelium including the periderm. However, earlier expression of *Tgfb3* in several

endodermal, mesodermal and ectodermal derivatives limits its usefulness in studies of

palatogenesis (Yang et al., 2008).

	Table 1-4. Cre driver lines used to study palatogenesis			
Driver	Time of recombination	Palatal tissue	Other tissues	Disadvantages for use in examining MES removal
Wnt1-Cre	E8.5	Mesenchyme	All neural crest derived tissues, Neural plate	Recombines in premigratory/early migratory neural crest cells
Osr2-Cre	E10-10.75	Mesenchyme	Mesonephros, specific domains of limb buds, maxillary-mandibular junction	Ectopic activation detected in a subset of embryos
Foxg1-Cre	E12.5	Epithelium	Dorsal and ventral telencephalon, developing ear, olfactory epithelium, foregut	Recombination pattern highly dependent of genetic background and is poorly characterized
K14-Cre	E12-14.5	Epithelium	All ectoderm-derived tissues	Does not recombine in the periderm
Tgfb3-Cre	E8	Epithelium	Heart, octic vesicles, limb buds, midbrain, somites, tail, lower jaw, tongue	Early recombination in several tissues
Pitx2-Cre	E11.5-13.5	Epithelium	None	Mostly in posterior of secondary palate, early recombination

1-9.   Summary

1-9.1. Smad4-independent signaling in the craniofacial neural crest

Tgfb3 is expressed specifically in the palatal epithelium and when it is removed globally

it results in a full cleft of the secondary palate. However, when Tgfb3 is removed in the palatal

epithelium, it results in a milder palatal phenotype. One hypothesis was that Tgfb3 is expressed

within the palatal epithelium and signals to the underlying mesenchyme, but when Tgfb3 was

removed in post-migratory neural crest cells (Wnt1-Cre), it did not result in a palatal phenotype

(Lane et al., unpublished and data not shown).   Although, the palatal phenotype of Tgfb3

mutants cannot be ascribed as a mesenchymal defect, we were interested in the role of Smad4

independent signaling, since loss of TGF-β receptors (Dudas et al., 2006; Xu et al., 2006) in the

craniofacial ectomesenchyme results in severe palatal defects.

TGF-β signaling in craniofacial growth and pattering is well established, yet the details of

the signaling mechanisms are not well known. The focus of many TGF-β signaling studies has

been on Smad-dependent signaling processes, yet the roles of Smad-independent signaling are

just now being addressed. In this thesis (Chapter 2), I address the role of Tak1 in the craniofacial

neural crest. I found that Tak1 is required for appropriate activation of p38 Mapk (Smad-

independent pathway) and TGF-β/ BMP R-Smads (Smad-dependent pathway) in the neural

crest-derived craniofacial ecto-mesenchyme.

1-9.2. Smad4-independent signaling in the pre-fusion palatal epithelium

Tgfb3 is strongly and specifically expressed in the midline epithelial seam and mice

lacking Tgfb3 have a complete cleft of the secondary palate due to lack of MES removal.

Epithelial specific deletion of the TGF-β receptors Alk5 and Tgfbr2 led to specific palatal

defects. However, it was surprising that epithelial removal of a critical TGF-β3 transducer, *Smad4*, did not result in a palatal phenotype. Xu et al further demonstrated in culture that simultaneous removal of *Smad4* and inhibition of *p38* led to a persistent midline epithelial seam. This suggests that both Smad-dependent and Smad-independent TGF-β signaling act redundantly for successful palatal epithelial fusion. In this thesis, I studied the downstream signaling components of the Smad-independent pathway and their role in MES removal (Chapter 3).

1-9.3. *Tgfb3* expression in pre-fusion palatal epithelium

Tgfb3 is expressed in the epithelial tips of pre-fusion palatal shelves and is needed for successful palatogenesis. Previously, it has been shown that conditional removal of *Alk5* or *Tgfbr2* in the palatal epithelium has a milder palatal phenotype when compared to the complete removal of *Tgfb3* (knock-out). I have found in this thesis (Chapter 4) that there is a milder phenotype when *Tgfb3* is removed specifically in the palatal epithelium (conditional knock-out) and is likely caused by the inability of the *K14-Cre* driver to recombine in peridermal cells (flattened layer of cells that cover the epithelial tips of pre-fusion palatal shelves). It is unknown how *Tgfb3* gene expression is specifically directed in the pre-fusion MEE and overlying periderm. In this thesis (Chapter 4), I identified the control elements responsible for palate-specific *Tgfb3* expression in the epithelium and in the overlying periderm.

Chapter 2:

TGF-β-activated Kinase I (Tak1) mediates agonist-induced Smad activation and linker region phosphorylation in embryonic craniofacial neural crest-derived cells

2-1. Summary

Although the importance of TGF-β superfamily signaling in craniofacial growth and patterning is well established, the precise details of its signaling mechanisms are still poorly understood. This is in part because of the concentration of studies on the role of the Smad-dependent (so-called "canonical") signaling pathways relative to the Smad-independent ones in many biological processes. Here, we have addressed the role of TGF-β-activated kinase 1 (Tak1, Map3k7), one of the key mediators of Smad-independent (noncanonical) TGF-β superfamily signaling in craniofacial development, by deleting *Tak1* specifically in the neural crest lineage. *Tak1*-deficient mutants display a round skull, hypoplastic maxilla and mandible, and cleft palate resulting from a failure of palatal shelves to appropriately elevate and fuse. Our studies show that in neural crest-derived craniofacial ecto-mesenchymal cells, Tak1 is not only required for TGF-β- and bone morphogenetic protein-induced p38 Mapk activation but also plays a role in agonist-induced C-terminal and linker region phosphorylation of the receptor-mediated R-Smads. Specifically, we demonstrate that the agonist-induced linker region phosphorylation of Smad2 at Thr-220, which has been shown to be critical for full transcriptional activity of Smad2, is dependent on Tak1 activity and that in palatal mesenchymal cells TGFβRI

and Tak1 kinases mediate both overlapping and distinct TGF-β2-induced transcriptional responses. To summarize, our results suggest that in neural crest-derived ecto-mesenchymal cells, Tak1 provides a critical point of intersection in a complex dialogue between the canonical and noncanonical arms of TGF-β superfamily signaling required for normal craniofacial development.

2-2. Introduction

Members of the transforming growth factor-β (TGF-β) superfamily are involved in many normal and pathologic events including development, inflammation, fibrosis and cancer (Blobe et al., 2000). TGF-βs and bone morphogenetic proteins (BMPs) form two important subgroups within the superfamily(Derynck et al., 1998; Massague, 1998). They bind to largely subfamily-specific membrane-spanning complexes of Type I and Type 2 receptors resulting in activation of components of intracellular Smad-dependent and Smad-independent pathways. In the Smad-dependent pathway, receptor-regulated Smads (R-Smads) become phosphorylated at their C terminals via Type I receptor kinase activity, complex with Smad4, and accumulate in the nucleus where they act as transcriptional co-regulators (Derynck et al., 1998; Massague, 1998). Initially it was thought that TGF-βs signal exclusively through TGF-β Type I and II receptors (TGFβRII and TGFβRI) to activate TGF-β R-Smads 2 and 3 and similarly BMPs signal through specific Type I and II receptors to activate BMP R-Smads 1,5 and 8 (Derynck and Zhang, 2003). However, a recent report showed that at least in certain specific cell lines TGF-βs can also signal via mixed receptor complexes resulting in activation of BMP R-Smads (Daly et al., 2008).

As well as C-terminal phosphorylation at a conserved –SSXS- sequence, more recent research has shown that R-Smads can also be phosphorylated in the linker region between their

Mad homology domains, which is important for both full activation and cessation of activation (Alarcon et al., 2009; Matsuzaki et al., 2009). Specific residues become phosphorylated as the result of distinct pathways: antagonists, such as EGF, which enable the activated R-Smads to remain in the cytoplasm and be degraded (Kretzschmar et al., 1997); and agonist-induced linker phosphorylation which is required for maximal transcriptional activity of R-Smad/Smad4 complexes as well as for rapid turnover of corresponding R-Smads (Alarcon et al., 2009; Aragon et al., 2011). In this 'action turnover switch' model the Thr/Ser residues adjacent to proline-rich sequences in R-Smads (Thr-220 in Smad2) are phosphorylated by nuclear Cdks creating a docking site for transcriptional co-regulators (Pin1 in case of TGF-β R-Smads; Yap in case of Bmp R-Smads). Moreover, it has been suggested that this phosphorylation may enable subsequent phosphorylation of other linker region residues, such as S250 in Smad2, providing a docking site for ubiquitin ligases, such as, Nedd4L, targeting R-Smads for proteasome-mediated degradation (Aragon et al., 2011; Gao et al., 2009).

In addition to Smad-dependent (canonical) TGF-β/BMP signaling, ligands in the TGF-β superfamily can also activate Smad-independent (non-canonical) pathways resulting in activation of the Map kinase signaling (Derynck and Zhang, 2003). A critical step in initiation of the non-canonical pathway is activation of TGF-β activated kinase-1 (Tak1, Map3k7) by Traf6-mediated polyubiquitination (Sorrentino et al., 2008; Yamashita et al., 2008). Other studies have shown that Tak1 is required for fine-tuning of BMP effects during bone development as well as for TGF-β-induced NF-κb and JNK activation, and also mediates cytokine-induced Ikkα activation (Gingery et al., 2008; Hoffmann et al., 2005; Wang et al., 2001).

Although the canonical pathway tends to be treated as the more important, recent studies suggest that the Smad-independent TGF-β signaling plays a more significant role *in vivo* than

47

previously thought (Holm et al., 2011; Iwata et al., 2012a). In a mouse model of Marfan syndrome in which TGF-β signaling is elevated, the aortic aneurysm phenotypes are made *worse by* reducing the canonical pathway component Smad4, and the phenotypes less severe by attenuation of *non*-canonical pathways (Holm et al., 2011). These results show that not only is the non-canonical pathway of importance in disease mechanisms but that the two pathways somehow interact with one another. Mutations in TGF- β type I and type II receptors (*TGFBR1* and *TGFBR2)* associated with Marfan's syndrome and Loeys-Dietz syndrome lead to an increase in TGF-β signaling activity in the absence of normal canonical signaling(Cardoso et al., 2012). The importance of maintaining the correct balance between the pathways for normal developmental events is implied by the presence of craniofacial defects including cleft palate in patients suffering from the Loeys-Dietz syndrome(Loeys et al., 2005) and in a mouse model when *Tgfbr2* is genetically removed from the neural crest cell population (which form the principal source of mesenchymal cells in the secondary palate precursor structures, the palatal shelves) resulting in cleft palate in the presence of excessive TGF-β-induced non-canonical signaling (Iwata et al., 2012a).

In the light of the important role played by the Smad-independent pathway implied by these studies, as well as the well-established importance on TGF-β and Bmp signaling in normal craniofacial development in mouse models (Iwata et al., 2012a), we examined the role of Tak1 in craniofacial neural crest development by deleting *Tak1* function in pre-migratory neural crest cells using the *Wnt1-Cre* driver line. The mutant mice display hypoplastic facial structures, and cleft palate, which is caused by a delayed palatal shelf elevation. We found that Tak1 is required for appropriate activation of both p38 Mapk (non-canonical pathway) and TGF-β/Bmp R-Smads (canonical pathway) in the neural crest-derived craniofacial ecto-mesenchyme. We also show

that Tak1 deficiency results in attenuated TGF-β R-Smad linker region phosphorylation, and that

Tak1 kinase mediates both distinct and overlapping agonist-induced transcriptional responses.

Collectively, these results imply that in neural crest-derived mesenchymal cells Tak1 mediates

both canonical and non-canonical arms of the TGF-β superfamily signaling.

2-3. Experimental Procedures

2-3.1. Mice

   Tak1-flox mice were generated by flanking a critical exon 2 with asymmetric loxP sites

(*Lox66* and *Lox71*) in opposing orientations (see Fig. 2-1; details will be described

elsewhere). *Wnt1-Cre* (from the Jackson Laboratories) and *Tgfbr1^{FX}* (kindly provided by S.

Karlsson) mice have been described earlier ((Danielian et al., 1998; Larsson et al.,

2001)).*Tak1^{FX+}/Wnt1-Cre$^+$* male mice were crossed with *Tak1^{FXFX}* female mice to obtain timed

pregnancies. The presence of a vaginal plug was designated as embryonic day 0 (E0). DNA for

genotyping was prepared from yolk sac or from tail tissue using DirectPCR lysis reagents

(Viagen Biotech). Mouse lines were maintained in mixed genetic backgrounds. All experiments

involving the use of animals were approved by the Institutional Animal Use and Care Committee

at the University of Michigan at Ann Arbor.

2-3.2. Genotyping

   Tak1^{FXFX} mice were genotyped by PCR using the following primer sequences (annealing

at 60$^{\text{o}}$C): *Tak1^{FX}*-sense: *5'-gataccttacactgggggacca-3'* and *Tak1^{FX}*-antisense *5'-*

ggcattcagttgtggagcatt-3'. *Wnt1-Cre* and *Tgfbr1^{FX}* mice were genotyped as previously described

(Danielian et al., 1998; Larsson et al., 2001).

2-3.3. Conventional RT-PCR

To assess the recombination efficiency of the *floxed Tak1 locus*, the total RNAs were
isolated from prefusion palatal shelves harvested at E14.0 or maxillary and mandibular first
pharyngeal arch at E11 (RNeasy mini kit; Qiagen), and cDNAs synthesized (Omniscript reverse
transcriptase, Qiagen) according to manufacturer's protocols. The following primers were used:
Tak1 exon 1-specific sense primer, 5′-GGGGATCATGTCGACAGCCTC-3′; Tak1 exon 3-
specific antisense primer, 5′-GTTCACACGTGACAACTGCCG-3′; and Tak1 exon 4-specific
antisense primer, 5′-GCATGCTGTGCAGGTAAGCCA-3′. β-Actin was used as a quality and
loading control: sense primer, 5′-GTGGGCCGGTCTAGGCACCAA-3′; and antisense primer,
5′CGGTTGCCTTAGGGTTCA-GG-3′.

2-3.4. Real-time quantitative PCR

Total RNAs were isolated, and cDNAs were synthesized as outlined above. Real time
quantitative PCR experiments were carried out using Universal Probe Library-based assays
(Roche Applied Science) with gene-specific primer sequences generated by the manufacturer's
online algorithm and TaqMan Universal PCR master mix (Applied Biosystems). 30-μl assays
were quantified using the ABI7300 PCR and detection system (Applied Biosystems) and
analyzed using 7500 System v1.2.2 software.

2-3.5. Histology, in Situ Hybridization, Cell Death, and Proliferation Assays

For histological analyses, tissues were processes, sectioned and stained by H&E
according to standard protocols. For whole-mount in situ hybridization, the tissues were fixed in

4% buffered formaldehyde for 12-16 hours and dehydrated though a graded methanol series

(20%, 50%, 70%, 95% and 100%) containing PBST. Antisense RNA probes were synthesized

with NTP DIG RNA labeling mix (Roche Applied Science) following manufacturer's

instructions. Probe templates for *Shox2, Tbx22* and *Shh* were obtained from Y-P Chen(Yu et al.,

2005), R. Jiang (Liu et al., 2008) and S. Bellusci (Bellusci et al., 1997), respectively. A probe

template for *Tgfb3* was prepared as described (Dudas et al., 2004). Apoptotic cells were detected

using TUNEL assay (Dead End from Promega) following manufacturer's instructions. For cell

proliferation analyses, cell proliferation labeling reagent (RPN201, Amersham) was used. BrdU-

positive cells were detected using anti-BrdU antibody (RPN202, Amersham). Fluorescent images

were viewed on an Olympus BX51 microscope and documented using an Olympus DP71

camera.

2-3.6. MicroCT analyses

Specimens were embedded in 1% agarose, placed in a 19-mm-diameter tube, and scanned

over the entire length of the skull using a microCT system (μCT100; Scanco Medical,

Bassersdorf, Switzerland). The scan settings were: voxel size 10 μm, medium resolution, 55

kVp, 109 μA, 0.5 mm AL filter, and integration time 500 ms. Images were created using the

manufacturer's evaluation software and a fixed global threshold to segment bone from non-bone.

Skull shape was analyzed by measuring the distance from the supraoccipital bone to the anterior

end of the frontal bone (length) and from the top of the parietal bone to the cranial base (height)

and calculating the height/length ratio. Mandibular length was measured as shown in Fig. 2-1.

2-3.7. Western Blotting

Tissues or cells were lysed in 2xLaemmli sample buffer (Harlow and Lane, 1988),

quantified by Quant-It protein assay system (Invitrogen), and samples (5 μg of protein per lane),

run on NuPage 4-12% Bis-Tris gradient gels (Invitrogen) and transferred by "iBlot dry blotting"

(Invitrogen) onto nitrocellulose filters. Immonoblotting and detection were done according to

standard protocols. Documentation and quantification was accomplished by using the UVP

BioSpectrum AC imaging system. Antibodies used were: pTak1 (#9339 – Cell Signaling),

Smad2 (#5339 –Cell Signaling), pSmad2-C (#3101 –Cell Signaling), Smad1 (#6944 –Cell

Signaling), pSmad1/5/8-C (#9511 – Cell Signaling), p-p38 Mapk (#4511-Cell Signaling), p-Jnk

(#4668- Cell Signaling), p42/44 Erk (#4376-Cell Signaling), β-Actin (#A1978 – Sigma-Aldrich),

pSmad2-L(S250) (#35741 – Immuno-Biological Laboratories), pSmad2-L(T220) and pSmad3-

L(T179) (#28087 – Immuno-Biological Laboratories), Histone H3 (#4499-Cell Signaling),

PSMA2 (#2455-Cell Signaling).

2-3.8. Primary craniofacial mesenchymal cell cultures

Mandibular and maxillary processes of the first mandibular arch, and prefusion palatal

shelves were dissected from E11.0 and E14.0 embryos, respectively. The cultures were

established as described by Thomas et al. (Thomas et al., 2010). The neural crest origin and

purity of cultures was confirmed by establishing cultures of embryos that carried both the *Wnt1*-

Cre transgene and were positive for the R26-lacZ reporter (Fig. 2-3B). β-galactosidase staining

was carried out as described (Behringer, 2003). After 7-10 days cells were stimulated with

growth factors (TGF-β2, 10ng/ml or BMP2, 100ng/ml) for 0, 10 or 40 minutes, and harvested for

western blot analyses. Chemical inhibitors Flavopiridol (Cdk inhibitor; 1 or 10 μM; Sigma-Aldrich), UO126 (Erk1/2 (and Jnk) inhibitor; 10mM; Sigma Aldrich), SB431542 (TGFβRI inhibitor; 10 μM; Sigma-Aldrich), 5Z-7-Oxozeaenol (Tak1 inhibitor; 2 μM; eMolecules) and SB202190 (p38 Mapk inhibitor; 10 μM; Sigma-Aldrich) were added to cells 60 min prior to TGF-β2 or BMP2 addition. Cells were not starved of serum prior to these treatments. Some cultures were transduced with replication-deficient recombinant adenoviral preparations using MOI 1000. *Ad-Gfp* and *Ad-Cre* (titer, 4 x 10^{12} vp/ml) were obtained from the University of Michigan Biomedical Research Core Facility. For immunofluorescence, cultured cells were fixed in 4% buffered formaldehyde (5 mins) and stained using anti-Smad2 (#5339, Cell signaling) antibody. Binding was detected using Alexafluor-594 goat anti-rabbit secondary antibody (Invitrogen), and slides mounted in Vectashield with DAPI (Vector Labs Inc.). Fluorescent images were viewed and documented as outlined above. In some experiments, nuclear and cytoplasmic fractions were separated using NE-PER Nuclear and Cytoplasmic Extraction kit (# 78833-Thermo Scientific) according to the manufacturer's instructions.

2-3.9. Neural crest stem cell cultures

The neural crest stem cell line O9-1 was obtained from M. Ishii. Undifferentiated cells were cultured in the presence of LIF and bFGF in SNL-cell-conditioned medium as described (Ishii et al., 2012).

2-3.10. Roller bottle organ cultures

Heads from embryos were collected at E13.5 and mandible, tongue and brain removed in PBS. The resulting mid-face samples were cultured for 24-48 hours at 37°C in roller bottles (60

rotations per minute) in serum-free BGJb medium without Pen-Strep. The bottles were gassed at the beginning of the culture and every 12 hours by gently bubbling the medium for 2 minutes with O_2/CO_2 (95%/5%). The palatal cultures were fixed, sectioned, and stained as described above.

2-3.11. Microarray analyses

Palatal mesenchymal cells were isolated and aliquoted to 4 groups as shown in Table 2-1 Confluent cultures were incubated in the presence of inhibitors (TGFβRI inhibitor SB431542, 10 μM; Tak1 inhibitor 5Z-7-oxozeaenol, 2 μM) for 1 h and then stimulated with TGF-β2 (10 ng/ml) for 2 h. Total RNAs were then isolated using an RNeasy kit (Qiagen). Concentration and purity were determined by spectrophotometry, and RNA integrity was confirmed by running aliquots on 1% agarose gel. 500 ng of total RNA of each sample was amplified and biotin-labeled according to the GeneChip 3′ IVT expression kit user manual (Affymetrix). Microarray analysis was performed with the GeneChip mouse genome 430 2.0 array (Affymetrix). The biotin-labeled RNAs were fragmented, and 10 μg of each was hybridized to a GeneChip at 45 °C for 16 h. Labeled bacterial RNAs of known concentrations were spiked in hybridization to generate an internal standard and to allow normalization between the chips. The chips were washed and stained with streptavidin R-phycoerythrin (Molecular Probes). After scanning the chips by GeneChip Scanner 3000 7G System, the data were analyzed by Affymetrix GeneChip-related software packages GCOS, Data Mining Tool, and Affymetrix web database "NetAffx." Microarray data were submitted to the GEO repository under accession number GSE45491.

2-4. Results

2-4.1. Neural crest-specific Tak1 mutants display mandibular hyperplasia and cleft palate

A recent study demonstrated that haploinsufficiency of *Tak1* in neural crest cells rescued the cleft palate phenotype of *Tgfbr2* mutant mice(Iwata et al., 2012a). However, the role of Tak1 itself in craniofacial development is currently unclear. To address this question, we crossed mice homozygous for the *floxed Tak1* allele (*Tak1^{FXFX};* for details see Fig. 2-1A) with transgenic *Wnt1-Cre* mice that also were heterozygous for the *floxed Tak1* allele (*Tak1^{FX+}/Wnt1-Cre$^+$)*. The expected Mendelian proportion of *Tak1^{FXFX}/Wnt1-Cre$^+$* mice (hereafter referred to as *Tak1/Wnt1-Cre* mutants)* survived to birth (n=16/66) but then died within 24 hours.

We used micro-CT analysis to compare the structure of control and *Tak1/Wnt1-Cre* mutant littermate heads at P0 in detail. The craniofacial skeleton appeared generally stunted in mutants (Fig. 2-1C). Many of craniofacial bones are largely derived from neural crest cells, including cranial base, mandible, maxilla, and frontal skull (Ishii et al., 2012). Although the average lengths of control and *Tak1/Wnt1-Cre* mutant cranial bases did not differ, those of the mandible and maxilla were about 20% and 5% shorter, respectively, in the mutants (Fig. 2-1C). The skulls in mutants were also shorter than in controls (length vs height ratio 1.74+/-0.04 (average+/-sem) and 1.49+/-0.02 in controls and mutants, respectively; n=3). The mutants also displayed cleft secondary palate with high penetrance (13/16, 80%).

To investigate the mechanism underlying the palatal defect, we collected mutant and control embryos at defined time points and analyzed palatal phenotype in detail by histology (Fig. 2-1D-F). At E13.5, the palatal shelves in both control and mutants were still growing vertically towards the floor of the mouth, parallel to the sides of, and separated by, the tongue, which was

almost square in cross section (Fig. 2-1D). By E14.5 (Fig. 2-1E), in controls the tongue had

changed shape in cross section, becoming wider than it was tall. It was no longer interposed

between the palatal shelves which had elevated to point towards one another parallel to the top of

the tongue, and commenced fusion with one another along the midline of the oral cavity in the

mid- and posterior regions, though a 'seam' of adhered epithelia from each shelf still remained.

In contrast, in *Tak1/Wnt1-Cre* mutants, the tongue remained interposed between the palatal

shelves, lying close to the nasal septum, and was still relatively square in cross section. The

shelves had failed to elevate very much. By E18 (Fig. 2-1F), in controls the secondary palates

had fused completely along their entire length: the seam formed where their epithelia had met in

the midline had disappeared so their mesenchymal cores were confluent, and differentiation into

cartilage commenced. In most *Tak1/Wnt1-Cre* mutants examined, secondary palate formation

had failed, leaving a cleft from anterior to posterior. Although the tongue was no longer

completely interposed between the palatal shelves, which had elevated, the shelves had failed to

adhere to or fuse with one another, although some cartilage formation had occurred. Although

now above the tongue in anterior and mid positions, the underside of the shelves and the top of

the tongue were very close compared to the same structures in controls.

As components of the head were smaller in mutants than controls at birth, we examined

the relative size of palatal shelves in littermates at E13.5, and found that shelves in mutants were

about 20% smaller in cross-sectional area than those in controls (Fig. 2-1G, left). BrdU

incorporation assays on pre-fusion palatal shelf sections from littermates showed a lower average

value in mutant versus control cells at the anterior level (not significantly different), but no

difference at the mid and posterior levels (Fig. 2-1G right). To determine if the smaller mutant

shelf area at E13.5 was the result of an earlier lower cell proliferation rate, we performed the

same assay at E11 on mandibular primordia (first pharyngeal arch mesenchyme) but no significant difference between control and mutant tissues was detected (data not shown). No differences in cell death were detected at E11 or E13.5 (data not shown)

Since *Tak1/Wnt1-Cre* mutants displayed a distinct reduction in craniofacial size at birth (Fig. 2-1) likely resulting in a hypoplastic oral cavity, and the position and shape of the tongue appeared abnormal in mutants during palatogenesis, we wondered whether the failure in palatal shelf elevation could be caused by the failure of the tongue to 'descend' appropriately. To address this we cultured mouse embryonic heads at E13.5 (when palatal shelves are still growing vertically), and from which we had removed the mandible and tongue. This was performed in roller bottles under chemically defined conditions. In both control and mutant samples sufficient elevation of palatal shelves occurred after 24 hours that, after a further 24 hours culture, fusion occurred, with equivalent mesenchymal confluence regardless of genotype (Fig. 2-2A-B). This suggests that in *Tak1/Wnt1-Cre* mutants the tongue obstructed palatal shelf elevation *in vivo*, contributing to the pathogenesis of cleft palate in *Tak1/Wnt1-Cre* mutants *in vivo* (see the manuscript of Song et al., co-submitted with this manuscript).

Previous studies have shown that TGF-β superfamily signaling is involved in the anterior-posterior patterning of the secondary palate (Hilliard et al., 2005; Liu et al., 2005; Yu et al., 2005; Zhang et al., 2002). Therefore, we compared expression patterns of established anterior (*Shox2)* and posterior (*Tbx22)* mesenchymal markers between *Tak1/Wnt1-Cre* mutant and control littermates using whole mount in situ hybridization. These experiments did not demonstrate detectable differences in *Shox2* and *Tbx22* expression patterns or intensities between controls and mutants (Fig. 2-2C) suggesting that in *Tak1/Wnt1-Cre* mutants the anterior-posterior patterning is not grossly affected.

Mesenchymal Bmp signaling has been shown to be important for maintenance of *Shh* expression in the rugae of the palatal epithelium (Zhang et al., 2002), which in turn plays a critical role in regulation of growth and patterning along the palatal oro-nasal axis (Han et al., 2009; Rice et al., 2004). Our experiments demonstrate that, unlike palatal mesenchyme-specific *Bmpr1a* mutant shelves (Baek et al., 2011), there was no reduction in *Shh* expression in the primary palate of *Tak1/Wnt1-Cre* mutants. However, while the amount of *Shh* expression in individual ruga was not decreased, at the time of palatal fusion (E14.5-E15.5) a marked delay in rugal formation suggests that the rate of expansion of the secondary palate was reduced (Fig. 2-2D).

In summary, *Tak1* deficiency in craniofacial neural crest resulted in facial (particularly mandibular) and palatal shelf hypoplasia, and cleft palate. Palatal shelf elevation was delayed, and the tongue abnormal in position and shape in mutants immediately prior to the normal stage of palatal fusion. No difference between control and *Tak1/Wnt1-Cre* mutants in anterior-posterior patterning of pre-fusion palatal shelves was detected by marker gene analysis, but a delay in ruga pattern formation suggests abnormal morphogenesis or maturation there. In rolling culture, removal of the tongue and mandible resulted in mutant palatal shelf elevation and fusion occurred in both control and mutant heads.
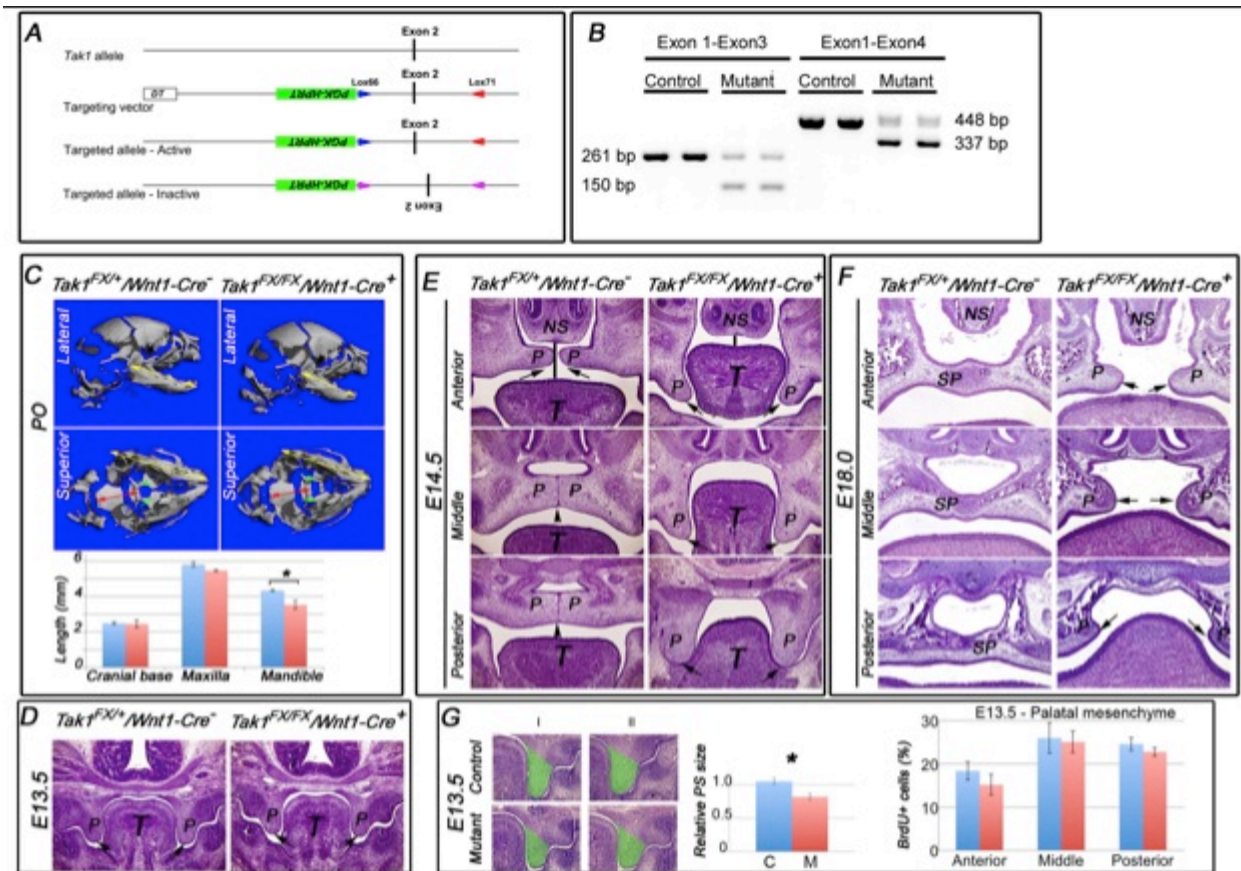
Figure 2-1. **Deletion of *Tak1* in neural crest cells leads to mandibular hypoplasia and cleft palate.** *A*, schematic presentation of the gene-targeting strategy. "Flipping" of exon 2, which encodes the kinase domain of Tak1, causes alternative splicing between exons 1 and 3 (*B*) inactivating the function of Tak1. *B*, RT-PCR analysis of RNA samples harvested from prefusion (at E14) palatal shelves of control (*Tak1$^{FX/+}$/Wnt1-Cre$^-$*) and mutant (*Tak1$^{FX/FX}$/Wnt1-Cre$^+$*) embryos. *Left panel*, exon 1-specific sense and exon 3-specific antisense primers result in amplification of 261-bp wild-type and 150-bp mutated PCR products, respectively. Exon 1-specific sense and exon 4-specific antisense primers result in amplification of 448-bp wild-type and 337-bp mutated PCR products, respectively. *C*, lateral and superior μCT images of control (*Tak1$^{FX/+}$/Wnt1-Cre$^-$*) and mutant (*Tak1$^{FX/FX}$/Wnt1-Cre$^+$*) heads at P0. The *yellow arrows* in the lateral images depict the length of the mandible. The *yellow arrows* in the superior views depict the length of the maxilla. The *red arrows* in the superior images depict the length of the cranial base, and the *green arrows* illustrate palatine bones in a control (fused palate) and mutant (cleft palate). The bar graph shows lengths of the cranial base, maxilla, and mandible of controls (*blue columns*) and mutants (*red columns*) (*n* = 3). *D–F*, histological comparison of palatal phenotypes of controls and *Tak1/Wnt1-Cre* mutants: frontal sections at anterior, middle, and posterior levels at E14.5 (*E*), E18.0 (*F*), and the level of the first molar at E13.5 (*D*). between controls and mutants. *Middle panel*, bar graph shows relative quantification of palatal shelf (*PS*) size in controls (*C*, *blue columns*) and mutants (*M*, *red columns*) (*n* = 3).

59

The *black arrows* point to tips of palatal shelves, the *black arrowheads* point to the midline seam (in a control), and the *black vertical lines* depict the distance between the tongue and nasal septum. *G, left-hand panel* shows sections from two independent control and mutant samples at the level of the first mandibular molar. The *green highlighting* illustrates the area measured to compare palatal shelf size between controls and mutants. *Middle panel*, bar graph shows relative quantification of palatal shelf (*PS*) size in controls (*C, blue columns*) and mutants (*M, red columns*) ($n = 3$). *Right panel*, bar graph summarizes results from BrdU incorporation assays on controls (*blue columns*) and *Tak1/Wnt1-Cre* mutants (*red columns*) palatal shelves at E13.5 ($n = 4$). *Error bars*, S.E. *, $p < 0.05$. *NS*, nasal septum; *P*, palatal shelf; *SP*, secondary palate.
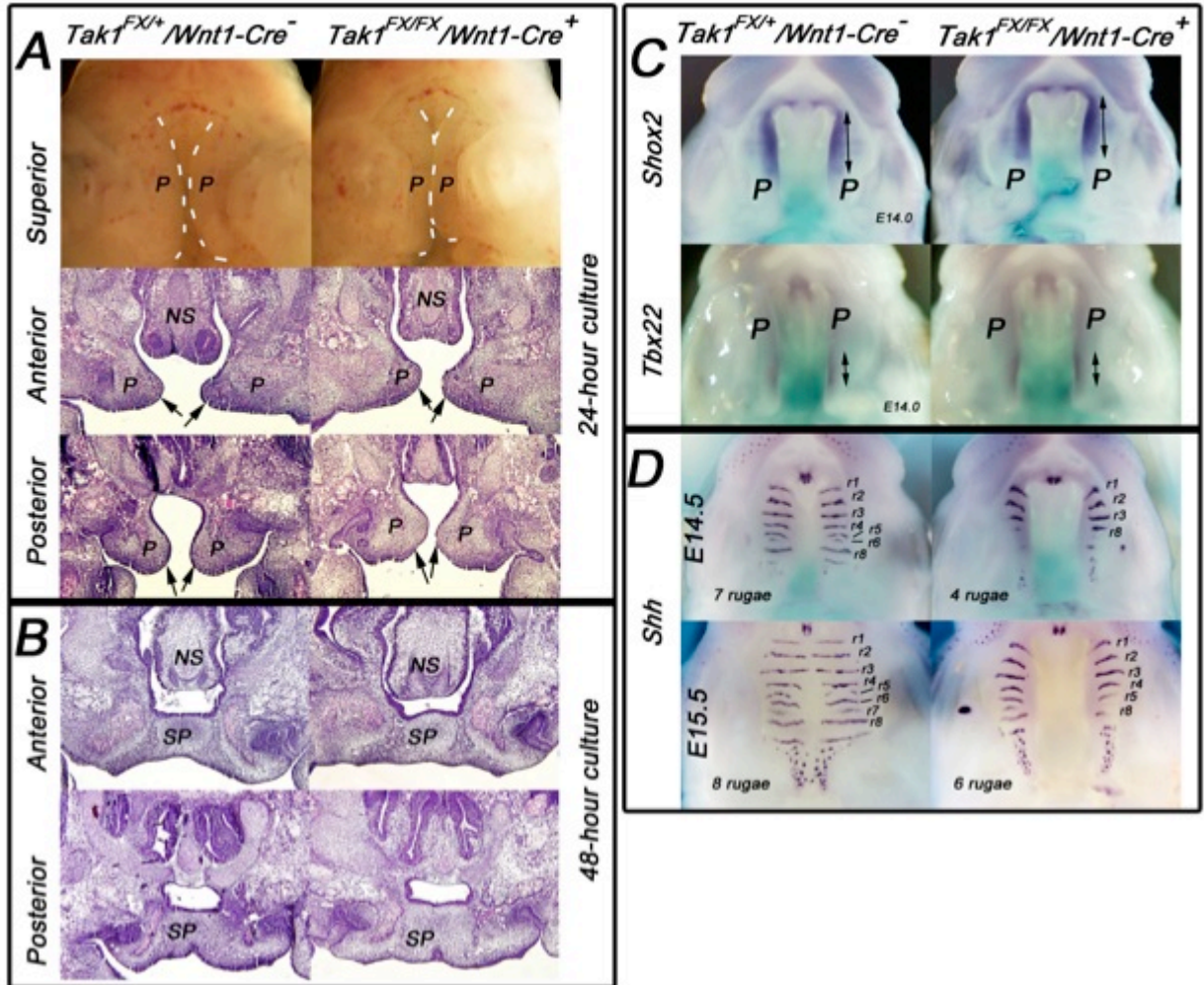
Figure 2-2. **Palatal shelves of *Tak1/Wnt1-Cre* mutants elevate and fuse *in vitro*, but show delayed rugal formation *in vivo*.** *A* and *B*, control (*left panels*) and mutant (*right panels*) embryos were harvested at E13.5, and dissected midfacial segments (without mandible, tongue, and brain) were cultured under chemically defined conditions in roller bottles for 24 h (*A*) or 48 h (*B*). The *arrows* point to the tips of elevated palatal shelves in both control and mutant samples cultured for 24 h (*n* = 3). *C* and *D*, comparison of *Shox2* and *Tbx22* (*C*, E14.0) and *Shh* (*D*, E14.5 and E15.5) expression in control and *Tak1/Wnt1-Cre* mutant palatal regions. The *double-headed arrows* in *C* illustrate the length of the positive signal. Rugal stripes (positive *Shh* expression) were identified and numbered (r1–r8) according to(Economou et al., 2012). *E–H*, *n* = 3. *NS*, nasal septum; *P*, palatal shelves; *SP*, secondary palate.

2-4.2. Both Canonical and Non-canonical TGF-β Superfamily Signaling Pathways Are Affected in *Tak1/Wnt1-Cre* Mutants

Neural crest cells make a contribution to all the craniofacial structures identified as showing abnormalities in *Tak1/Wnt1-Cre* mutants, including palatal shelves, tongue and mandible. Of these, the palatal shelf mesenchyme is the most uniformly composed of neural crest cells. To identify signaling processes influenced by *Tak1* deficiency *in vivo*, we harvested prefusion palatal shelves from control and *Tak1/Wnt1-Cre* embryos and analyzed their protein for Tak1, phosphorylation of Tak1 and its downstream signaling target p38 Mapk, the TGF-β signaling target Smad2 and BMP signaling targets Smad1/5/8 (Fig. 2-3A). The level of Tak1 and Tak1 C-terminal phosphorylation at Ser-412 (S412) was significantly less in *Tak1/Wnt1-Cre* mutant samples demonstrating an efficient Cre-induced recombination in the *Tak1* locus. The level of p38 Mapk phosphorylation was also markedly and consistently less in these mutant palatal shelves when compared to corresponding control samples. Similarly, C-terminal Smad2 phosphorylation was consistently lower in mutant shelves, while there were no differences in Smad2 protein levels. C-terminal Smad1/5/8 phosphorylation was lower on average in mutant samples but not significantly so. These results show that *Tak1* deficiency leads to decreased signaling activity in both non-canonical and canonical TGF-β signaling pathways.

2-4.3. Tak1 Mediates C-terminal Smad Phosphorylation in Craniofacial Mesenchymal Cells

To gain a deeper insight into processes regulated by Tak1-mediated signaling in postmigratory neural crest cells, we established control and*Tak1/Wnt1-Cre* mutant craniofacial mesenchymal primary cultures from both prefusion palatal shelves (at E14) and first pharyngeal arches, which give rise to maxilla and mandible (at E11), and analyzed their ability to respond to

TGF-β stimulation (Fig. 2-3, B and C). As expected, control mesenchymal cells isolated from the secondary palate showed an increase in Tak1 Ser-412 phosphorylation in response to TGF-β stimulation and beyond a clearly detectable base-line Tak1 phosphorylation level (Fig. 2-3C). In *Tak1/Wnt1-Cre* cells, there was no detectable Tak1 phosphorylation, with or without TGF-β stimulation. A modest increase in phosphorylation of Smad-independent pathway targets p38 Mapk, Jnk, and Erk1/2 was induced by TGF-β2 in control cells, but in mutant cells no such change was observed (Fig. 2-3C). TGF-β2 stimulation induced C-terminal phosphorylation of both TGF-β Smads (Smad2) and BMP Smads (Smad1/5/8) in control palatal mesenchymal cells. In mutant cells, Smad2 C-terminal also became phosphorylated in response to TGF-β2 stimulation, but less so than in control cells (Fig. 2-3, B and C), and BMP Smads did not show detectable C-terminal phosphorylation. In all samples, Smad2 protein levels remained stable for 90 min after TGF-β stimulation (Fig. 2-3B). Similar results were obtained using cells isolated from first pharyngeal arches (which also contribute to mandible and tongue) at E11, using a neural crest stem cell line in conjunction with the Tak1 kinase inhibitor (5Z-7-oxozeaenol) (Fig. 2-3F and data not shown).

In summary, the relative pattern of phosphorylation of downstream targets shown by control and mutant palatal shelf primary culture cells in response to TGF-β stimulation is similar to that found between control and mutant E14 palatal shelves recovered *in vivo*. Because Tak1 has also been shown to be involved in BMP signaling, we stimulated both the control and *Tak1/Wnt1-Cre* mutant ecto-mesenchymal cells with BMP2 and monitored the phosphorylation of signaling molecules as above (Fig. 2-3D). Unlike TGF-β2 and as expected, BMP2 was not able to induce Tak1 phosphorylation at Ser-412 in control cells, nor did mutant cells show detectable phospho-Tak1 levels. Control cells were responsive to BMP2 stimulation

in their progressive increase in C-terminal BMP-Smad (Smad 1/5/8) phosphorylation, but Smad2 phosphorylation was not altered. In mutant cells, base-line C-terminal Smad1/5/8 phosphorylation levels were lower, and their responsiveness to BMP2 stimulation was reduced, when compared with control cells. Collectively, the results of these experiments suggest that in neural crest-derived mesenchymal cells, Tak1 contributes more to TGF-β than BMP-induced C-terminal phosphorylation of the corresponding R-Smads. BMP2 induced progressive p38 Mapk and Jnk phosphorylation in controls cells, but no increase was detected in mutant cells.

To provide additional evidence for the role of Tak1 in C-terminal phosphorylation of Smad2, we transduced palatal mesenchymal cells carrying the homozygous *Tak1-flox* allele with recombinant adenoviruses expressing the Cre recombinase and analyzed the transduced and control cells (transduced with AdGfp) for Tak1 and Smad2 phosphorylation (Fig. 2-3E). These results confirm that the reduction in C-terminal phosphorylation of Smad2 is an immediate result of Tak1 deficiency rather than just a long term adaptation to severely reduced Tak1 levels in our*Tak1/Wnt1-Cre* mutants.

To conclude, we show that Tak1 is required for appropriate activation of both canonical and noncanonical TGF-β and BMP signaling pathways in neural crest-derived mesenchymal cells. Moreover, in the presence of Tak1, TGF-β2 was able to induce activation of both TGF-β and BMP R-Smads, *i.e.* Smad2 and Smad1/5/8, respectively.
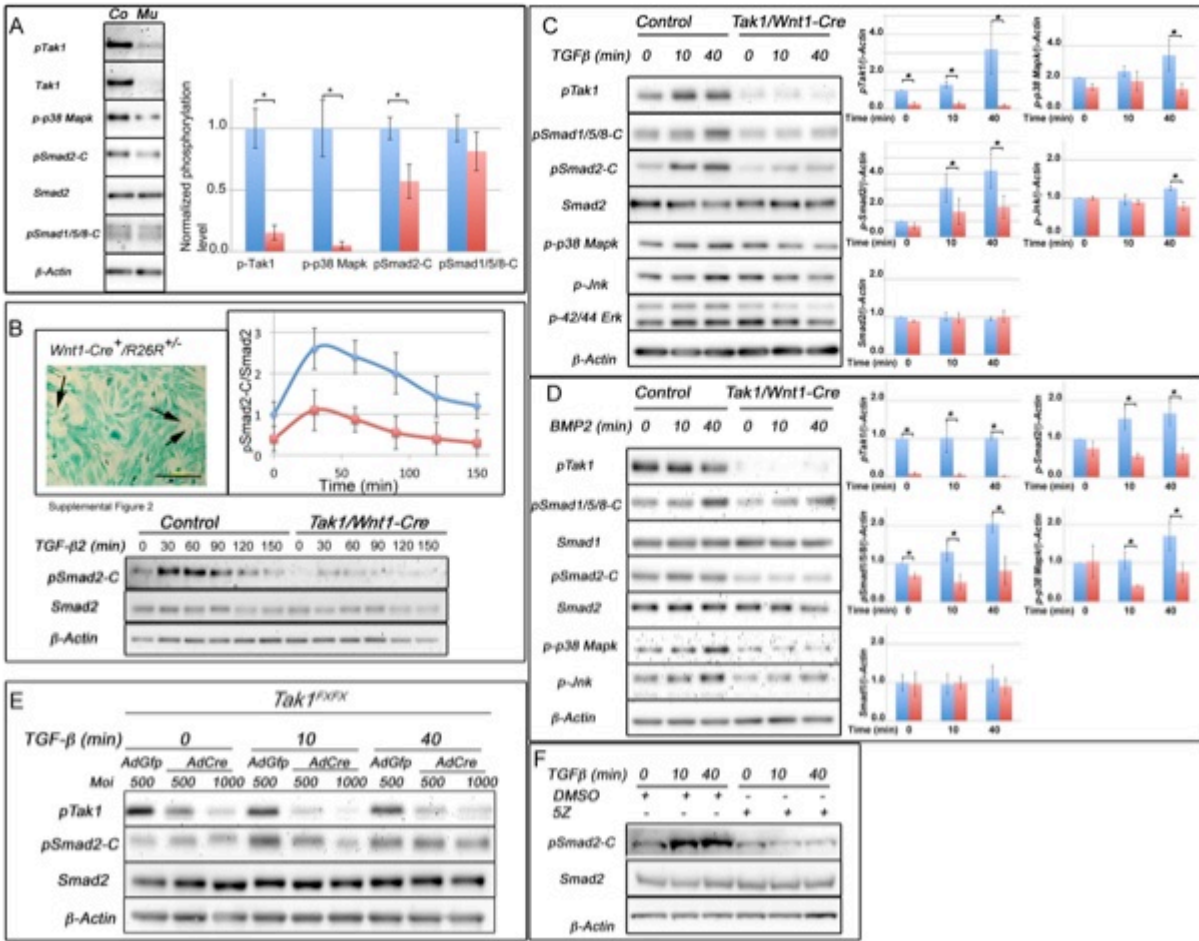
Figure 2-3. **Activation of R-Smads and Mapks is less in *Tak1/Wnt1-Cre* embryos.** *A*, representative immunoblot from prefusion palatal shelves harvested from control and *Tak1/Wnt1*-Cre mutant embryos at E14.0 and analyzed for phosphorylation of Tak1, Smad1/5/8 (BMP Smads), Smad2 (TGF-β Smad), and p38 Mapk. *Co*, control sample; *Mu*, *Tak1/Wnt1-Cre* mutant sample. The bar graph shows relative quantification of pTak1, p38 Mapk, pSmad2-C, and pSmad1/5/8-C in controls (*blue columns*) and mutants (*red columns*) (normalized to β-actin; *n* = 4). *B*, primary palatal mesenchymal cell cultures were established (see "Experimental Procedures") from prefusion palatal shelves (at E14.0) of mouse embryos carrying both the *Wnt1-Cre* transgene and the *R26R^{lacz}* reporter (*top left*). Cells stained *blue* are derived from the neural crest. The *black arrows* point to a few negatively staining cells. *Scale bar*, 200 μm. A representative immunoblot of primary palatal mesenchymal cells stimulated with TGF-β2 and analyzed for C-terminal Smad2 phosphorylation is shown. *Top right*, the diagram illustrates the differences in amount of normalized Smad2-C phosphorylation between control (*blue data points* and *blue line*) and *Tak1/Wnt1-Cre* mutant (*red data points* and *red line*) cells. The values were normalized to Smad2. *C*, representative immunoblot from primary palatal mesenchymal cells stimulated with TGF-β2 (10 ng/ml), and protein lysates were analyzed for Tak1, C-terminal Smad1/5/8, C-terminal Smad2, total Smad2, p38 Mapk, Jnk, and Erk1/2 phosphorylation. The bar graphs show relative quantification of pTak1, p38 Mapk, pSmad2-C, pJnk, and Smad2 in controls (*blue columns*) and mutants (*red columns*) (normalized

65

to β-actin; *n* = 3). *D*, representative immunoblot of primary palatal mesenchymal cells stimulated with BMP2 (100 ng/ml) and analyzed for Tak1 phosphorylation, C-terminal Smad1/5/8 phosphorylation, total Smad1, C-terminal Smad2 phosphorylation, total Smad2, p38 Mapk phosphorylation, and Jnk phosphorylation. The bar graphs show relative quantification of pTak1, p38 Mapk, pSmad1/5/8-C, and total Smad1 in controls (*blue columns*) and mutants (*red columns*) (normalized to β-actin; *n* = 3). *Error bars*, S.E. *, *p* < 0.05. *E*, representative immunoblot of primary *Tak1^{FX/FX}* palatal mesenchymal cells transduced with AdGfp (control) or AdCre (mutant). The transduced cells were stimulated with TGF-β and analyzed for Tak1 phosphorylation, C-terminal Smad2 phosphorylation, total Smad2, and β-actin. *Moi*, multiplicity of infection. *F*, representative immunoblot of O9-1 neural crest stem cells stimulated with TGF-β2 in the presence or absence of the Tak1 kinase inhibitor 5*Z*-7-oxozeaenol (*5Z*) and analyzed for C-terminal Smad2 phosphorylation, total Smad2, and β-actin.

2-4.4. Agonist-induced Linker Region Phosphorylation Is Affected in Palatal Mesenchymal Cells Deficient in Tak1 Mutants

Several studies have shown that in R-Smads the intervening sequence that links the DNA binding domain and transcriptional domain, the so-called linker region, becomes phosphorylated by a set of divergent stimuli (including FGFs, EGFs, stress signals) via Map kinases, and also by members of the TGF-β superfamily (Massague et al., 2005; Wang et al., 2009; Wrighton and Feng, 2008). This agonist-induced linker region phosphorylation (ALP) at T220 in Smad2 (T179 in Smad3) located immediately upstream of a PY motif is of particular interest, since it was recently suggested that, in addition to priming Smads for turnover, phosphorylation of this threonine residue is required for a full transcriptional activity of Smad complexes (Alarcon et al., 2009; Aragon et al., 2011). Therefore, we stimulated both control and Tak1-deficient primary mesenchymal cells (from both the first pharyngeal arch and the palate) with TGF-β2 and analyzed phosphorylation of these key residues (Smad2-L(T220), Smad3-L(T179)) and of Smad2-L(S250) using phospho-residue-specific antibodies. Our results demonstrate that in control cells TGF-β2 induced efficient phosphorylation of the Smad2 linker region at S250 and T220, and at T179 in Smad3, while cells deficient in Tak1 failed to show comparable induction of ALP (Fig. 2-4A). As before, practically identical results were obtained using cells isolated from first pharyngeal arches at E11.0 (data not shown). Moreover, O9-01 neural crest stem cells showed similar increases in TGF-β2-induced linker region phosphorylation at Smad2-L(T220) and Smad3-L(T179), and that this induction was largely inhibited by 5Z-7-Oxozeaenol (Fig. 2-4A, lower panel).

To investigate whether these *in vitro* results were reflective of palatal shelf mesenchyme *in vivo*, we prepared protein lysates directly from pre-fusion palatal shelves of control and

Tak1/Wnt1-Cre mutant embryos and analyzed them for the Smad2/3 linker region

phosphorylation. Endogenous levels of Smad2 linker phosphorylation at T220 and S250 and

Smad3 phosphorylation at T179 were all significantly lower in mutant palatal samples than in

those of controls (Fig. 2-4B).

It has previously been shown that in several established cell lines, e.g., HEK293T and

HaCaT, that T220 in the linker region of Smad2 is directly phosphorylated by nuclear cyclin-

dependent kinases Cdks8 and 9 (Alarcon et al., 2009; Aragon et al., 2011). Therefore we

examined the effect of Tak1 inactivation on subcellular localization of total Smad2 both on

palatal mesenchymal cells (harvested at E14) (Fig. 2-4C) and on first pharyngeal arch

mesenchymal cells (harvested at E11 – data not shown). In both cell types, TGF-β2-induced

Smad2 nuclear accumulation was effectively inhibited by the Tak1 kinase inhibitor (5Z-7-

Oxozeaenol), and by the TGFβRI kinase inhibitor (SB431542) (Fig. 2-4C, and data not shown).

Tak1 kinase inhibitor also inhibited both TGF-β2–induced Smad2-C-terminal and linker region

phosphorylation at Smad2-L(T220), Smad3-L(T179) and Smad2-S250 (Fig. 2-5A). Certain

Tak1-mediated ALP were also dependent on the presence of the TGFβRI protein, and the kinase

activity of TGFβRI, since both the Cre-mediated *Tgfbr1* deletion and TGFβRI inhibition by the

SB431542 could attenuate TGF-β2-induced phosphorylation at Smad2-L(T220)/Smad3-L(T179)

(Fig. 2-5A, B). As expected, agonist-induced phosphorylation of Smad2 at the C-terminus was

also inhibited by the physical loss of *Tgfbr1* and by SB431542 (Fig. 2-5A, B). In palatal

mesenchymal cells, flavopiridol (Cdk inhibitor) inhibited ALP at T220 and S250 (Smad2) (Fig.

2-5A), while UO126 (Erk1/2 & Jnk inhibitor) could effectively prevent TGF-β2-induced Smad2-

L(S250) phosphorylation, but could only weakly inhibit ALP at T220 (Fig. 2-5A). The effect of

SB202190 (p38 Mapk inhibitor) on phosphorylation at Smad2-L(T220) was very similar to that

of UO126 (data not shown). Our cell fractionation experiments confirmed that most of the

Smad2 molecules with TGF-β2-induced phosphorylation at T220 could be detected in the

nucleus and that this phosphorylation was effectively inhibited by flavopiridol (Fig. 2-5C).

In summary, our results show that in craniofacial mesenchymal cells Tak1 deficiency

lead to reduced agonist-induced C-terminal phosphorylation and decreased nuclear accumulation

of R-Smads, and that agonist-induced linker phosphorylation of Smad2 both at T220 (which is at

least partially mediated by Cdks) and at S250 (mediated by Erk1/2 and/or Jnk) was dependent on

the functional Tak1 protein (Fig. 2-5D-E).
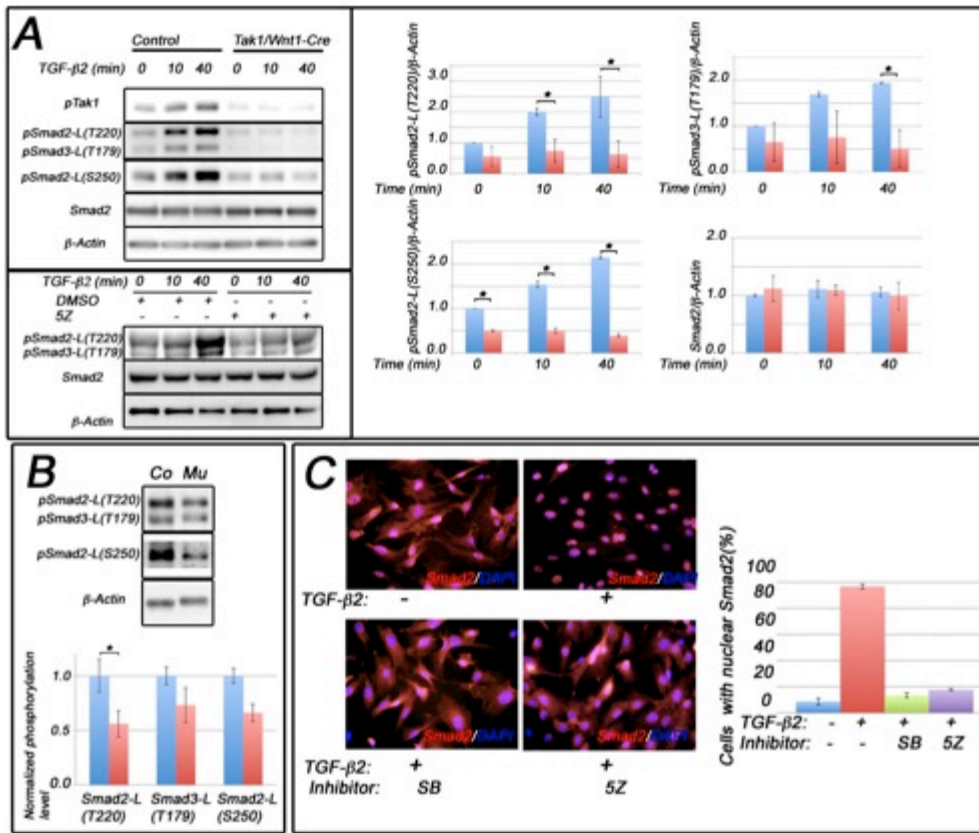
Figure 2-4. **Tak1 is required for appropriate Smad2 nuclear localization and agonist-induced Smad2/Smad3 linker-region phosphorylation in palatal mesenchymal cells.** *A*, *upper panel*, primary palatal mesenchymal cells were stimulated with TGF-β2. Shown are representative Western blots of protein lysates analyzed for Smad2 linker region phosphorylation at Thr-220 (*pSmad2-L(T220)*) and Ser-250 (*pSmad2-L(S250)*) and for Smad3 linker region phosphorylation at Thr-179 (*pSmad3-L(T179)*). The bar graphs show relative quantification of pSmad2-L(T220), pSmad3-L(T179), and pSmad2-L(S250) in controls (*blue columns*) and mutants (*red columns*) (normalized to β-actin; *n* = 3). *A,lower panel*, representative immunoblot of O9-1 neural crest stem cells stimulated with TGF-β2 in the presence or absence of the Tak1 kinase inhibitor 5Z-7-oxozeaenol (*5Z*) or vehicle (dimethyl sulfoxide, *DMSO*) and analyzed for Smad2 linker region phosphorylation at Thr-220 (*pSmad2-L(T220)*), Thr-179 (*pSmad3-L(T179)*), total Smad2, and β-actin. *B*, representative immunoblot of prefusion palatal shelves harvested from control (*Co*) and *Tak1/Wnt1-Cre* mutant (*Mu*) embryos at E14.0 and analyzed for linker region phosphorylation at Thr-220 (*pSmad2-L(T220)*) and Ser-250 (*pSmad2-L(S250)*) and for Smad3 linker region phosphorylation at Thr-179 (*pSmad3-L(T179)*). The bar graph shows relative quantification of agonist-induced linker region phosphorylation in controls (*blue columns*) and mutants (*red columns*) (normalized to β-actin; *n* = 3). *C*, representative images showing subcellular localization of Smad2 in unstimulated cells (*upper left*), cells stimulated with TGF-β2 (*upper right*), cells stimulated with TGF-β2 in the presence of the TGFβRI kinase inhibitor (SB431542 (*SB*), *lower left*), and cells stimulated with TGF-β2 in the presence of Tak1 inhibitor (5Z-7-oxozeaenol (*5Z*), *lower right*). *Red*, immunostaining for

Smad2; *blue*, nuclear counterstaining with DAPI. The bar graph shows quantification of nuclear localization of Smad2 ($n = 3$; *error bars*, S.E.).

2-4.5. Tak1 as a TGF-β Signal Transducer in Neural Crest-derived Facial Mesenchymal Cells

Previous studies have demonstrated that TGF-β-induced Tak1 activation is dependent on the presence of TGFβRI protein and is mediated by an adaptor protein Traf6 (Sorrentino et al., 2008; Yamashita et al., 2008). However, whether or not this activation is dependent on the TGFβRI kinase activity is still controversial (Sorrentino et al., 2008; Yamashita et al., 2008). As shown above, the presence of either TGFβRI or its kinase activity is sufficient for agonist-induced Tak1-mediated linker region phosphorylation of Smad2 in ecto-mesenchymal cells (Fig.2-5A, B). To better define the relationship between Tak1 kinase-mediated and TGFβRI kinase-mediated transcriptional responses, we compared expression profiles of TGF-β2-responsive genes in primary palatal mesenchymal cells in the presence of inhibitors for either TGFβRI kinase or Tak1 kinase using a genome-wide transcriptomic analysis (Fig. 2-6). Of TGF-β2-responsive genes (>2-fold change; p<0.05), 58 were dependent on TGFβRI kinase, 27 were dependent on Tak1 kinase and 18 were dependent on both (>2.5-fold change; p<0.05) (Fig. 2-6A). Among the up-regulated genes (120 genes; >2-fold change; p<0.05), 47 were TGFβRI kinase-dependent, 20 were Tak1 kinase-dependent and 12 were dependent on both (>2.5-fold change; p<0.05) (Fig. 2-6B). Among the down-regulated (45 genes; >2-fold change; p<0.05) 11 were TGFβRI kinase-dependent, 7 were Tak1 kinase-dependent and 6 were dependent on both (>2.5-fold change; p<0.05) (Fig. 2-6C). Differential expression of several Tak1 kinase/TGFβRI kinase-dependent genes was confirmed by real-time RT-PCR (Fig. 2-5D). When more stringent criteria were used and only the genes that displayed >3-fold expression change when stimulated with TGF-β2 were analyzed, 10 genes were dependent on both TGFβRI and Tak1 kinase

activities, while 8 genes and 1 gene were dependent on only TGFβRI or only Tak1 kinase activities, respectively (data not shown).

To examine whether any of the kinase-dependent gene expression findings reflected those between control and Tak1-deficient cells *in vivo*, we harvested NC-derived craniofacial mesenchymal tissues (both mandibular arch at E11 and palatal shelves at E14) from control and *Tak1/Wnt1-Cre* mutant embryos and compared expression levels of TGF-β-responsive genes using real-time RT-PCR (Fig. 2-6E). Among the analyzed genes, *Nfatc2,* which was induced by TGF-β2 in cultured palatal mesenchymal cells dependent on both kinases, was clearly down-regulated in *Tak1/Wnt1-Cre* mutant first pharyngeal arch tissues at E11 and slightly decreased though not significantly in mutant palatal shelves at E14. Similarly, *Osr1*, which was repressed by TGF-β2 in cultured palatal mesenchymal cells dependent on both kinases, was expressed at higher levels both in *Tak1/Wnt1-Cre* mutant first pharyngeal arch (2.2-fold higher) and prefusion palatal shelf tissues (2.8-fold higher) than in corresponding control tissues. Any differences in average expression of other genes tested, e.g., *Wnt11* and *Bmp4*, were relatively modest, but some still showed tendencies consistent with the findings made in mesenchymal cell culture assays *in vitro*.

To conclude, TGFβRI and Tak1 kinases mediated both distinct and overlapping transcriptional responses in palatal mesenchymal cells, when stimulated by TGF-β2. In this cell type, agonist-induced Tak1 activation could occur independently of TGFβRI kinase activity.
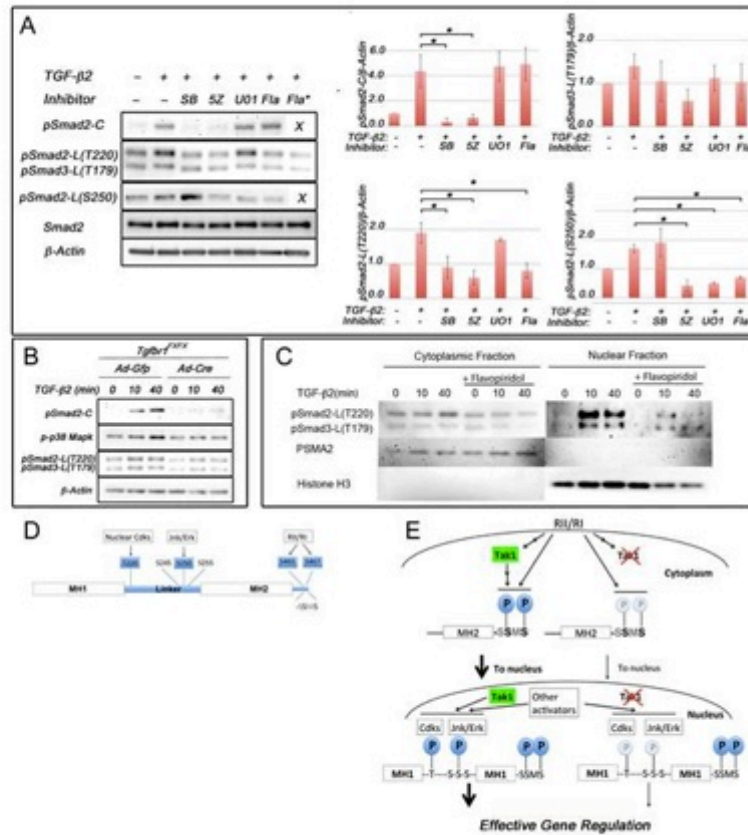
Figure 2-5. **Smad2 linker-region at Thr-220 is phosphorylated by nuclear kinases in palatal mesenchymal cells.** *A*, representative immunoblot of primary palatal mesenchymal cells stimulated with TGF-β2 in the presence of SB431542 (*SB*), 5Z-7-oxozeaenol (*5Z*), UO126 (*UO1*), and flavopiridol (*Fla*; 1 and 10 μm (*asterisk*)). Protein lysates were analyzed for Smad2 C-terminal phosphorylation, Smad2 linker region phosphorylation (at Thr-220 and Ser-250), and Smad3 linker region phosphorylation (at Thr-179). The bar graphs show relative quantification of pSmad2-C, pSmad-L(T220), pSmad3-L(T179), and pSmad2-L(S250) (normalized to β-actin; *n* = 3). *Error bars*, S.E. *, $p < 0.05$. *B*, representative immunoblot of primary palatal mesenchymal cells from *Tgfbr1[FX/FX]* embryos were transduced with *Ad-Gfp* or *Ad-Cre*, the cells were stimulated with TGF-β2, and protein lysates were analyzed for C-terminal Smad2 phosphorylation, p38 Mapk phosphorylation, and linker region phosphorylation at Smad2-L(T220) and at Smad3-L(T179). β-actin was loading control. *C*, palatal mesenchymal cells were stimulated by TGF-β2 in the presence and absence of flavopiridol. Cytosolic and nuclear lysates were analyzed for Smad2 linker region phosphorylation at Thr-220 (*pSmad2-L(T220)*) and for Smad3 linker region phosphorylation at Thr-179 (*pSmad3-L(T179)*). Antibodies against PSMA2 and histone H3 were used to assess the purity of cytosolic and nuclear fractions (*middle* and *bottom panels*). *D*, schematic representation of Smad2 depicting Thr/Ser residues phosphorylated by nuclear Cdks and Jnk/Erk in the linker region and by TGFβRI (*RI*) at the C terminus examined in this study. *E*, schematic summary illustrating the role(s) of Tak1 in phosphorylation of Smad2 (*left side* of diagram) in which Smad2 C-terminal phosphorylation

74

levels were greatly enhanced in response to TGF-β stimulation when Tak1 was present, as well as *Tgfbr1*. Cdk-dependent phosphorylation of Thr-220 occurs in the nucleus. Phosphorylation of Ser-250 is Mapk-dependent but also inhibited by Cdk inhibitor, which may be due to some dependence on the prior phosphorylation of Thr-220 in the model of Aragón *et al.* (Aragon et al., 2011). Deletion of *Tak1* results in reduced C-terminal phosphorylation, leading to a reduced nuclear accumulation of Smad2, and reduced linker region phosphorylation (*right side* of diagram), which would be expected to reduce effectiveness in gene regulation according to the model of Aragón *et al.* (Aragon et al., 2011).

A

Tgf-β responsive genes (>2x; 165 genes total)
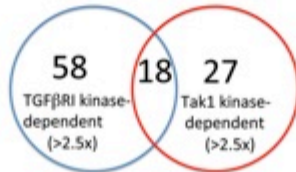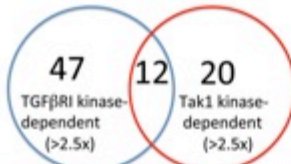
58 | 18 | 27
TGFβRI kinase-dependent (>2.5x) | | Tak1 kinase-dependent (>2.5x)

B Upregulated by Tgf-β (>2x; 120 genes total)

47 | 12 | 20
TGFβRI kinase-dependent (>2.5x) | | Tak1 kinase-dependent (>2.5x)

Dependent on TGFβRI kinase[#]	Dependent on both TGFβRI kinase and Tak1 kinases	Dependent on Tak1 kinase
Fmod[1]	Bhlhe40 (Dec1)[2]	Hbegf[3]
Jag1[4]	Egr2[5]	Ngf[6]
Rnx1[7]	Has2[8]	Sphk1[9]
Wnt9a[10]	Nfatc2[11]	
	Wnt11[12]	

[#]1. Baffi, M. et al (2006) Dev Biol 296, 363-374. 2. Zawel, L. et al (2002) Proc Natl Acad Sci U S A 99, 2848-2853. 3. Hoshino, H. et al. (2007) Mol Biel Cell 18, 1143-1152. 4. Humphreys, R. et al (2012) Hum Mol Genet 21, 1374-1383. 5. Sarnat, H. B. and Flores-Sarnat, L. (2005) J Child Neurol 20, 637-643. 6. Amano, O. et al (1999) Dev Dyn 216, 299-310. 7. Yamashiro, T. et al (2004) J Bone Mineral Res 19, 1671-1677. 8. Casini, P. et al (2012) Dev Dyn 241, 294-302. 9. Yamanaka, M. et al (2004) J Biol Chem 279, 53994-54001. 10. Curtin, E. et al (2011) Mech Dev 128, 104-115. 11. Ranger, A. M. et al (2000) Journal Exp Med 191, 9-22. 12. Lee, J. M. et al (2008) Dev Biol 314, 341-350.

C Downregulated by Tgf-β (>2x; 45 genes total)
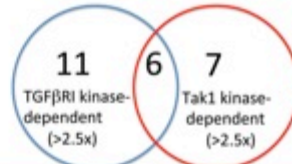
11 | 6 | 7
TGFβRI kinase-dependent (>2.5x) | | Tak1 kinase-dependent (>2.5x)

Dependent on TGFβRI kinase[#]	Dependent on both TGFβRI kinase and Tak1 kinases	Dependent on Tak1 kinase
Ahr[13]	Alx1[14]	Mllt3[15]
Hey1[16]	Bmp4[17]	Run1tl[18]
Pdk4[19]	Gas1[20]	Sesn1[21]
Rgs3[22]	Id4[23]	
Snai2[24]	Osr1[25]	

[#]13. Abbott, B. D. et al (1998) Teratology 58, 30-43. 14. Uz, E. et al (2010) Am J Hum Genet 86, 789-796. 15. Collins, E. C. et al (2002) Mol Cell Biol 22, 7313-7324. 16. Zuniga, E. et al (2010) Development 137, 1843-1852. 17. Zhang, Z. et al (2002) Development 129, 4135-4146. 18. Yeh, K. T. et al (2011) Epigenetics 6, 727-739. 19. Stockert, J. et al (2011) Nucleic Acids Res 39, 119-131. 20. Seppala, M. et al (2007) J Clin Invest 117, 1575-1584. 21. Peeters, H. et al (2006) Hum Mol Genet 15, 3369-3377. 22. Yau, D. M. et al (2008) Mol Pharmacology 73, 1356-1361. 23. Kee, Y. and Bronner-Fraser, M. (2001) Mech Dev 109, 341-345. 24. Perez-Mancera, P. A. et al (2006) Cytogenet Genome Res 114, 24-29. 25. Gao, Y. et al (2009) Dev Biol 328, 200-209.

D

Stimulated by TGF-β2   Suppressed by TGF-β2

Relative expression

- unstimulated
- TGF-β2
- TGF-β2 + SB
- TGF-β2 + 5Z

Egr2, Has2, Kcnn4, Nfatc2, Wnt11, Ahr, Snai2, Alx1, Bmp4, Dbp, Id4, Osr1, Mllt3

E

1st pharyngeal arch   palatal shelves

Relative expression

Nfatc2, Wnt11, Osr1, Nfatc2, Wnt11, Osr1, Bmp4, Id4

76
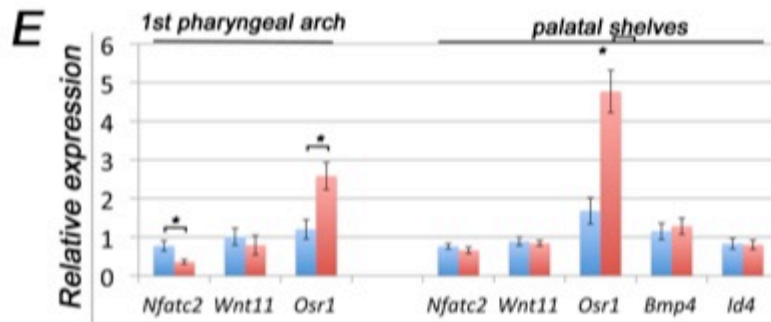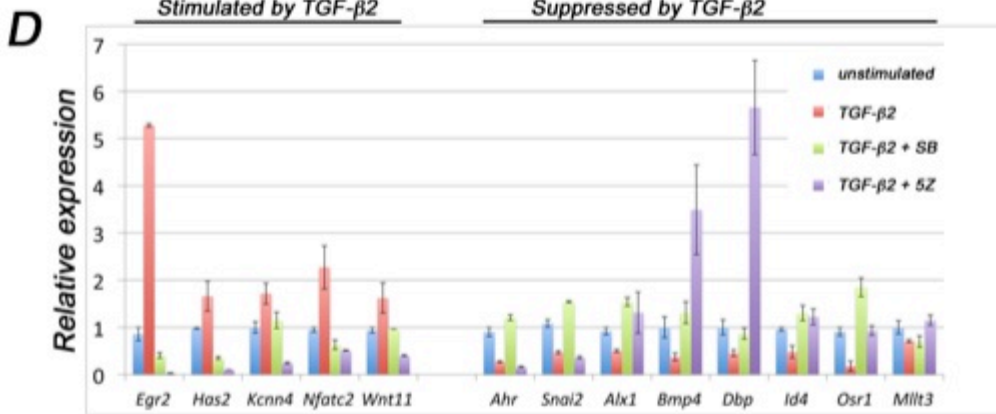
Figure 2-6. **Tak1 and TGFβRI mediate both distinct and overlapping gene responses in palatal mesenchymal cells.** Total RNAs from unstimulated palatal mesenchymal cells, from cells stimulated with TGF-β2, from cells treated with the TGFβRI kinase inhibitor (SB431542 (*SB*), 10 μm, 60 min prior stimulation) and stimulated with TGF-β2 (2 h), and cells treated with Tak1 inhibitor (5Z-7-oxozeaenol (*5Z*), 2 μm, 60 min prior stimulation) and stimulated with TGF-β2 (2 h) were subjected to genome-wide transcriptomic analysis on the MOE 430A 2.0 microarray. *A*, Venn diagram showing a summary of the number TGFβRI kinase- and Tak1 kinase-dependent TGF-β2 responsive genes (>2-fold change; *p* < 0.05). *B*, summary of number of TGFβRI kinase- and Tak1 kinase-dependent genes up-regulated by TGF-β2 in palatal mesenchymal cells (five examples of genes are shown in each group). *C*, summary of number of TGFβRI kinase- and Tak1 kinase-dependent genes that are down-regulated by TGF-β2 (3–5 examples of genes in each group). # in *B* and *C* denotes references highlighting relevance of a listed gene either in TGF-β signaling or in craniofacial/neural crest biology. *D*, real time RT-PCR quantification of differentially expressed genes. *Blue columns*, no inhibitor, no TGF-β2; *red columns*, no inhibitor, stimulated with TGF-β2; *green columns*, 10 μm SB431542 60 min prior stimulation with TGF-β2; *purple column*, 2 μm 5Z-7-oxozeaenol 60 min prior to stimulation with TGF-β2. *E*, bar graph showing relative real time RT-PCR quantification of selected TGF-β-responsive Tak1-dependent genes (identified by the microarray screen) in the craniofacial mesenchyme. *Blue columns*, control; *red columns*, Tak1/Wnt1-Cre mutant (*n* = 3). *Error bars*, S.E. *, *p* < 0.05. *1st pharyngeal arch*, first pharyngeal arch harvested at E11.0; *palatal shelves*, prefusion palatal shelves harvested at E14.0.

2-5. Discussion

Although Tak1, a member of the Map kinase-kinase-kinase subfamily, was originally shown to mediate TGF-β signaling pathways (Yamaguchi et al., 1995), its physiological role in TGF-β superfamily signaling *in vivo*, particularly during embryogenesis, is still poorly elucidated. Here we show that Tak1 plays a critical non-redundant role in craniofacial development, and that, in embryonic neural crest-derived craniofacial cells, Tak1 is required not only for Smad-independent TGF-β superfamily signaling, but also for maximal ligand-induced C-terminal and linker phosphorylation of R-Smads.

2-5.1. Role of Tak1 in craniofacial development

Previous studies have shown that TGF-β and Bmp signaling plays an essential role in the neural crest-derived palatal mesenchyme(Baek et al., 2011; Dudas et al., 2006; Ito et al., 2003). Of particular note is a recent report which demonstrates that cleft palate in *Tgfbr2/Wnt1-Cre* mutants results from TGF-β2-induced activation of an alternative pathway via TGFβRI and TGFβRIII which induces activation of Tak1 and hence p38 Mapk (Iwata et al., 2012a). This aberrant activation results in attenuated expression of *Fgf9* and *Pitx2* leading to reduced mesenchymal cell proliferation and cleft palate(Iwata et al., 2012b). These results raised the questions of what role neural crest-expressed Tak1 normally plays in craniofacial development, and in the activation of signaling pathway components downstream of TGF-β2 signaling.

Here we report that Tak1 is required for normal facial and mandibular growth and palatogenesis *in vivo* and that it mediates both Smad-dependent and Smad-independent TGF-β and Bmp signaling in neural crest cells *in vitro*. The overall craniofacial phenotypes of *Tak1/Wnt1-Cre* mutants were relatively mild when compared to those of corresponding *Tgfbr1,*

Tgfbr2 or *Bmpr1a* mutants. Unlike in *Tgfb* receptor mutants, palatal mesenchymal cell proliferation in general was only slightly affected in *Tak1* mutants, as we did not detect any significant differences at the time points examined. Although over-activation of Tak1 in the *Tgfbr2/Wnt1-Cre* mutants led to a reduction in cell proliferation (Holm et al., 2011), removal of *Tak1* in our *Tak1/Wnt1-Cre* mutants resulted in moderate hypoplasia. As we could not detect increased apoptosis between embryonal days 11-14, generalized *hyper*plasia in NC-derived tissues as the result of the absence of Tak1 does not seem to occur.

Normal formation of the secondary palate requires distinct developmental events; not just formation and growth of two palatal shelves but their elevation, physical contact with one another, fusion, loss of epithelial seam and differentiation into cartilage and bone. Of these steps, shelf elevation and patterning (ruga formation) showed developmental delay in *Tak1Wnt1Cre* mutants. It was recently shown that a Turing-type reaction-diffusion mechanism establishes the normal pattern of rugae (Economou et al., 2012). Although the delay in ruga formation may indicate an intrinsic defect in palatogenesis, it also is possible that a failure of the tongue to descend disturbs the shelf tissue proportions, altering the distribution of signals for ruga formation, and slowing their increase in number. An essential role for Tak1 in palatal shelves themselves in the processes of palatal shelf elevation onwards is hard to define as these processes occurred indistinguishably in control and *Tak1/Wnt1-Cre* mutant heads in rolling culture *in vitro* when tongue and mandible were absent but their morphology looked different from normal palatal shelves *in vivo* (Figure 2-1B). This result, along with histological observations, suggests that the failure of the tongue to descend sufficiently in mutants most likely contributes to the cleft palate phenotype *in vivo* by physically impeding shelf elevation. Consistent with these

findings, Song et al. have recently shown that Tak1 plays an important role in tongue development by controlling Fgf10 expression (Song et al., 2013) .

At the protein level, *Tak1/Wnt1-Cre* mutant tissues showed reduced levels of activation of both Smad- independent and -dependent pathways rather than an upregulation of Smad-dependent pathway signaling. As our studies on primary culture cells also showed, Tak1 functions as a modulator of signal strength rather than an 'on/off switch' for the Smad-independent pathway in the NC-derived craniofacial mesenchyme. Our results do not exclude that altered TGF-β/Bmp-independent Tak1-mediated signaling in these cells may also contribute to the relatively mild phenotype.

2-5.2. Role of Tak1 in TGF-β-induced signaling events

Our studies of the dependence of TGF-β2-induced signaling on Tak1 in embryonic neural crest cells have revealed important details not only of phosphorylation of components of signaling pathways but of their cell type-dependent variation. We show that in NC-derived craniofacial mesenchymal cells Tak1 mediates both TGF-β and BMP-induced activation of their corresponding R-Smads. Shim et al showed that in chondrocytes Tak1 can phosphorylate the C-terminal residues of an R-Smad (Smad1) only as part of the Bmp signaling pathway (Shim et al., 2009). Moreover, we show that in neural crest cells TGF-β stimulation is able to stimulate BMP R-Smad activation directly, and that this process is, in part, mediated by Tak1. In fact, a recent study on established immortalized cell lines (of both epithelial, endothelial and mesenchymal origins) suggested that this unconventional TGF-β-induced Bmp R-Smad activation is required for a subset of critical TGF-β-induced cellular functions (Daly et al., 2008). While our studies show that this unconventional R-Smad activation takes place in primary NC-derived craniofacial

mesenchymal cells *in vitro*, it remains to be shown whether it plays a role in craniofacial

ectomesenchyme during embryogenesis *in vivo*.

Linker regions in both TGF-β and BMP R-Smads are Ser/Thr-rich and are known to be

phosphorylated by several different kinases, e.g., GSK, Mapks and Cdks, and it has been

suggested that these post-translational modifications have both activatory and inhibitory

regulatory functions in TGF-β signaling (Wrighton and Feng, 2008). Here we show that palatal

and pharyngeal arch mesenchymal cells deficient in Tak1 show reduced agonist-induced linker

region phosphorylation both at T220 and S250 in Smad2 *in vitro,* and that particularly T220

phosphorylation in the Smad2 linker region is reduced in neural crest cell-specific *Tak1* mutants

in vivo. Moreover, our results suggest that in NC-derived mesenchymal cells T220 and S250 are

phosphorylated by Cdks and Mapks, respectively. These findings differ from those made in

fibroblast and melanoma cell lines, which showed that Mapks rather than Cdks are the primary

kinases responsible for the linker region phosphorylation (Cohen-Solal et al., 2011; Hough et al.,

2012). Therefore, there seems to be distinct cell type-specific differences between the potency of

particular kinases phosphorylate the specific residues.

It was recently suggested that ALP at Smad2-L (T220) plays a role in the so-called

"action-turnover switch" function of R-Smads, and may be required both for maximal TGF-β-

induced transcriptional activity and efficient termination of the signal in immortalized cell lines

(Aragon et al., 2011; Gao et al., 2009). Our present results show that, in primary craniofacial

mesenchymal cells, Tak1, by functioning as an amplifier of C-terminal R-Smad phosphorylation,

could have indirectly regulated ALP at Smad T220 as deficient Tak1 activity would result in

reduced ligand-induced R-Smad activation, and hence decreased R-Smad nuclear accumulation,

and less linker-region phosphorylation at T220 by nuclear CDKs (Fig. 2-5E). However, our

results do not exclude the possibility that Tak1 could also contribute to linker region phosphorylation by other mechanisms, such as regulating activity of other downstream kinases (Fig. 2-5E). Endogenous levels of Smad2-C phosphorylation and Smad T220 phosphorylation, were also reduced in *Tak1/Wnt1Cre* mutant palatal shelves, implying that Tak1 may modulate TGF-β superfamily signaling *in vivo* in the same way.

2-5.3. Interdependence of TGFβRI and Tak1 Signaling?

Two recent studies addressed the mechanism of TGF-β-induced Tak1 activation in HEK 293 cells (Sorrentino et al., 2008; Yamashita et al., 2008). While these studies agree that a ligand-induced interaction between TGFβRI and Traf6 results in Traf6 auto-ubiquitination and subsequent Tak1 activation, they did not agree on a role for TGFβRI kinase activity in TGF-β-induced Tak1 activation. Here we show that, in craniofacial mesenchymal cells, the presence of TGFβRI or its kinase activity are sufficient for Tak1-mediated signaling events downstream of TGF-β2. To explore whether all the Tak1-dependent TGF-β transcriptional responses are dependent on the TGFβRI kinase activity we performed a genome-wide transcriptomic analysis on prefusion palatal mesenchymal cells stimulated with TGF-β2 in the presence or absence of either TGFβRI or Tak1 kinase inhibitors. This assay demonstrated that many of the TGF-β-induced transcriptional responses (both stimulatory and repressive) are simultaneously dependent on both TGFβRI kinase and Tak1 kinase activities, and that surprisingly few genes, e.g., *Mllt3,* respond to TGF-β2 stimulation if TGFβRI kinase activity is inhibited.

In conclusion, our combined evidence implies that Tak1 has a novel multi-modal role in the craniofacial neural crest-derived mesenchyme in regulating activation of both TGF-β- and Bmp-induced Smad-dependent and Smad-independent signaling processes. *Tak1* deficiency in

NC-derived mesenchymal cells leads to attenuation of both canonical and non-canonical TGF-β

and Bmp signaling, which contribute to relatively subtle but consistent growth distortions in

craniofacial structures. This dis-coordination in craniofacial growth likely results in delayed

elevation of palatal shelves, which will never form a contact in the midline, resulting in cleft

secondary palate.

Chapter 3:

Tak1, Smad4 and Trim33 cooperatively mediate TGF-β3 signaling during palate

development

3-1. Summary

Transforming growth factor-beta3 (TGF-β3) plays a critical role in palatal epithelial cells by inducing palatal epithelial fusion, failure of which results in cleft palate, one of the most common birth defects in humans. Recent studies have shown that Smad-dependent and Smad-independent pathways work redundantly to transduce TGF-β3 signaling in this context. However, detailed mechanisms by which this signaling is mediated still remain to be elucidated. Here we show that TGF-β activated kinase-1 (Tak1) and Smad4 interact genetically in palatal epithelial fusion. While simultaneous abrogation of both *Tak1* and *Smad4* in palatal epithelial cells resulted in characteristic defects in the anterior and posterior secondary palate, these phenotypes were less severe than those seen in the corresponding *Tgfb3* mutants. Moreover, our results demonstrate that Trim33, a novel chromatin reader and regulator of TGF-β signaling, is functionally redundant with Smad4. Unlike the epithelium-specific *Smad4* mutants, epithelium-specific *Tak1:Smad4-* and *Trim33:Smad4*-double mutants display reduced expression of *Mmp13* in palatal medial edge epithelial cells, suggesting that both of these redundant mechanisms are required for appropriate TGF-β signal transduction. Moreover, we show that inactivation of Tak1

in *Trim33:Smad4* double conditional knockouts leads to the palatal phenotypes which are identical to those seen in epithelium-specific *Tgfb3* mutants. To conclude, our data reveal added complexity in TGF-β signaling during palatogenesis and demonstrate that redundant pathways involving Smad4, Tak1 and Trim33 regulate palatal epithelial fusion.

3-2. Introduction

Cleft palate, one of the most common birth defects in humans, is caused by a failure in palatogenesis (Chai and Maxson, 2006). During mammalian development, the secondary palate, which separates the oral cavity from the nasal cavity, develops as bilateral outgrowths (palatal shelves) of the maxillary processes of the first pharyngeal arch (Bush and Jiang, 2012). Palatal shelves first grow vertically down along the sides of the tongue, then they rapidly elevate and fuse in the midline (Ferguson, 1987). Failure in any of these three processes can result in cleft palate. The palatal shelf growth and patterning are governed by complex interactions between the ectoderm-derived epithelium, and the underlying mesenchyme derived from the cranial neural crest. One of the later events in palatogenesis, albeit a critical one, is epithelial fusion. During this process the medial edge epithelium (MEE) in tips of the apposing palatal shelves first forms the midline seam, which subsequently disappears. Many studies, both in humans and mice, have shown that signaling initiated by TGF-β3 is required for successful epithelial fusion (Dudas et al., 2007).

TGF-β3 binds and activates a heterotetrameric receptor complex composed of two type II and two type I receptors. Ligand-receptor interactions result in phosphorylation of TGF-β R-Smads 2 and 3 and subsequent complex formation with a common Smad (Co-Smad or Smad4). R-Smad/Co-Smad complexes then accumulate in the nucleus, where they function as

transcriptional co-regulators (Shi and Massague, 2003). This so called canonical (or Smad-dependent) signaling is regulated by many proteins interacting either with receptor complexes or Smads, e.g., SARA, Axin, inhibitory Smads (I-Smads) and Trim33. Previous studies have shown that Trim33 (Tif1γ, ectodermin) may regulate TGF-β superfamily signaling in different ways depending on the biological context. Dupont et al. suggested that Trim33 is a negative regulator of TGF-β signaling by functioning as a monoubiquitin ligase capable of disrupting activated R-Smad/Co-Smad complexes , while He et al. showed that Trim33 can bind to activated R-Smads in competition with Smad4 and mediate distinct TGF-β signaling processes (He et al., 2006). It also has been suggested that Trim33/R-Smad complexes can function as chromatin readers by making target genes accessible to R-Smad/Co-Smad complexes or by controlling the time the Smad complexes are bound to promoter sequences . In addition to the canonical (Smad-dependent) pathway, TGF-βs can also trigger non-canonical (Smad-independent) signaling processes leading to activation of various downstream mediators, such as, small rho-related GTPases, TGF-β-activate kinase-1 and downstream map kinase cascades including p38 Mapk, and Ikk-α (Derynck and Zhang, 2003).

Tgfb3 is strongly and specifically expressed in the MEE , and mouse embryos deficient in *Tgfb3,* as well as epithelium-specific *Tgfbr1* or *Tgfbr2* mutants suffer from defective palatal epithelial fusion (Dudas et al., 2006; Xu et al., 2006). Xu et al. previously showed that, at least in palatal explant cultures *in vitro*, Smad-dependent (Smad4-mediated) and Smad-independent (p38Mapk-mediated) pathways act redundantly during palatal epithelial fusion. Here, we show that redundancy between different TGF-β downstream mediators is even more extensive. By using tissue-specific mouse mutants in conjunction with a whole-head roller culture assay we demonstrate that both *Tak1:Smad4-* and *Trim33:Smad4*-double conditional mutants display

specific palatal fusion defects, and that simultaneous deletion/inactivation of all three proteins in palatal epithelial cells results in palatal phenotypes typically seen in tissue-specific *Tgfb3* mutants.

3-3. Experimental Procedures

3-3.1. Mice

$Tgfb3^{FX}$, $Ikka^{FX}$ and $Trim33^{FX}$ mice have been described earlier (Doetschman et al., 2012; Kim and Kaartinen, 2008; Liu et al., 2008) . *K14-Cre* and $Smad4^{FX}$ mice were obtained from S. Millar(Andl et al., 2004) and C. Deng (Yang et al., 2002), respectively. To generate mutant embryos, Cre-positive male mice heterozygous for floxed gene(s) were crossed with female mice carrying corresponding homozygous floxed allele(s) (see Table 3-1). For timed matings, the presence of a vaginal plug was designated as embryonic day 0 (E0). DNA for genotyping was prepared from tail tissues using DirectPCR lysis reagents (Viagen Biotech). Mouse lines were maintained in mixed genetic backgrounds. All experiments involving the use of animals were approved by the Institutional Animal Use and Care Committee at the University of Michigan-Ann Arbor (Protocol #00004320).

3-3.2. Histology, Immunohistochemistry and cell death assays

Embryos were collected into sterile DPBS and fixed at 4°C overnight in freshly prepared 4% paraformaldehyde in PBS. Samples used for wax embedding were washed, dehydrated through a graded ethanol series (20, 50, 70, 95 and 100%) and an overnight step in 50% Ethanol/50% Toluene, one hour step in 100% toluene, one hour step in 50% toluene/50% fresh Blue Ribbon Tissue Embedding/Infiltration Medium (Leica Surgipath) before being oriented and

embedded in fresh Blue Ribbon Tissue Embedding/Infiltration Medium (Leica Surgipath) after three changes. 7μm sections (histology and immunohistochemistry) were cut, mounted on Superfrost plus slides (Fisher) and stained with hematoxylin and eosin according to standard protocols. For immunohistochemistry, sections were rehydrated, and after antigen retrieval (5-20 minutes at 95-100°C in 10 mM citrate buffer, pH6.0) proliferating cell were detected using Ki67 antibody (#M7249; Dako). Cells positive for phosphorylated p38 Mapk were detected using p-p38 Mapk antibody (#4511; Cell Signaling). Antibody binding was visualized with Alexfluor-594 secondary antibody (Life Technologies). Apoptotic cells were detected using a TUNEL assay (Dead End, Promega) following manufacturer's instructions. Fluorescent images were viewed on an inverted fluorescent Leica DMI3000B microscope and documented using an Olympus DP72 camera.

Table 3-1. Crosses used to generate mutant embryos

Male mouse	Female mouse
$Tgfb3^{FX/+}K14Cre$	$Tgfb3^{FXFX}$
$Smad4^{FX/+}K14Cre$	$Smad4^{FXFX}$
$Tak1^{FX/+}Smad4^{FX/+}K14Cre$	$Tak1^{FXFX}Smad4^{FXFX}$
$Ikka^{FX/+}Smad4^{FX/+}K14Cre$	$Ikka^{FXFX}Smad4^{FXFX}$
$Trim33^{FX/+}Smad4^{FX/+}K14Cre$	$Trim33^{FXFX}Smad4^{FXFX}$

3-3.3. In situ hybridization

Embryos were processed and embedded in paraffin as described above. 10μm sections were cut and mounted on glass slides. RNA probes were labeled using a DIG-labeled NTP mix (Roche Applied Science) according to manufacturer's instructions, stored at -80°C and diluted in hybridization buffer. Section ISH was performed as described (Moorman et al., 2001). After staining, sections were fixed and mounted in Immumount (Thermo Scientific). Probe templates for *Tgfb3* and *Mmp13* were prepared as described .

3-3.4. Real-time quantitative PCR

Tissues were harvested from tips of palatal shelves from E14 and E15 mouse embryos, placed into 200μl of RLT (RNeasy mini kit, Qiagen), and RNAs were isolated by using RNeasy columns (Qiagen). cDNAs were synthesized by using Omniscript reverse transcriptase (Qiagen) according to the manufacturer's protocols. Real time quantitative PCR experiments were done either by using Universal Probe library-based assays (Roche Applied Science) or by using TaqMan assay reagents (Applied Biosystems) (see Table 3-2). 30μl assays were quantified using Applied Biosystems ABI7300 PCR and ViiA7 detection systems and software.

Table 3-2. Real-time quantitative PCR primers

Q-RTPCR using the Universal Probe System (Roche)			
Gene	Forward Sequence	Reverse Sequence	Universal Probe
Cytokeratin 14 (K14)	atcgaggacctgaagagcaa	tcgatctgcaggaggacatt	#83
Tp63 (delta N-p63)	ggaaaacaatgcccagactc	aatctgctggtccatgctgt	#45
Cdkn1a (p21)	cagatccacagcgatatcca	ggcacactttgctcctgtg	#21
Q-RTPCR using the TaqMan approach (Life Technologies)			
Gene		TaqMan Reference	
Irf6		Mm00516797_m1	
Mmp13		Mm00439491_m1	
Cdkn2a (p16)		Mm00494449_m1	
Cdkn1c (p57)		Mm01272135_g1	

3-3.5. Whole-head roller culture assays

Roller culture assays were modified from Goudy et al. (Goudy et al., 2010) Heads from

E15 embryos were collected in DPBS and mandibles, tongues, and brains were removed. The

resulting mid-face samples were cultured for 24 hours at 37°C in roller bottles (60ml serum

bottles) (60 rotations/minute) in serum free BGJb medium without penicillin and streptomycin.

The bottles were gassed at the beginning of the culture and again every 12 hours by gently

bubbling the medium for 2 minutes with O_2/CO_2 (95%/5%).   The palatal cultures were fixed,

sectioned and stained as described above. In 5Z-7-oxozeanenol (Tak1 inhibitor; 10μM;

eMolecules) treated samples, the inhibitor was added directly into the culture medium.

3-3.6. Western-blot assays

Palatal shelf edges were removed and cultured as described above in 2ml cryovials (60

rotations/minute) at 37°C in BGJb medium for 1 hour and then stimulated with TGF-β3

(10ng/ml) (#243-B3-002; R&D Systems) for 40 minutes. Tissues were then isolated and lysed in

2x Laemmli sample buffer (Harlow and Lane, 1988), ran on NuPage 4-12% Bis-Tris gradient

gels (Invitrogen) and transferred by "iBlot dry blotting" (Invitrogen) onto nitrocellulose filters.

Immunobloting and detection were done using standard protocols. The antibodies used were p-

38 (N-20) (#SC-728; Santa Cruz Biotechnology) and p-p38 MapK (#4511; Cell Signaling).

3-3.7. Statistical analysis

For histological and real-time quantitative PCR analyses three or more samples were analyzed. Averages, standard error and probability (Student's t-test, 2-tailed) were calculated. Probability (p) equal or less than 0.05 was marked as statistically significant.

3.4. Results

3-4.1. Epithelium-specific *Smad4* mutants display mild defects in palatogenesis

Smad-dependent and Smad-independent pathways have been shown to play functionally redundant roles during palatal epithelial fusion (Iwata et al., 2013) . To confirm and expand these findings, we first compared palatal phenotypes of epithelium-specific *Tgfb3* mutants (*Tgfb3$^{F/F}$K14-Cre = Tgfb3-cKO*) to those of corresponding *Smad4-cKOs (Smad4$^{F/F}$:K14-Cre)*. *Tgfb3*-cKOs display a fusion defect in the anterior palate, failure of the anterior palate to fuse to the nasal septum, variable degree of fusion in the mid-palate, persistent midline seam and occasionally a cleft in the posterior palate (Fig. 3-1 A-F). These observed phenotypes are less severe than those seen in *Tgfb3* germline mutants , but are practically identical to those seen in epithelium-specific *Tgfbr1* and *Tgfbr2* mutants suggesting that the phenotypic difference between *Tgfb3* germ line mutant and *Tgfb3-cKO* results, at least in part, from the inability of *K14-Cre* to recombine in the periderm as shown by ((Lane et al., 2014); Chapter 4). In contrast to phenotypes seen in *Tgfb3-cKOs,* palatal phenotypes displayed by Smad4-cKOs were very mild (Fig. 3-1G-I, M and Table 3-1), yet consistent and previously unappreciated . These include posterior epithelial triangles and occasional failure of the anterior palate to fuse, and the nasal septum to fuse to the anterior palate (1/4).

3-4.2. Simultaneous deletion of TGF-β activated kinase-1 and Smad4 results in anterior and posterior palate defects

To further examine cooperation between Smad-independent and Smad-dependent pathways during palatal epithelial fusion in vivo, we generated an allelic series of double mutants lacking one or both alleles of *Tak1 (w*hich, at least in some cell and/or tissue types, is an upstream activator of p38 Mapk) and *Smad4* in epithelial cells by crossing transgenic *K14-Cre* male mice that also were heterozygous for both *Tak1^{FX}* and *Smad4^{FX}* alleles with double homozygote *Tak1^{FXFX}Smad4^{FXFX}* female mice (Table 3-3). Epithelium-specific double heterozygotes showed no palatal phenotypes, while corresponding *Tak1:Smad4* double mutants (herein called *Tak1:Smad4cdKO*) displayed specific and consistent defects in palatogenesis (Fig. 3-1J-L, M, and Table 3-1), e.g., persistent epithelial seam, anterior fusion defect and a failure of the nasal septum to fuse to the anterior secondary palate. *Cre*-positive embryos heterozygous for the *floxed Tak1* allele and homozygous for the *floxed Smad4* allele showed similar but milder defects as dcKO with variable penetrance (Table 3-3).
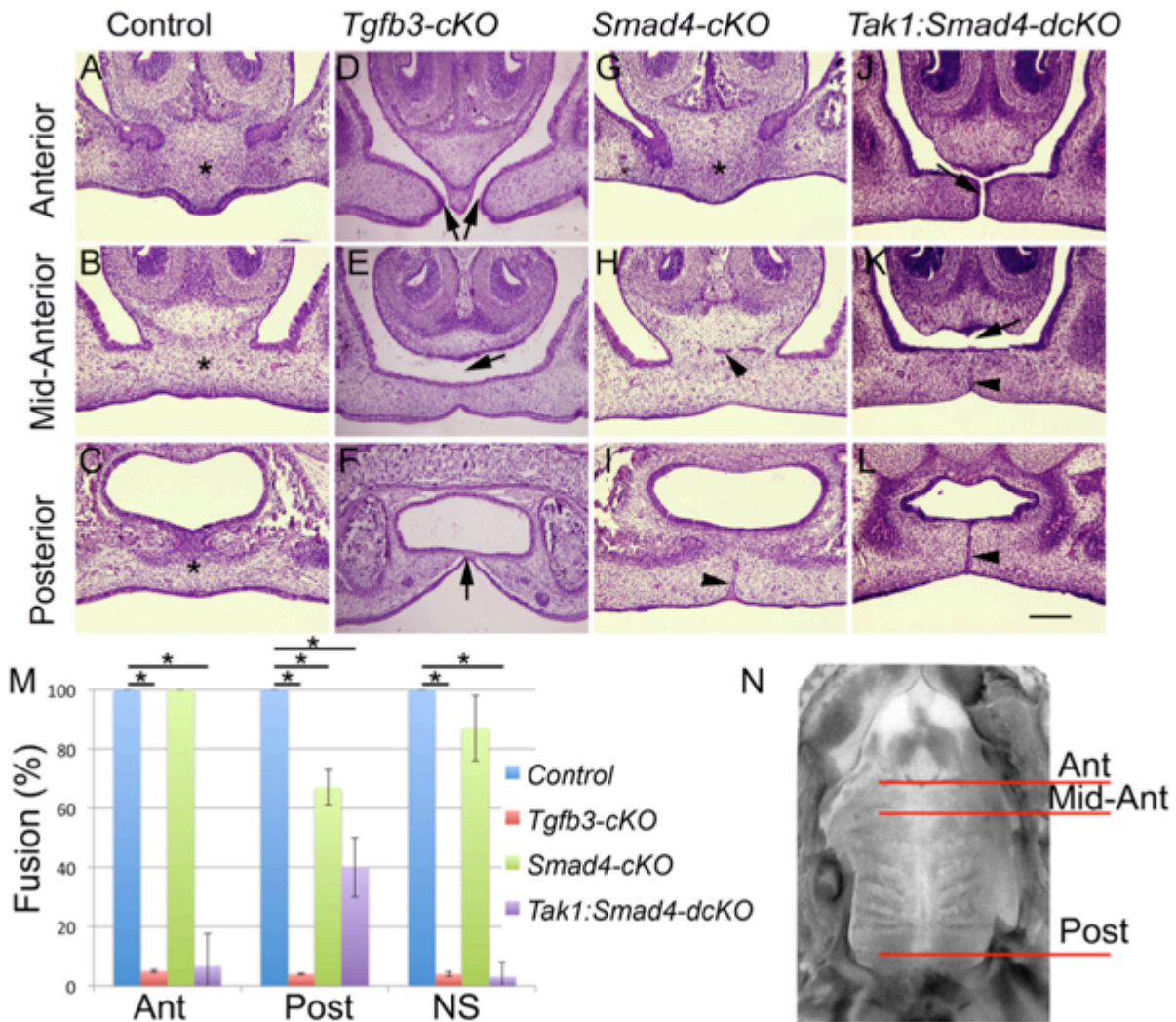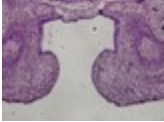
Figure 3-1. Epithelium-specific deletion of **Tak1** and **Smad4** results in defects in palatogenesis. Frontal sections on the anterior level (A, D, G, J), mid anterior (B, E, H, K) and posterior (C, F, I, L) levels (see N for levels of sections along the anterior-posterior axis). A-C, Control; D-F, *Tgfb3-cKO*, G-I, *Smad4-cKO,* J-L, *Tak1:Smad4-dcKO*. Asterisks in A, B, C, G illustrate the palatal mesenchymal confluence, black arrows in D and J point to the sites of failed fusion in the anterior palate, black arrows in E and K point to a gap between the nasal septum and the secondary palate, the black arrow in F points to an epithelial bridge in the posterior palate and black arrowheads in H, I, K and L point to persistent epithelial seams. Scale bar, 200 μm. Bar graph (M) illustrates the degree of fusion (mesenchymal confluence); Error bars, SEM; *, p<0.05; Ant, anterior level; Post, posterior level; NS, fusion between the nasal septum and secondary palate. N, mouse mouth roof at E18; superior view; red lines illustrate the levels of frontal sections shown in A-L (n=3).

Table 3-3. Summary of palatal defects in *Tgfb3*, *Smad4*, *Tak1 cKOs* and *Tak1:Smad4 –dcKOs*.

Genotype	Anterior cleft/ persistent seam	Nasal septum fusion defect/ persistent seam	Posterior midline seam/ epithelial triangle	Posterior cleft
Control (*Cre*⁻); n=3	0/3	0/3	0/3	0/3
Tgfb3^{FxFx}*K14Cre*; n=3	3/3	3/3	2/3	1/3
Smad4^{FXFX}*K14Cre*; n=4	1/4	1/4	4/4	0/4
Tak1^{FXFX}*K14Cre*; n=3	0/3	0/3	0/3	0/3
Tak1$^{FX/+}$*Smad4*^{FXFX}*K14Cre*; n=3	1/3	2/3	2/3	0/3
Tak1$^{FX/+}$*Smad4*$^{F/+}$*K14Cre*; n=3	0/3	0/3	0/3	0/3
Tak1^{FXFX}*Smad4*^{FXFX}*K14Cre*; n=4	4/4	4/4	4/4	1/4

3-4.3. Additional modifiers of TGF-β signaling during palatal epithelial fusion

Our results suggested that Tak1 plays a redundant regulatory role in TGF-β signaling, perhaps by functioning upstream of p38 Mapk in palatal epithelial cells. Yet, the *Tak1:Smad4-dcKO* palatal phenotypes (Fig. 1J-L) were noticeably less severe than those seen in corresponding *Tgfb3-cKOs* (Fig. 1D-F) or *Tgfbr1-cKOs* (Dudas et al., 2006)). Therefore we wondered whether, in addition to the Tak1-mediated pathway, other signal mediators could be involved in TGF-β3-induced palatal epithelial fusion. As candidates, we chose Ikk-α (Chuk) and Trim33 (Tif1γ; ectodermin), because both proteins modulate TGF-β signaling both by Smad-dependent and Smad-independent mechanisms contingent on the biological context (Descargues et al., 2008; Xi et al., 2011). Our results showed that epithelium-specific single mutants (i.e., *Ikka-cKOs* and *Trim33-cKOs)* did not show palatal phenotypes, and that *Ikka:Smad4-dcKO* mutants did not significantly differ from those of Smad4-cKOs (Fig. 2A-F,M) suggesting that Ikk-α does not contribute to TGF-β-triggered MEE removal. However, *Trim33:Smad4-dcKO* mutants consistently showed the persistent midline epithelial seam both in the anterior and in the posterior palate, and between the nasal septum and the anterior palate (Fig. 2G-L,M and Table IV). This phenotype differs from that seen in *Smad4-cKOs* or in *Tak1:Smad4-dcKOs* (compare Fig.1 and 2) suggesting that Trim33 and Smad4 play functionally redundant roles in palatal epithelial fusion that are at least in part distinct from that of a combined role of Tak1 and Smad4.
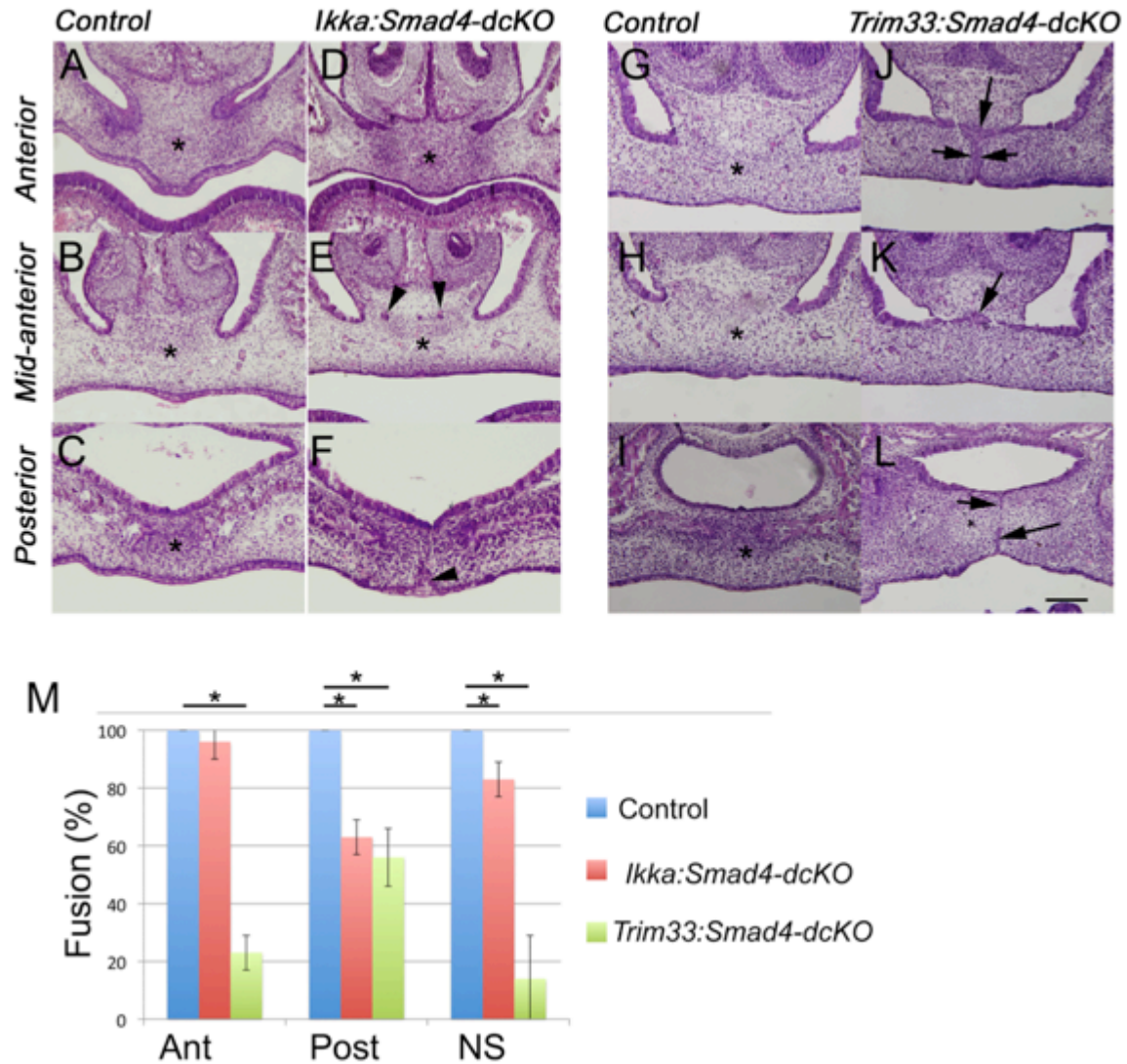
Figure 3-2. Simultaneous deletion of **Trim33** and **Smad4** in epithelial cells leads to persistence of the midline seam. Frontal sections on the anterior level (A, D, G, J), mid anterior (B, E, H, K) and posterior (C, F, I, L) levels (see Fig 1N). A-C and G-I, Control; D-F, *Ikka:Smad4-dcKO,* J-L, *Trim33:Smad4-dcKO.* Asterisks in A, B, C, D, E, G, H, I illustrate the palatal mesenchymal confluence, black arrowheads in E point to epithelial islands between the nasal septum and the posterior palate, black arrows in F, J, K, and L point to persistent epithelial seams. Scale bar, 200 μm. Bar graph (M) illustrates the degree of fusion (mesenchymal confluence); Error bars, SEM; *, p<0.05; Ant, anterior level; Post, posterior level; NS, fusion between the nasal septum and secondary palate (n=3).

Table 3-4. Summary of palatal defects in *Ikka* and *Trim33* cKOs and *Ikka:Smad4* and

Trim33:Smad4-dcKOs.

Genotype	Anterior cleft/ persistent seam	Nasal septum fusion defect/ persistent seam	Posterior midline seam/ epithelial triangle	Posterior cleft
Control (*Cre-*); n=3	0/3	0/3	0/3	0/3
Ikka^{FF}K14Cre; n=3	0/3	0/3	0/3	0/3
Trim33^{FF}K14Cre; n=3	0/3	0/3	0/3	0/3
Ikka^{FXFX}Smad4^{FXFX}K14Cre; n=3	0/3	1/3	2/3	0/3

3-4.4. Expression of a TGF-β signaling target Mmp13 is affected in Tak1:Smad4 and Trim33:Smad4 double conditional mutants

It has been previously shown that *Mmp13* expression is rapidly induced by TGF-β3-signaling in the midline seam during palatogenesis (Dudas and Kaartinen, 2005). To analyze whether Tak1 and Smad4- or Trim33 and Smad4-mediated pathways are involved in regulation of *Mmp13* expression, we first harvested palatal shelves from control, *Tgfb3-cKO, Smad4-cKO, Tak1:Smad4-cKO* and *Trim33:Smad4-cKO* embryos at E15.0 and used qRT-PCR to quantify their *Mmp13* mRNA levels. As shown in Fig. 3A, *Mmp13* expression was significantly reduced in *Tgfb3, Tak1:Smad4-dcKO* and *Trim33:Smad4-dcKO* samples, while the reduction in *Smad4-cKO* samples was rather modest and not statistically significant (Fig. 3A). We also used section ISH to analyze *Mmp13* and *Tgfb3* expression in the MES and nasal septum epithelium (Fig. 3B-I). Cre-negative control and *Smad4-cKO* samples displayed strong *Tgfb3* and *Mmp13* expression both in the MES and in the nasal septal epithelium. In *Tak1:Smad4-cdKOs* there was a notable reduction in *Mmp13* expression, while in *Trim33:Smad4-cKOs Mmp13* expression was barely detectable. In both samples, *Tgfb3* mRNA levels did not differ from those seen in controls. These results suggest that a known TGF-β signaling target *Mmp13* is regulated both by *Tak1:Smad4-* and *Trim33:Smad4*-mediated pathways in palatal medial edge epithelial cells.

3-4.5. Altered gene expression in TGF-β pathway mutants

Iwata et al. recently reported that signaling via TgfβRII stimulates *Irf6* expression, which in turn suppresses dNp63 expression allowing appropriate *p21 (Cdkn1a, p21Cip1)* expression . In prefusion palatal shelves at E14, we could not detect any differences in *Irf6* or *dNP63* expression levels between the control, *Tgfb3-cKO, Smad4-cKO, Tak1:Smad4-cKO* or

Tak1:Smad4-dcKO samples *(*Fig.3J). In the fusing palatal shelves at E15, *Irf6* was reduced only in *Tak1:Smad4-dcKO* samples, while dNP63 levels were increased in *Tgfb3-* and *Smad4-cKO* samples. In contrast to the lack of differences in *Irf6* and *dNP63* expression at E14, *p21* expression levels were reduced in all samples lacking *Smad4 (i.e., Smad4-cKO, Tak1:Smad4-dcKO and Trim33:Smad4-dcKO),* but not in *Tgfb3-cKO* samples (Fig. 3J). In addition to p21, TGF-β signaling has been shown to regulate expression of other cyclin-dependent kinase inhibitors in the MEE . Therefore, we compared expression levels of *p15 (Cdkn2b, p15Ink4b), p16 (Cdkn2a, p16Ink4a)* and *p57 (Cdkn1c, p57Kip2)* as outlined above (Fig. 3K and data not shown). At E14, *p16* expression was significantly reduced in *Tgfb3-cKOs* and in *Tak1:Smad4-dcKOs,* but not in *Trim33:Smad4-dcKOs,* whereas *Tgfb3-cKO* samples showed a dramatic increase in *p57* expression at E15 (expression levels of p15 were very low and did not show detectable differences between controls and different mutants; data not shown). Taken together, differences in expression level of candidate genes between *Tak1:Smad4-dcKOs* and *Tgfb3*-cKOs suggest that Tak1 and TGF-β3 can affect at least in part distinct pathways that act together to promote palatal epithelial fusion. Similarly, differences in gene expression between *Trim33:Smad4* and *Tak1:Smad4* double mutants imply that these molecules mediate distinct arms of TGF-β signaling.
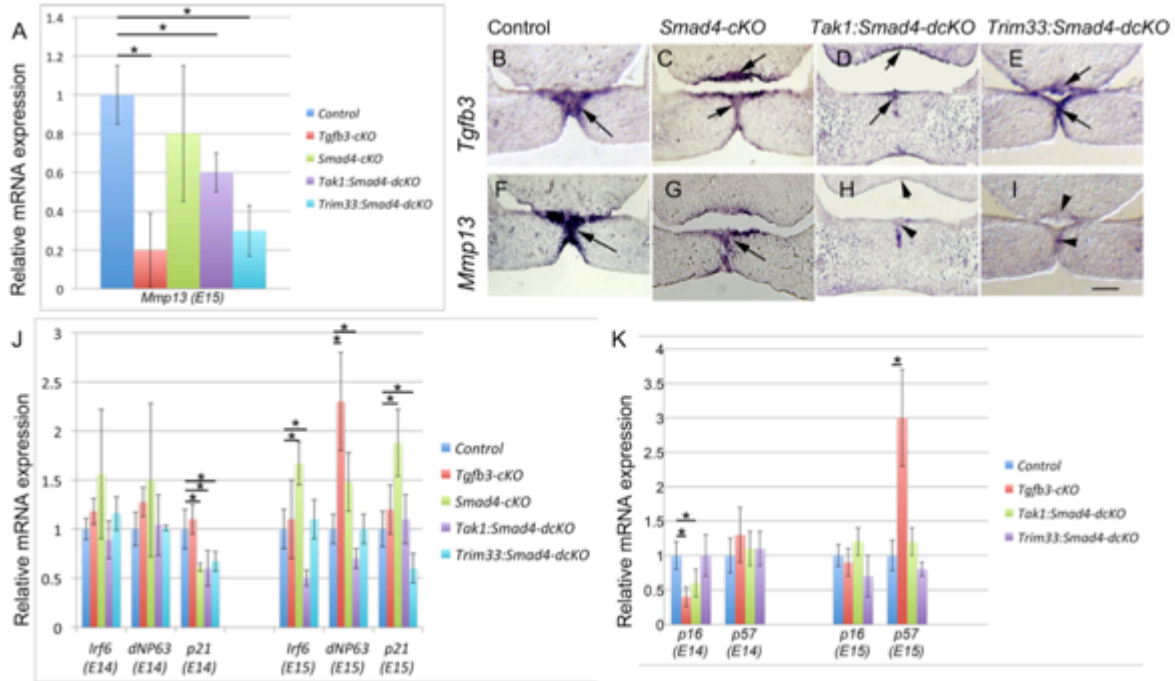
Figure 3-3. Gene expression differences in prefusion and fusing palatal shelves between controls and TGF-β pathway mutants. A, QRT-PCR analysis of *Mmp13* expression in palatal tissues of control (blue), *Tgfb3cKO* (red), *Smad4-cKO* (green), *Tak1:Smad4-dcKO* (purple) and *Trim33:Smad4-dcKO* (turquoise) at E15 (Error bars, SEM; *, p<0.05, n=3). B-I, In situ hybridization for *Tgfb3* (B, C, D, E) and for *Mmp13* (F, G, H, I). B, F, Control; C, G, *Smad4-cKO; D, H,* Tak1:Smad4-dcKO; E, I, *Trim33:Smad4-dcKO.* Frontal sections of E15 embryos; anterior level. Scale bar in I, 100μm (for B-I). J, QRT-PCR analysis of *Irf6, dNP63* and *p21* expression in palatal tissues from control, *Tgfb3-cKO, Smad4-cKO, Tak1:Smad4-dcKO* and *Trim33:Smad4-dcKO* embryos harvested at E14 and E15 (Error bars, SEM; *, p<0.05, n=3). K, QRT-PCR analysis of *p16,* and *p57* expression in palatal tissues from control, *Tgfb3-cKO, Smad4-cKO, Tak1:Smad4-dcKO* and *Trim33:Smad4-dcKO* embryos harvested at E14 and E15 (Error bars, SEM; *, p<0.05; n=3).

3-4.6. Epithelial cell proliferation and apoptosis are variably affected in *Tak1:Smad4-* and *Trim33:Smad4-dcKOs*

Previous studies showed that TGF-β signaling in the palatal epithelium induces cell cycle arrest that is a prerequisite for the disappearance of the midline seam by apoptosis and other possible mechanisms . To examine whether cell proliferation in the MES was affected in *Tak1:Smad4-* or *Trim33:Smad4-dcKOs,* we used Ki67 immunostaining on anterior frontal sections obtained from control (cre-negative) and *dcKO* embryos at E14.5 (Fig. 4A-C). Both *Tak1:Smad4* and *Trim33:Smad4-dcKOs* showed an increased number of positively staining epithelial cells in the tip of the nasal septum and in epithelial tips of prefusion palatal shelves when compared to the controls (Fig. 4A-C, J). In contrast, the number of TUNEL-positive apoptotic cells was significantly reduced in the control and mutant samples in the anterior palate on the level of nasal septum (Fig. 4D, F, H). MEE cells of *Tak1:Smad4-dcKO*s showed reduced phosphorylation (activation) of apoptosis-associated TGF-β-induced signaling molecule p38 Mapk, while *Trim33:Smad4-dcKOs* did not demonstrate comparable changes (Fig. 4 E, G, I).
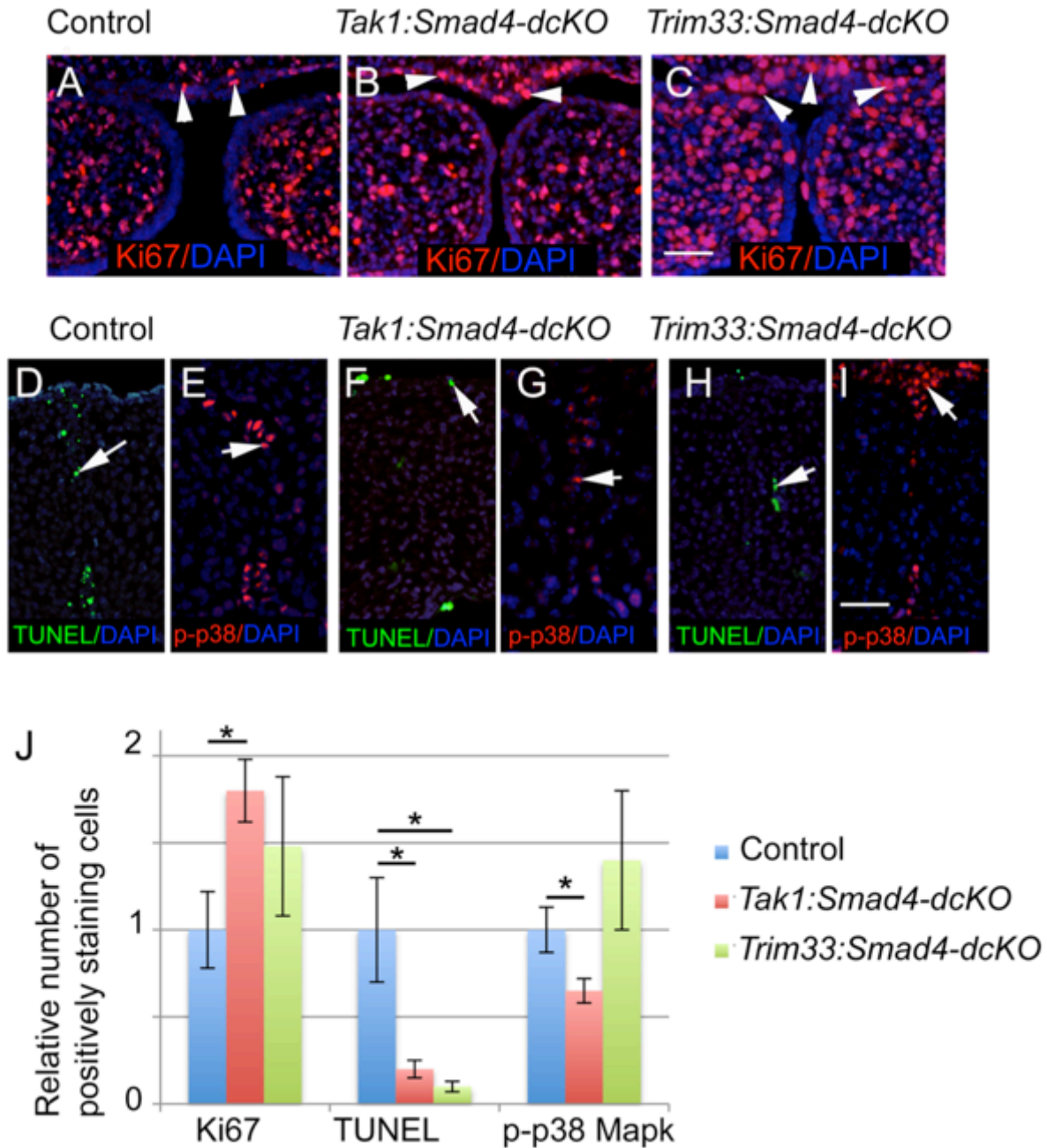
Figure 3-4. Proliferation and cell death are affected in *Tak1:Smad4* and *Trim33:Smad4*-dcKOs. Immunostaining for Ki67 (red) in control (A), *Tak1:Smad4-* (B) and *Trim33:Smad4-dcKO* (C) at E14.5. Frontal sections, anterior level. Counterstaining with DAPI (blue nulei). White arrowheads in A-C point to Ki67-positive cells in the nasal septum epithelium. TUNEL staining to detect apoptotic/necrotic cells (white arrows in D, F, H; green nuclei) in control (D), *Tak1:Smad4:dcKs* (F) and in *Trim33:Smad4-dcKO(H)* samples. Frontal sections, anterior level; counter staining with DAPI (blue). Immunostaining for phosphorylated p38 Mapk (p-p38, red staining) in control (E), *Tak1:Smad4:dcKs* (G) and in *Trim33:Smad4-dcKO* (I) samples. White arrows in E, G, and I point to positively-staining cells. Frontal sections, anterior level; counter

staining with DAPI (blue). J, Bar graph shows quantification of proliferation (Ki67) apoptosis (TUNEL) and phopho-p38 Mapk assays (Error bars, SEM; *, p<0.05; n=3).

3-4.7. Inactivation of Tak1 in *Trim33:Smad4-dcKOs* phenocopies the palate defects seen in *Tgfb3-dcKOs*

As outlined above, the palatal phenotypes of both *Tak1:Smad4-* and *Trim33:Smad4-dcKOs,* while consistent and clear, were still less severe than those seen in *Tgfb3-cKOs.* Therefore, we wondered whether combined loss of *Tak1, Smad4* and *Trim33* would result in palatal phenotypes similar to those seen in *Tgfb3-cKOs.* To this end, we used a potent Tak1 inhibitor, 5Z-7-oxozeaenol, in conjunction with *Trim33:Smad4-dcKOs in vitro* by using a whole-head roller culture assay. Control cultures treated with 5Z-7-oxozeaenol, which efficiently blocked p38 Mapk phosphorylation (Fig. 3-5I), showed consistent and reliable fusion identical to that seen in untreated cultures (Fig. 3-5A-D). Furthermore, *Smad4-cKO* cultures with the Tak1 inhibitor did not demonstrate detectable phenotypes (data not shown). Under similar culture conditions, *Trim33:Smad4-dcKOs* without the Tak1 inhibitor showed a persistent midline seam both in the anterior and posterior palate, comparable to that seen in *Trim33:Smad4-dcKOs* in vivo (Fig. 3-5E,F). However, treatment of double-cKO cultures with the Tak1 inhibitor resulted in palatal phenotypes practically identical to those seen in *Tgfb3-cKOs*, i.e., an anterior hole and a posterior epithelial bridge (Fig. 3-5G,H). These data suggest that Tak1, Smad4 and Trim33 are redundantly transducing TGF-β3 signaling to remove the midline epithelial seam, and to facilitate palatal anterior and posterior fusion during palatogenesis (Fig. 3-6).
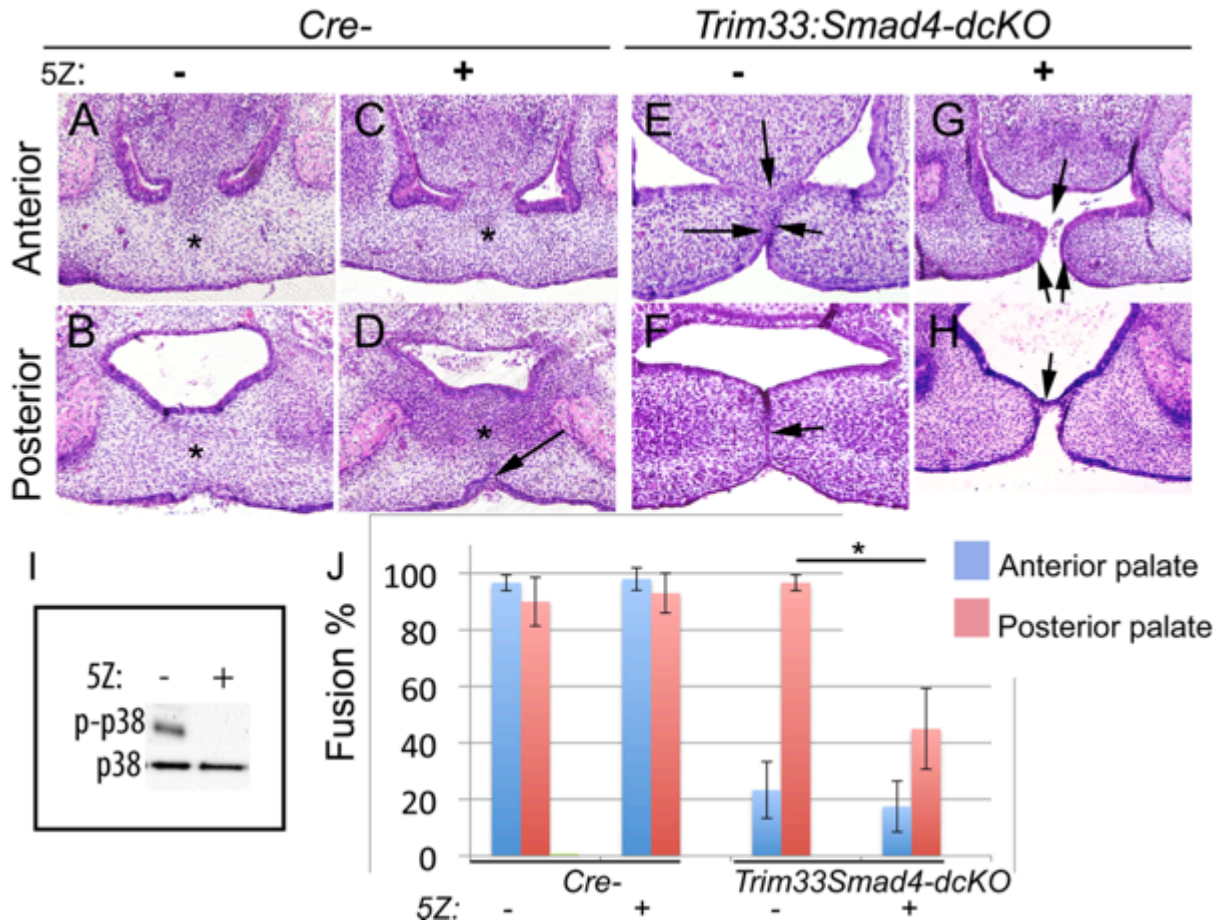
Figure 3-5. Conditional removal of **Trim33** and **Smad4** along with Tak1 inhibition recapitulates the palatal phenotype seen in **Tgfb3-cKO** embryos.

A whole-head roller culture assay of Cre-negative controls (A-D) and Trim33:Smad4-dcKOs (E-H) in the absence (A,B, E, F) and presence of Tak1 inhibitor (C, D, G, H). A, C, E, G, frontal sections, anterior level; B, D, F, H, frontal sections, posterior level. Asterisks in A, B, C, D illustrate mesenchymal confluence, black arrow in D points to oral epithelial triangle, black arrows in E point to intact MEE cells in palatal shelves and nasal septum, black arrow in F points to the persistent epithelial seam, black arrows in G point to the anterior cleft and black arrow in H points to the posterior epithelial bridge. Scale bar, 100μm. I, Tak1 inhibitor 5Z-7-oxozeaenol (5Z) prevents p38 Mapk phosphorylation in palatal shelves harvested from whole-head roller cultures. J, bar graph shows a degree of palatal fusion in control and *Trim33:Smad4-cKO* samples cultured a presence or absence of 5Z in a whole-head roller culture assay. Error bars, SEM; *, $p<0.05$; n=3). Blue columns, anterior palate; red columns, posterior palate.
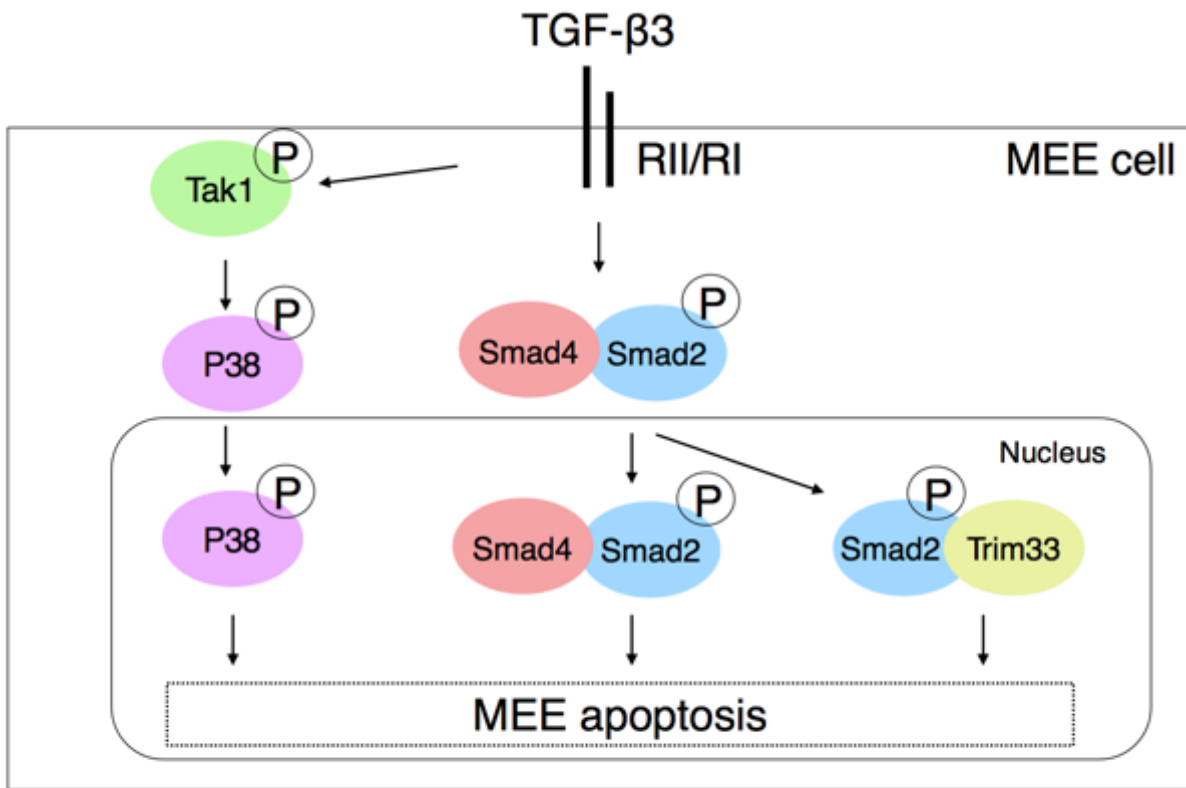
Figure 3-6. Schematic of redundant functions of Tak1, Smad4 and Trim33 during palatal epithelial fusion.

3-5. Discussion

Palatogenesis is a complex developmental process involving appropriate growth, elevation and fusion of palatal shelves (Ferguson, 1988). While the role of TGF-β3 in the palatal epithelium (MEE) is well established , recent studies have shown that mechanisms by which the downstream signaling is transduced are surprisingly complicated, involving redundantly acting canonical and non-canonical arms of TGF-β signaling . Here we show that in MEE cells, redundancy of TGF-β signal transduction is even more extensive, since recapitulation of the *Tgfb3-cKO* palatal phenotype required inactivation of three separate genes/gene products (*Tak1, Smad4, Trim33)* mediating different arms of TGF-β signaling.

Developing palatal shelves are composed of the mesenchyme (largely derived from the cranial neural crest with a minor contribution coming from the cranial paraxial mesoderm) and from the ectoderm-derived surface epithelium, which is covered by a thin layer of peridermal cells (Lane and Kaartinen, 2014). Recent studies have shown that peridermal cells play a key role in palatal shelf adherence, and that this layer has to be removed for a normal palatal adhesion and fusion to take place . *Tgfb3* is expressed in both cell types (Lane et al., 2014) and interestingly, the cleft palate phenotype of *Tgfb3* null mutants can be partially rescued by transducing *Tgfb3* exclusively in peridermal cells . Likewise, *Tgfb3-cKO* mice, which lack *Tgfb3* in epithelial cells including the MEE but not in peridermal cells, display significantly milder palatal phenotypes than those seen in systemic *Tgfb3* mutants ((Lane et al., 2014) and the present study), suggesting that TGF-β3 signaling is important for peridermal cell removal and is thus required for adhesion and fusion between the palatal shelves in the mid-palate. In fact, *Tgfb3-cKO* palatal phenotypes are practically identical to those seen in epithelium-specific *Tgfbr1* or *Tgfbr2* mutants . Moreover, this distinct palatal phenotype can be seen in mice expressing *Tgfb1*

in the *Tgfb3* locus (Yang and Kaartinen, 2007) suggesting that *Tgfb1* can functionally replace *Tgfb3* in peridermal cells but not in MEE cells. Nevertheless, the consistent defects of *Tgfb3-cKO* embryos in the anterior and posterior palate (anterior hole, nasal septum fusion defect and posterior epithelial bridge/submucous cleft) show that TGF-β3-mediated signaling is crucial also in the MEE, and that the *K14-Cre* driver line is a useful tool to study gene functions in this cell type during palatogenesis.

A previous study on epithelium-specific *Tgfbr2:K14-Cre* mice suggested that TGF-β via TgfbRII triggers a Smad4-Irf6 signaling cascade, which downregulates *dNP63* resulting in p21 induction, cell cycle arrest and removal of MEE cells . Using the same *K14-Cre* transgenic line we demonstrate that *Tgfb3-cKO* embryos, which display clear and consistent palatal defects similar to those seen in *Tgfbr2:K14-Cre* mutants, do not show differences in *p21* expression in prefusion or fusing palatal shelves. In addition, *Smad4-dcKOs*, which display a very mild phenotype in the posterior palate, consistently show reduced levels of *p21* expression. Based on these results we conclude that changes in *p21* expression are not causally related to the observed palatal phenotypes. Despite the obvious reduction in *p21* expression in *Smad4-cKOs* as well as in *Tak1:Smad4-* and *Trim33:Smad4dcKOs*, we could not see significant differences in *Irf6* or *dNP63* expression in prefusion palatal shelves at E14. In fusing palatal shelves at E15, *Tak1:Smad4-dcKOs* palatal shelves showed reduction in *Irf6* expression while palatal tissues harvested from *Tgfb3-ckos* at E15 showed an increase in *dNP63*. Whether these discrepancies between our current findings and those reported by others are caused by experimental variables, e.g., timing and/or technique of tissue harvest and differences in genetic backgrounds, or whether they are caused by other currently unknown causes, remains to be shown.

In epithelial cells, TGF-βs are well-known growth inhibitory cytokines . It has been suggested that inhibition of MEE proliferation by TGF-β signaling triggers a cascade of events that results in the removal of MEE via apoptosis (and to some extent by transdifferentiation/migration) . Despite some differences in gene expression patterns between *Tak1:Smad4-dcKOs* and *Trim33:Smad4-dcKOs,* we show that both of these epithelium-specific double mutants show increased levels of proliferation, particularly in the epithelial tips of the nasal septum, while increased levels of TUNEL-positive nuclei could be seen both in the epithelial tips of palatal shelves and nasal septum. Increased cell proliferation is consistent with our finding that p21 expression levels are reduced in both *dcKO*s. However, it is likely that expression of other negative cell cycle regulators, e.g., p16, is also regulated by TGF-β, as p21 expression levels are not reduced in *Tgfb3* mutants, although they display a well-documented failure to suppress cell proliferation in the prefusion MEE .

A role of Tak1 in regulation of TGF-β3-induced p38Mapk activation is currently controversial. Several studies have suggested that Traf6-Tak1 signaling module mediates TGF-β-induced p38 Mapk activation , while other studies have proposed that instead of Tak1 other Map3Ks, e.g., Map3K4 and Map3K10, play the key role in transducing TGF-β signaling that results in p38 Mapk phosphorylation . We previously showed that neural crest-derived ectomesenchymal cells lacking *Tak1* fail to demonstrate TGF-β-induced p38 Mapk activation . Our present results imply that also in MEE cells Tak1 is at least partially responsible for mediating p38 Mapk activation, since we could see reduction in p38Mapk phosphorylation in *Tak1:Smad4-dcKOs* when compared to controls or *Trim33:Smad4-dcKOs*. Moreover, similar to palatal explant cultures with inactivated p38 Mapk , inactivation of Tak1 alone, which totally abolished the p38Mapk phosphorylation (Fig. 3-5I), did not result in defects in palatogenesis

111

(Fig. 3-5), while simultaneous inactivation of Tak1 and deletion of *Smad4* in explant cultures resulted in palatal phenotypes similar to that seen in *Tak1:Smad4-dcKOs* in vivo (Supplemental Fig. 3-1).

Mutations in the *IRF6* gene cause van der Woude syndrome, an autosomal dominant syndrome characterized by cleft lip and/or palate . Mouse embryos lacking *Irf6* display early differentiation defects of the ectoderm, which are practically identical to those seen in *Ikka* knockout mice . Therefore, it is surprising that deletion of *Ikka* in epithelial cells including the MEE does not result in noticeable defects in palatogenesis. Instead we discovered that in MEE cells, concomitant deletion of a novel chromatin reader *Trim33* and *Smad4* led to defective palatal fusion. Several recent reports have demonstrated that epigenetic mechanisms involving appropriate histone modifications are crucial for successful craniofacial development and palatogenesis. In humans, haploinsufficiency of histone-3 demethylases, e.g., *PHF8* and *KATB6,* has been shown to result in cleft palate , while neural crest specific deletion of *Hdac3* resulted in severe craniofacial defects including cleft palate in mouse embryos . Trim33 is a multifunctional protein , which has been shown to both facilitate and antagonize TGF-β signaling. In differentiating stem cells, Trim33, when complexed with Smad2, is able to bind to specific poised chromatin marks found in the promoter regions of master regulators, rendering them accessible to R-Smad/Co-Smad complexes (Xi et al., 2011). In other cellular systems, Trim33 has been shown to mono-ubiquitinate Smad4 disrupting Smad4-chromatin complexes and limiting their residence time at TGF-β-responsive enhancer s (Agricola et al., 2011). Here we show in MEE cells Trim33 does not function as a negative regulator of canonical TGF-β signaling, but rather that Trim33 and Smad4 function cooperatively during palatal fusion (Fig.

112

3-6). A similar cooperative role of Smad4 and Trim33 in a control of neural stem cell proliferation was recently shown to take place in the developing cortex (Falk et al., 2013)

In conclusion, our data indicate that complex and largely cooperative mechanisms involving both non-canonical and canonical arms of TGF-β signaling control disappearance of MEE cells during palatal fusion. These involve Tak1 functioning upstream of p38Mapk, Smad4 and a novel Smad2 binding partner and a putative chromatin reader Trim33 (Fig. 3-6). While the roles of Tak1 and Trim33 appear fully cooperative with Smad4, our results also reveal a subtle but consistent, and previously unappreciated, non-cooperative role for Smad4 in MEE cells during palatogenesis.

Chapter 4:

Control elements targeting *Tgfb3* expression to the palatal epithelium are located intergenically and in introns of the upstream *Ift43* gene

4-1. Summary

Tgfb3 is strongly and specifically expressed in the epithelial tips of pre-fusion palatal shelves where it plays a critical non-redundant role in palatal fusion in both medial edge epithelial (MEE) cells and in a thin layer of flattened peridermal cells that covers the MEE. It is not known how *Tgfb3* expression is regulated in these specific cell types. Using comparative genomics and transgenic reporter assays, we have identified cis-regulatory elements that could control *Tgfb3* expression during palatogenesis. Our results show that a 61-kb genomic fragment encompassing the *Tgfb3* gene drives remarkably specific reporter expression in the MEE and adjacent periderm. Within this fragment, we identified two small, non-coding, evolutionarily conserved regions in intron 2 of the neighboring *Ift43* gene, and a larger region in the intervening sequence between the *Ift43* and *Tgfb3* genes, each of which could target reporter activity to the tips of pre-fusion/fusing palatal shelves. Identification of the cis-regulatory sequences controlling spatio-temporal *Tgfb3* expression in palatal shelves is a key step towards understanding upstream regulation of *Tgfb3* expression during palatogenesis and should enable the development of improved tools to investigate palatal epithelial fusion.

4-2. Introduction

Failure of palatogenesis (palate formation) results in cleft palate, which is one of the most common congenital birth defects in humans. In mice, palatogenesis starts around embryonic day 11.5 (E 11.5) when bilateral outgrowths of the maxillary process called palatal shelves start to grow down vertically on each side of the tongue. Co-ordinated growth of palatal shelves themselves, the tongue and the rest of the oral cavity is followed by rapid palatal shelf elevation (~ E14) and fusion (~E15) (Bush and Jiang, 2012). Palatal shelves are composed of the neural crest-derived mesenchyme covered by epithelial cells (Bush and Jiang, 2012). Before palatal fusion, the epithelial layer is composed of a basal layer of cuboidal medial edge epithelial (MEE) cells and an apical periderm layer of flattened cells. This periderm layer is shed from the tips of the apposed elevated palatal shelves just before they form contact with each other, allowing adhesion and intercalation of the underlying MEE cells (Yoshida et al., 2012) to form a midline epithelial seam. Epithelial cells in this seam are subsequently lost and the underlying basement membrane degraded resulting in palatal mesenchymal confluence (Gritli-Linde, 2007).

Several studies have demonstrated that signaling triggered by transforming growth factor-β3 (TGF-β3) plays a critical role in palatal epithelial fusion. *Tgfb3* is strongly and specifically expressed in MEE cells (Fitzpatrick et al., 1990; Millan et al., 1991; Pelton et al., 1990), and mice lacking *Tgfb3* display 100% penetrant cleft secondary palate (Kaartinen et al., 1995; Proetzel et al., 1995), which results from defects in TGF-β3-induced palatal MEE differentiation and/or apoptosis (Ahmed et al., 2007; Iwata et al., 2013; Kaartinen et al., 1997; Taya et al., 1999). Results of a recent study also suggest that TGF-β3 is required for peridermal desquamation (Wu et al., 2013). Mutations in the human *TGFB3* have been linked to cleft palate (Carinci et al., 2007; Lidral et al., 1998), and a recent report described a disease-causing

mutation in the coding region of *TGFB3* in patients showing abnormalities in palate and muscle development(Rienhoff et al., 2013).

A commonly used approach to study complex developmental processes has been to manipulate gene function in mouse models using the *Cre-lox* system (Rajewsky et al., 1996). In the context of palatogenesis, an epithelium-specific *keratin14-Cre (K14-Cre)* driver line (Andl et al., 2004) has been frequently used, since it recombines with a very high efficiency in the MEE (Dudas et al., 2006; Xu et al., 2006). Yet abrogation of the *Tgfbr1* gene encoding the TGF-β type I receptor (Dudas et al., 2006) or *Tgfb3* in the palatal epithelium (this study) resulted in a significantly milder palatal phenotype than systemic deletion of the *Tgfb3* gene encoding the TGF-β3 ligand (Kaartinen et al., 1995; Proetzel et al., 1995). Here we show that this phenotypic difference is likely caused by an inability of the *K14-Cre* driver to recombine in peridermal cells.

To better understand how gene expression is specifically directed in the pre-fusion MEE and overlying peridermal cells, we decided to identify control elements responsible for palate-specific *Tgfb3* expression. We surveyed more than 400 kilobases (kb) of mouse genomic DNA sequences on mouse chromosome 12, and identified a 61-kb fragment around the *Tgfb3* gene that directs reporter expression specifically in the MEE and adjacent periderm. Using transient transgenic approaches, we identified three smaller cis-regulatory regions: one in the proximal intergenic region and two in intron 2 of the upstream *Ift43* gene. These more distal elements may function as 'shadow' enhancers assuring robust and reliable control of *Tgfb3* expression in the MEE and adjacent periderm.

4-3. Experimental Procedures

4-3.1. BACs and BAC recombineering

Mouse *BACs RP23-76M13 (=5'BAC) and RP24-299H18 (=3'BAC)* were obtained from

Children's Hospital Oakland Research Institute (http://bacpac.chori.org) (see Fig. 4-2A). Their

identity was verified using a standard restriction mapping technique (data not shown).

4-3.2. Insertion of the *SA-lacZ-PA* cassette into exon1 of the 5' BAC *RP23-76M13* and the 3'

BAC *RP24-299H18* (see Fig. 4-2A)

Targeting arms were generated by PCR using BAC *RP23-76M13* as a template and the following

primers:

Tgfb3-L1: 5'-TCCTAGCTCTACCCAGCACACG-3'

Tgfb3H3Xh-L2:5-'AAGCTTCTCGAGTGTGTGAGCCCAGGAACGAG-3'

Tgfb3XhH3-R1:5'-CTCGAGAAGCTTGCAAAGGGCTCTGGTAGTCCTG-3'

Tgfb3R2: 5'-TGATAGGGGACGTGGGTCATC-3'

pNASSβ (*SA-lacZ-PA* cassette) was inserted into exon 1 of the BACs *RP23-76M13* and *RP24-*

299H18 using standard BAC recombineering techniques (Warming et al., 2005). *Neo 452* (a

loxP-Neo-PA-loxP cassette) was added to the generated BAC to enable selection with

kanamycin. Integrity of the recombineered BACs was confirmed by PCR after amplification.

4-3.3. Preparation of the 61-kb and 28-kb BACs

The 61-kb BAC: A 128-kb 3'fragment from the recombineered BAC *RP24-299H18* was deleted

in two steps. First, a targeting vector to replace the large 3'fragment with *pGalK* was generated

by using the primers:

3'del-F: 5'-

TGACAGATATAGGCAGTGTAAGAACTCGCCATTAGCGGGAGGCGCCATCAGTGCCC

C

CTTCTGAATTCTACCTGTTGACAATTAATCATCGGCA-3'

3'del-R:

5'-

CTTTTCCCCTTGAGATAAGGCCTCTCATTGAACCTGAAACTTACTTTGATTGGGCTGG

CTT

CAGCACTGTCCTGCTCCTT-3'

After successful recombineering, a targeting vector to delete the *pGalK* selection marker was

generated by PCR using the following primers:

3'del-pGalK-F:

5'-AGAACTCGCCATTAGCGGGAGGCGCCATCAGTGCCCCCTTCTGAATTCTAACAAA

GTCTATACAGTTCCTCACCCTCTGGGAAAAGTAAGTGCTCAAAAC-3'

3'del-pGalK-R:

5'-GTTTTGAGCACTTACTTTTCCCAGAGGGTGAGGAACTGTATAGACTTTGTTAG

AATTCAGAACGGGGGCACTGATGGCGCCTCCCGCTAATGGCGAGTTCT-3'

The targeting vector was deleted as described (Warming et al., 2005).

The 28kb BAC: A 33-kb 5' fragment was deleted from the 5'end of the 61-kb BAC as outlined

above. Primers to generate the targeting vector were:

5'3'del-F:

5'-

TGACCAGGGAGAGGGGCTGTTATGAGGTACTGGGCATCCTGATGGGATGAGAGAAC

ATTCTCCTGTTGACAATTAATCATCGGCA-3'

5'3'del-R:

5'-GGGCAATGGAGATGTCAAACACGGGCTGCCTAATCTGGAAAGGCATTATTTT

AACTTGTATCAGCACTGTCCTGCTCCTT-3'

The targeting vector to delete the *pGalK* selection marker was generated by PCR and the

following primers:

5'3'del-pGalK-F:

5'-AGGGGCTGTTATGAGGTACTGGGCATCCTGATGGGATGAGAGAACATTCTTA

CAAGTTAAAATAATGCCTTTCCAGATTAGGCAGCCCGTGTTTGACATC3'

5'3'del-pGalK-R:

5'-GATGTCAAACACGGGCTGCCTAATCTGGAAAGGCATTATTTTAACTTGTAAGAA

TGTTCTCTCATCCCATCAGGATGCCCAGTACCTCATAACAGCCCCT-3'

BAC DNAs were purified for microinjections using Nucleobond AX alkaline lysis protocol

according to the manufacturer's instructions (Clontech).

4-3.4. Preparation of smaller reporter constructs

The *2xcHS4-hsp68-lacZ-PA-2xcHS4* vector was generated by replacing a *Sac*II-*Sac*I fragment

from the *pUbC-SH-Gm-4xcHS* plasmid (kindly provided by R. Behringer) with the *hsp68-lacZ-*

PA cassette. A unique *Not*I site just upstream of the *hsp68* minimal promoter was generated by

using the Quikchange-II site-directed mutagenesis kit (Agilent). Regions of interest were PCR-

amplified using SuperMix High Fidelity polymerase (Invitrogen) (primer sequences shown in

Table 4-1), and the generated fragments inserted into the *Not*I site using the In-Fusion HD

cloning kit (Clontech). Plasmid DNAs were purified using endonuclease-free Maxi-Prep columns (Qiagen) and the purified DNAs were linearized by *Sal*I for microinjection.

4-3.5. Alignment of orthologous sequences and identification of putative binding motifs

Multi-species sequence comparisons around the *Tgfb3* gene were performed using the UCSC genome browser (http://genome.ucsc.edu) and VISTA tools for Comparative Genomics (http://genome.lbl.gov/vista) using the global pair-wise and multiple alignment (LAGAN) program. The threshold used for evolutionary conservation was 70% sequence similarity within 100bp region of DNA sequence. Predicted transcription factor binding sites were identified by using RankVISTA and TRANSFAC matrices.

4-3.6. Generation of transgenic mouse lines and transient transgenic mouse embryos

The transgenic mouse lines and transient transgenics were generated in the Transgenic Animal Model Core facility at the University of Michigan – Ann Arbor.

4-3.7. Other mouse lines used in this study

We generated epithelium-specific *Tgfb3* mutants by crossing mice heterozygous for the floxed *Tgfb3* allele *(Tgfb3^{FXWT})* (Doetschman et al., 2012) and carrying the epithelial *K14-Cre* driver (Andl et al., 2004) with homozygous floxed *Tgfb3 (Tgfb3^{FXFX})* mice. *R26R-YFP* reporter mice were obtained from the Jackson Laboratories, and generation of *Tgfb3-Cre* mice has been previously described (Yang et al., 2008).

4-3.8. X-Gal staining

To detect expression of β-galactosidase encoded by the *lacZ* reporter gene, embryos were collected, washed and fixed in freshly prepared 4% para-formaldehyde-0.5% glutaraldehyde for 20 minutes, washed 3 x 20 minutes in the detergent wash solution and stained from 4 hours to overnight in X-Gal staining solution as described (Behringer, 2003). The stained samples were examined using a Leica MZ95 dissecting microscope and photographed using an Olympus DP71 camera and DP controller and manager software. Selected samples were processed for paraffin embedding using Histoclear, sectioned, rehydrated and mounted in Immumount (Fisher) or couterstained with eosin or Nuclear Fast Red and mounted in DPX.

4-3.9. Histology and Immunohistochemistry

For paraffin embedding, embryos were harvested and fixed in 4% para-formaldehyde for 24 hours at +4°C, washed, dehydrated and embedded in Leica Histowax. Sections (7 μm) were stained with hematoxylin and eosin using standard protocols. For immunohistochemistry, the paraformaldehyde fixed samples were allowed to sink in sterile 10% sucrose in PBS, then in 7% gelatin/15% sucrose in PBS, oriented and embedded in fresh 7% gelatin/15% sucrose in PBS on ice, then dry ice, and stored at -80°C. Cryosections (10μm) were cut and stored at -80°C. The sections were stained with αSSEA-1 (MC-480 from DSHB) and αGFP (A11122 from Life Technology) antibodies, which were detected by Alexafluor-594 and Alexafluor-488 secondary antibodies (Invitrogen) respectively. The stained sections were mounted with Vectashield mounting medium containing DAPI (Vector Labs Inc). Sections were viewed using an Olympus BX51 microscope and documented using an Olympus DP71 digital camera as described above.

Table 4-1. Primer sequences used for In-Fusion cloning.		
Fragment	Forward primer	Reverse Primer
-(6.1-0.8)	TTGGCGCCTCCCGCGGCCGCgatgagcccggcgtcccatctt	GTTTGGATGTTCGCGGCCGCcctttctaagaggcctggttctgg
-(6.1-3.7)	TTGGCGCCTCCCGCGGCCGCgatgagcccggcgtcccatctt	GTTTGGATGTTCGCGGCCGCtctctgagaagctgggagtctg
-(3.7-0.8)	TTGGCGCCTCCCGCGGCCGCttgaatcatttgagaagtgagttt	GTTTGGATGTTCGCGGCCGCcctttctaagaggcctggttctgg
-(13.7-6.1)	TTGGCGCCTCCCGCGGCCGCggatccttctctgtaaagtagac	GTTTGGATGTTCGCGGCCGCgtcgactcaggctgagaatt
-(13.7-9.7)	TTGGCGCCTCCCGCGGCCGgatccttctctgtaaagtagac	GTTTGGATGTTCGCGGCCGCgtgctgcgagccaactgagcc
-(9.7-6.1)	TTGGCGCCTCCCGCGGCCGCcatcaggttagctggaac	GTTTGGATGTTCGCGGCCGCgtcgactcaggctgagaatt
-(7.9-7.6)	TTGGCGCCTCCCGCGGCCGCggcaagccctgtgtctccct	GTTTGGATGTTCGCGGCCGCcccccctggaaacagggtgt
-(7.4-6.6)	TTGGCGCCTCCCGCGGCCGCcacacacacccctgcacaac	GTTTGGATGTTCGCGGCCGCaggcactgggatcaggc
-(13.0-12.5)	TTGGCGCCTCCCGCGGCCGgatggagccgctgattctga	GTTTGGATGTTCGCGGCCGCggggagcagggttggaatcc
-(26.9-24.0)	TTGGCGCCTCCCGCGGCCGCagaccaaggtctgcaagt	GTTTGGATGTTCGCGGCCGCggaactaacacttgtcctg
Capital letters indicate the sequences that are homologous to the vector.		

4-4. Results

4-4.1. Palatal peridermal cells are not recombined in a commonly used *K14-Cre* mouse line

　　　Comparison of the palatal phenotypes of global *Tgfb3* knockout mice (*Tgfb3$^{-/-}$*) and epithelium-specific *Tgfb3 (Tgfb3:K14-Cre)* mice revealed that, despite the efficient recombination in the MEE, the germline mutants consistently displayed a more severe phenotype than the tissue-specific mutants (Fig. 4-1, A-I): *Tgfb3$^{-/-}$* mice had a complete cleft of the secondary palate (Kaartinen et al., 1995; Proetzel et al., 1995), while *Tgfb3:K14-Cre* mice had a cleft anteriorly, but superficial or complete fusion in the mid-palate, and an aberrant posterior epithelial bridge. Since the *Tgfb3:K14-Cre* palatal phenotype was practically identical to that observed in the epithelium-specific TGF-β receptor mutants *(*both *Tgfbr1:K14-Cre* and *Tgfbr2:K14-Cre)* (Dudas et al., 2006; Xu et al., 2006), we wondered whether this milder palatal phenotype was caused by an inability of the *K14-Cre* driver line (Andl et al., 2004) to induce recombination in peridermal cells. To address this question we harvested tissues from *K14-Cre, R26R-YFP* reporter embryos at E13.5, and assessed the Cre-induced recombination in MEE and peridermal cells (Fig. 4-1, J and K). Our results showed that while the MEE was efficiently recombined, we could not detect reporter expression in the adjacent periderm. In contrast, *Tgfb3* was strongly and specifically expressed both in the periderm and underlying MEE as demonstrated by both in situ hybridization, and *R26R-lacZ* reporter expression in the *Tgfb3-Cre^{KI}* mouse line (Yang et al., 2008) (Fig. 4-1, L and M).
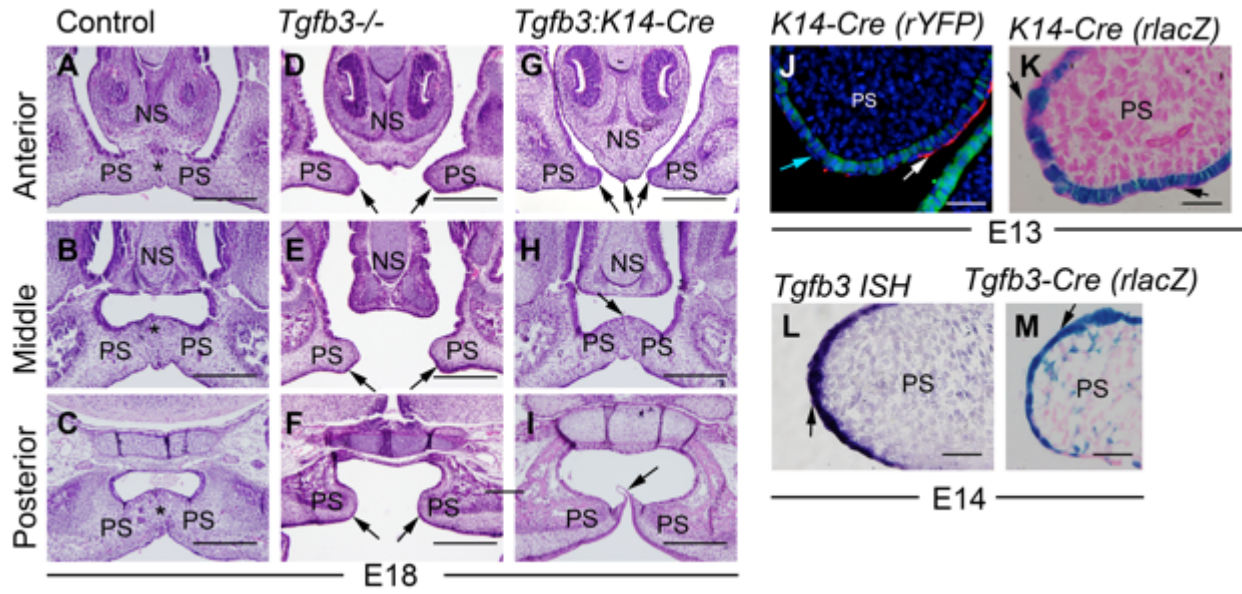
Figure 4-1. Milder palatal phenotype of epithelium-specific *Tgfb3:K14-Cre* mutants than that of *Tgfb3* null mutants results from an inability of *K14-Cre* to recombine in peridermal cells. A-C, control; D-F, *Tgfb3-/-* mutant; G-I, *Tgfb3:K14-Cre* (A-I, frontal orientation; all at E18). A, D, G, on the level of the nasal septum (anterior); B, E, H, mid-eye level (middle); C, F, I, on the level of soft palate (posterior). Asterisks in A-C indicate confluent midline mesenchyme, black arrows in D-E point to unfused palatal shelves, black arrows in G-I point to unfused elements of the anterior palate (G), a persistent epithelial seam in the mid-palate (H), and an epithelial bridge in the posterior soft palate (I). J, a frontal palatal section of a *K14-Cre:R26R-YFP* embryo at E13; double immuno-fluorescence staining to detect YFP-positive recombined cells (green) and an SSEA1-positive subset of non-recombined peridermal cells (red, white arrow). Light blue arrow points to the DAPI-positive nucleus of a peridermal cell that is SSEA-1-negative and has not been recombined by *K14-Cre*. K, a frontal palatal section of a X-Gal-stained *K14-Cre:R26R-lacZ* embryo at E13, counterstaining with eosin. Black arrows point to apical peridermal cells that were not recombined with *K14-Cre*. L, in situ hybridization for *Tgfb3* at E14 (palatal frontal section). Black arrow points to a positively staining flattened cell with peridermal appearance. M, a frontal palatal section of X-Gal-stained *Tgfb3-Cre:R26R-lacZ* embryo, counterstained with eosin. Black arrow points to an X-Gal-positive flattened cell with peridermal appearance. PS, palatal shelf; NS, nasal septum. Scale bars in A-I, 200µm; J-M, 50µm.

4-4.2. Survey of the *Tgfb3* cis-regulatory function using recombinant reporter *BACs*

Since *Tgfb3* is strongly and specifically expressed in peridermal and MEE cells, we reasoned that identification of cis-regulatory elements controlling palate-specific *Tgfb3* expression would be invaluable for development of new improved genetic tools to examine palatal epithelial fusion *in vivo*. The *Tgfb3* gene, composed of 7 evolutionarily conserved exons, is located on mouse chromosome 12 between the *Ift43* (intraflagellar transporter 43) and *Ttl5* (tubulin tyrosine ligase-like 5) genes, which both lie in the opposite orientation to the *Tgfb3* gene (Fig. 4-2A). The intergenic flanking sequences are remarkably short (3-3.5kb) but the neighboring genes are not expressed in pre-fusion palatal shelves (Fig. 4-4Ab).

To assess large regions upstream and downstream of the *Tgfb3* gene for regulatory elements, we obtained two overlapping BACs. The 5' BAC *(RP23-76M13)* contained a 289-kb region from -263kb to +26kb (defining *Tgfb3* transcriptional start site (TSS) as 0) which included the *Tgfb3, Ift43* and *Gpatch2l* genes (Fig. 4-2A). The 3' BAC *(RP24-299H18)* contained the 189-kb region from -35kb to +154kb which included the *Tgfb3* gene and the *Ttll5* (variant 4) gene (Fig. 4-2A). The sequences of the two BACs overlapped by 61kb, which includes all the *Tgfb3* exons and some of those of the neighboring genes.
To prepare reporter constructs, we inserted an *SA-lacZ-pA* cassette into *Tgfb3* exon 1 of each BAC using standard recombineering techniques (Warming et al., 2005). These recombinant *lacZ* reporter BACs were used to generate transgenic mice and β-galactosidase activity assessed at E14.0 using X-Gal staining as *Tgfb3* is usually strongly expressed in palatal shelf MEE and nasal septal epithelium around this stage. Both *5'* and *3' lacZ*-BACs were able to target reporter activity correctly to the palatal midline and nasal septal tissues (Fig. 4-2, B and F).
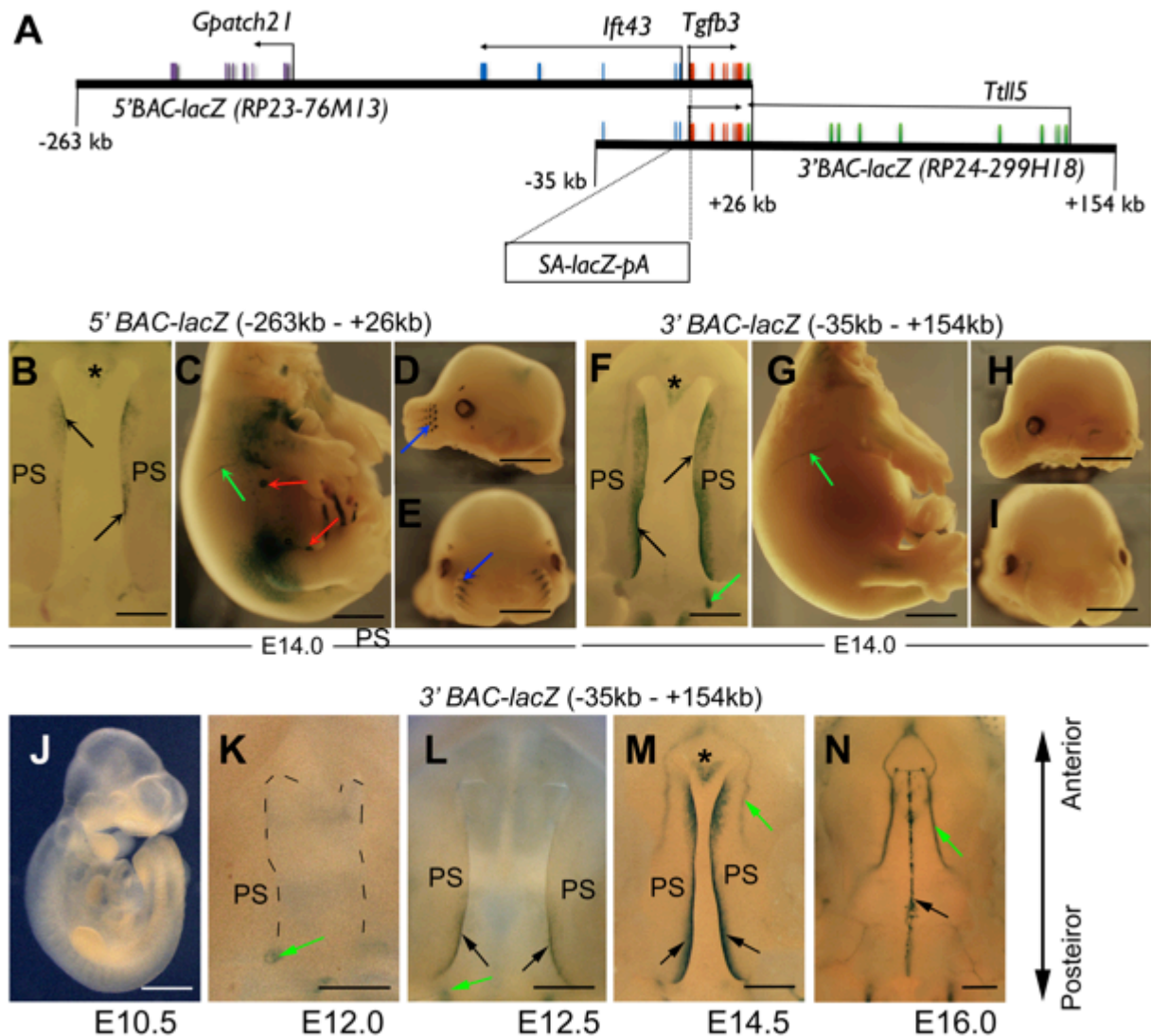
Figure 4-2: Recombinant reporter BACs used to detect *Tgfb3* regulatory regions. A, schematic representation of *Tgfb3*-containing *lacZ* BAC clones. Exons of the *Tgfb3* gene are shown as red vertical bars and exons of *Ttll5*, *Ift43* and *Gpatch21* genes are shown as green, blue and purple vertical bars, respectively. Horizontal black arrows show the direction of transcription of each gene. B-E, *5' lacZ* BAC transgenic embryos showing β-gal reporter activity (blue staining) in tips of palatal shelves (B, black arrows), nasal septum (B, asterisk, at anterior end of palate), blood vessels (C, green arrow), mammary placodes (C, red arrows) and in whisker follicles (D, E, blue arrows). F-I, 3' *lacZ* BAC transgenic embryos showing β-gal reporter activity (blue staining) in tips of palatal shelves (F, black arrows), nasal septum (F, asterisk), blood vessels (F, G, green arrows). B, F, roof of mouth at E14, inferior view; C, G, torso at E14, right lateral view, D, H, head (mandible removed), left lateral view; E, I, head (mandible removed), frontal view. J-N, Reporter activity in *3' lacZ*-BAC transgenic embryos between embryonic days 10.5 and 16.0. Black arrows point to expression in tips of pre-fusion palatal shelves (K, L) and midline seam (N); green arrows point to positively staining blood vessels (K,

126

L, M, N); asterisk (in M) marks the nasal septum PS, palatal shelf. B, F, K-N, anterior, top; posterior, bottom. Scale bars in K, 450μm; B, F, J, L, M, N, 500μm; C, D, E, G, H, I, 1mm.

The 5' *lacZ*-BAC transgenic embryos were also stained in mammary placodes, whisker follicles, nostrils and vasculature (Fig. 4-2, C-E), while the 3'*lacZ*-BAC embryos showed additional staining principally in vasculature (Fig. 4-2G, and Fig. 4-3, which illustrates the positions of all DNA fragments tested for enhancer activity in this study and summarizes expression data). Stable transgenic mouse lines carrying *3' lacZ*-BAC did not show detectable reporter activity until E12.0-E12.5, when staining was seen first in blood vessels and soon afterwards in the tips of the posterior palatal shelves (Fig. 4-2, K-L). At E14.5 strong staining occurred along the entire A-P axis of the palatal shelf tips, and continued during and after palatal epithelial fusion when it could still be detected in the degrading midline seam and in vasculature at E16.0 (Fig. 4-2, M and N).

As the 5' and 3' BAC sequences overlapped, and both the *5'* and *3' lacZ*-BAC reporters drove expression in the palatal shelf tips, we hypothesized that sequences in the region common to each *BAC* may be responsible. We tested this by making a reporter *lacZ*-BAC containing only this sequence, from -35kb to +26kb (Fig. 4-3A, 4-4Aa). This 61-kb fragment of mouse genomic DNA consistently drove highly specific reporter expression in the MEE and the adjacent periderm, and in peridermal cells covering the nasal septum where anterior secondary palatal fusion occurs (Fig. 4-4B, F, G, H). The only other tissue showing detectable though weak X-Gal staining was the lens (Fig. 4-4, D and E).

Figure 4-3. **Enhancer screening across the *Tgfb3* region.** A, Schematic presentation of the regions examined to locate cis-regulatory sequences directing reporter activity to the MEE/periderm cells. (a) 417-kb of genomic DNA (black line) including the *Tgfb3* gene (red boxes represent exons); colored lines beneath correspond to the positions of BAC sequences
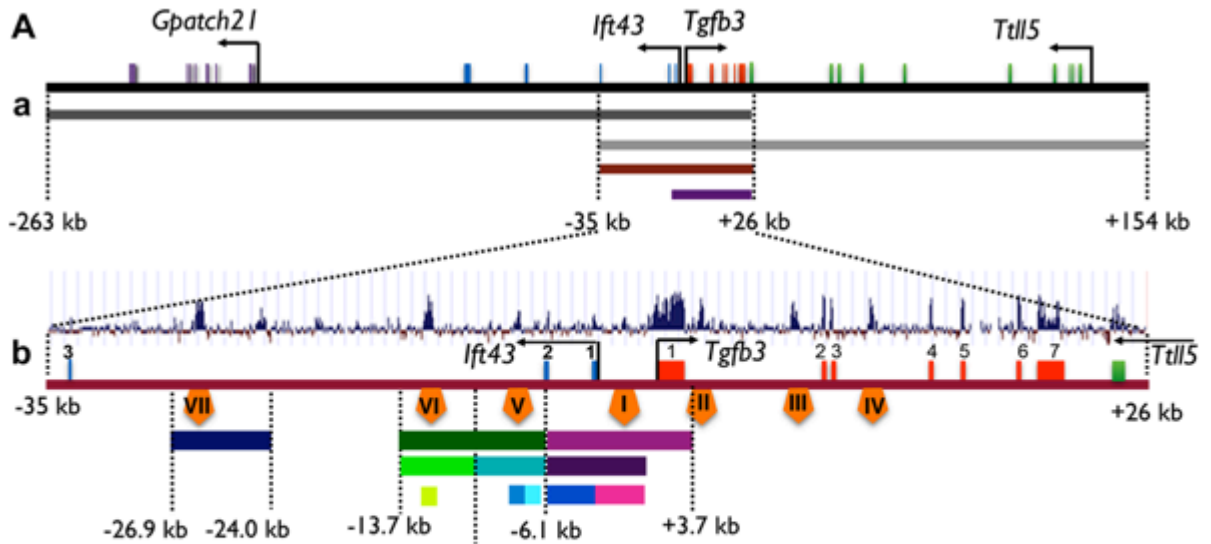
B. Enhancer screen across the *Tgfb3* region

Fragment (kb) (TSS=0)	-263 - +26	-35 - +154	-35 - +26	-3 - +26	-26.9 - -24.0	-13.7 - -6.1	-13.7 - -9.7	-12.5 - -11.9	-9.7 - -6.1	-7.9 - -7.6	-7.4 - -6.6	-6.1 - +3.7	-6.1 - -0.8	-6.1 - -3.7	-3.7 - -0.8	ECRs I-IV
MEE	4/5	3/3	4/5	0/5	0/10	4/5	0/7	0/8	7/14	2/6	2/4	2/5	2/3	0/5	0/5	0/8
Nasal Septum	4/5	3/3	4/5	0/5	0/10	4/5	0/7	0/8	7/14	1/6	0/4	2/5	1/3	0/5	0/5	0/8
Primary palate	1/5	0/3	1/5	0/5	4/10	2/5	2/6	0/8	2/14	2/6	0/4	0/5	0/3	0/5	1/5	0/8
Nasal cartilage	2/5	0/3	0/5	0/5	0/10	0/5	0/7	0/8	0/14	2/6	0/4	0/5	0/3	0/5	0/5	0/8
Molars	0/5	0/3	0/5	3/5	2/10	0/5	0/7	0/8	0/14	0/6	0/4	0/5	0/3	0/5	0/5	4/8
Incisors	0/5	0/3	0/5	1/5	1/10	0/5	0/7	1/8	2/14	0/6	1/4	0/5	1/3	0/5	2/5	2/8
Whisker follicles	3/5	1/3	0/5	3/5	1/10	3/5	6/7	3/8	3/14	2/5	1/4	1/5	0/3	0/5	1/5	4/8
Outer ear	0/5	1/3	0/5	0/5	3/10	0/5	0/7	2/8	0/14	2/6	0/4	2/5	1/3	0/5	0/5	0/8
Nostrils	3/5	0/3	0/5	3/5	5/10	4/5	2/7	6/8	13/14	4/6	1/4	1/5	1/3	0/5	3/5	6/8
Olfactory bulbs	0/5	2/3	1/5	2/5	0/10	1/5	0/7	0/8	0/14	0/6	0/4	1/5	1/3	0/5	3/5	3/8
Midbrain	2/5	0/3	2/5	0/5	0/10	0/5	0/7	0/8	0/14	1/6	1/4	0/5	0/3	0/5	0/5	0/8
Hindbrain	0/5	0/3	3/5	0/5	0/10	0/5	0/7	0/8	2/14	2/15	0/4	0/5	0/3	0/5	0/5	0/8
Forebrain	2/5	0/3	0/5	4/5	0/10	0/5	2/7	0/8	0/14	0/6	0/4	0/5	0/3	0/5	0/5	6/8
Lens	2/5	0/3	4/5	1/5	3/10	0/5	2/7	4/8	6/14	0/5	1/4	1/5	1/3	0/5	3/5	2/8
Mammary placodes	3/5	0/3	0/5	0/5	0/10	0/5	0/7	0/8	0/14	0/6	0/4	0/5	0/3	0/5	0/5	0/8
Surface ectoderm	2/5	1/3	0/5	2/5	4/10	0/5	1/7	4/8	3/14	2/6	1/4	2/5	2/3	5/5	2/5	1/8
Blood vessels	3/5	3/3	3/5	2/5	1/10	5/5	5/7	6/8	3/14	0/6	2/4	0/5	0/3	5/5	1/5	5/8
Long bones/ vertebrae	2/5	1/3	0/5	0/5	4/10	0/5	3/7	7/8	3/14	1/6	0/4	0/5	1/3	0/5	3/5	3/8

used for expression regulation analysis (see B, first four columns). (b) The 61-kb region in common between the 5' and 3' BACs (brown line); graph above shows evolutionary sequence conservation among placental mammals (UCSC genome browser) along this sequence; red boxes represent the *Tgfb3* exons; colored lines beneath correspond to the positions of regions used for regional expression regulation analysis (see B; fourth column onwards); orange pentagons illustrate the ECRs I-VII (see main text). B, a table summarizing findings of reporter activity driven by the sequences in the regions indicated by colored bars in A in various tissues of transgenic embryos at E14. Data entries show the number of embryos displaying positive reporter activity in selected tissues (rows) over the total number of *lacZ*-positive embryos for each sequence (identified by color bar in each column; dark yellow highlight, 50% or more staining; pale yellow highlight, >0%, <50% staining.
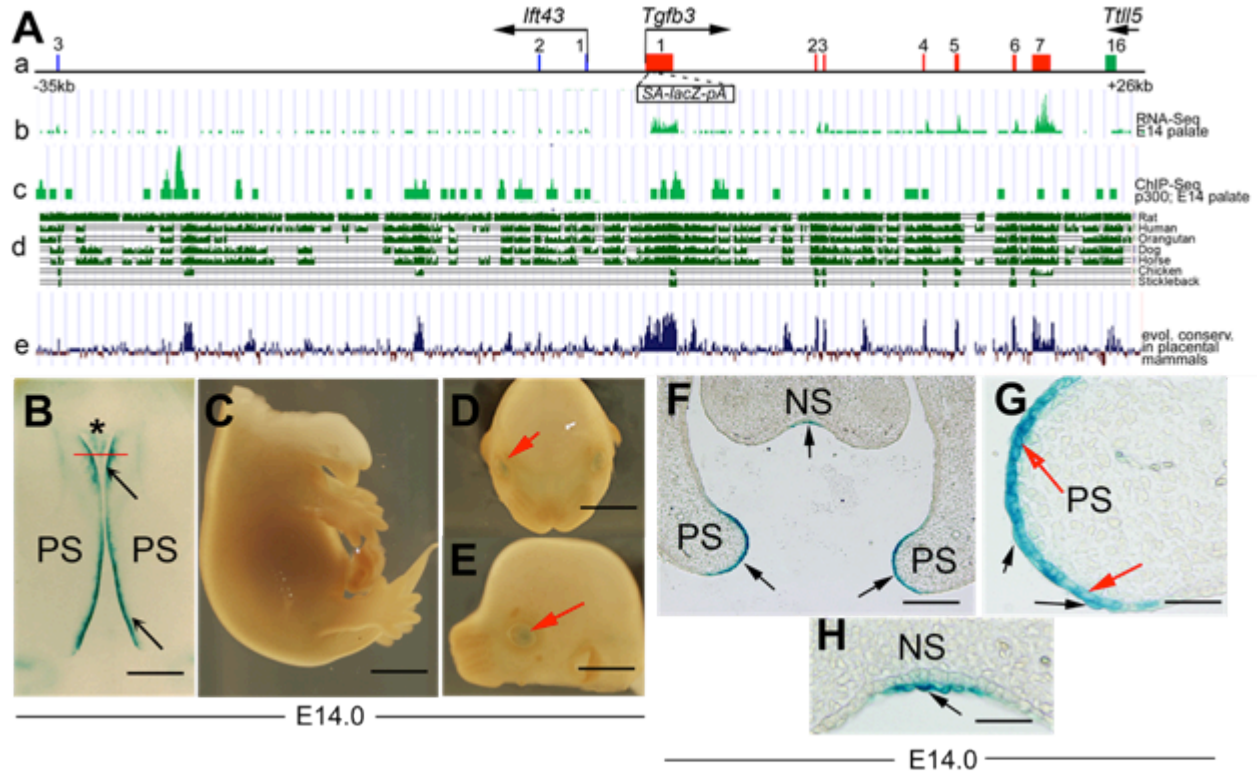
Figure 4-4. **A 61-kb genomic region including the*Tgfb3* gene targets reporter activity to the MEE and adjacent periderm.** A, Schematic representation of the 61-kb region (see main text) includes (a) the *Tgfb3* gene (exons in red); exons 1-3 of the *Ift43* gene (blue boxes) and exon 16 of the *Ttll5* gene (green box). That *Tgfb3* but neither of its neighbors is actively expressed at E14.5 is shown in (b, RNA-seq profile in mouse palate at E14.5 -FaceBase Enhancer Project; A Visel). Different types of sequence analysis are suggestive of possible enhancer sites: (c) p300 Chip-seq profile in mouse palate at E14.5 (ref: FaceBase Enhancer Project; A Visel), (d) evolutionary sequence conservation among selected vertebrate species in this sequence (UCSC genome browser) and (e) evolutionary sequence conservation among placental mammals (UCSC genome browser). B-E, 61-kb *BAC-lacZ* embryos showing β-gal activity (blue staining) in tips of palatal shelves (B, black arrows), nasal septum (B, asterisk), and lens (D, E, red arrows). B, mouth roof at E14, inferior view, anterior on the top; C, torso at E14, right lateral view; D, head (mandible removed), left lateral view; E, head (mandible removed), frontal view. F-H, Frontal sections of an X-Gal stained 61-kb *lacZ*-BAC embryo at the level of nasal septum (indicated by the red line in B). F, X-Gal staining (black arrows) at the tips of the pre-fusion palatal shelves (PS) and in the nasal septum (NS) is present in cells of both the basal MEE layer (red arrows in G) and the overlying periderm layer (black arrows in G), and periderm in the nasal septum (black arrow in H). Scale bars in B, 500μm; C, D, E, 1mm; F, 200μm; G, H, 50μm.

4-4.3. Noncoding evolutionarily conserved sequences within the *Tgfb3* gene are not responsible for the MEE-specific gene expression

We analyzed the 61-kb overlapping region using the UCSC Genome Browser (http://genome.ucsc.edu) (Fig. 4-4Ac-e) to identify non-coding evolutionarily conserved regions (ECRs), which are likely to include tissue-specific enhancers and found four: ECR-I (2kb upstream of TSS), ECR-II and ECR-III (in *Tgfb3* intron 1) and ECR-IV (in *Tgfb3* intron 3) (Fig. 4-5). As these are all highly conserved in placental mammals, which develop a complete secondary palate, but not in avians (or fish), which do not express *Tgfb3* in tips of palatal shelves and do not develop the fused secondary palate (Sun et al., 1998), they were good candidates to regulate palate-specific expression. To test this, the ECRs (I-IV) were PCR-amplified and subcloned upstream of the minimal *hsp68* promoter and *lacZ-PA* reporter, and the resulting ECR-(I-IV)–*hsp68-lacZ-PA* cassette cloned between concatamerized pairs of genomic insulators (cHS4), which have been shown to reduce positional effects of transgenes and alleviate promoter interference(Griswold et al., 2011);Yahata, 2007 #3977}(Fig. 4-5). Transient transgenic embryos were generated and analyzed for reporter activity at E14.0. While the ECRs were consistently able to target the reporter activity to several tissues (teeth, whisker follicles, nostrils and forebrain), no staining was seen in the MEE (n=15) (Fig. 4-5). We also modified the 61-kb *lacZ-*BAC by deleting sequences from -35kb to -3kb. This 28-kb BAC was also unable to direct *lacZ* reporter expression to the MEE (Fig. 4-3). These data suggest that the sequences from -3.0kb to +26kb, including the entire *Tgfb3* gene and ECRs I-IV, are not responsible for the MEE/periderm-specific gene expression in mouse embryos during palatogenesis.

4-4.4. Cis-regulatory elements directing gene expression in the MEE are located in intron 2 of the upstream *Ift43* gene

In addition to the noncoding ECRs I-IV, the 61-kb region from -35kb to +26kb contains three additional highly conserved regions in intron 2 of the *Ift43* gene: ECR-V at position –(7.9 - 7.6)kb, ECR-VI at -(13.0 - 12.5)kb and ECR-VII at –(26.9 – 24.0)kb. To assess these regions for the possible presence of MEE/periderm-specific cis-regulatory elements, we first subcloned the ECRs -V and -VI into the 2xcHS4-*hsp68-lacZ-2xcHS4* vector as a single 7.6-kb fragment (Fig. 4-5A) and ECR-VII as a 2.9-kb fragment (Fig. 4-5A). Analysis of X-Gal-stained transient transgenic embryos at E14 revealed that the region surrounding ECR-VII targeted the reporter activity to vascular and skeletal structures, but did not direct reporter activity in the MEE (Fig. 4-3, and data not shown). In contrast, the 7.6-kb region containing both ECRs -V and -VI was able to drive expression not only in the MEE/periderm with high efficiency (7/14) (Fig. 4-3B and Fig. 4-6C, V, X), but also in the vasculature (including palatal vessels), nostrils and whisker follicles (Fig. 4-6C-F). Within this region, ECR-V is conserved only in mammals but ECR-VI is conserved in both mammals and avians suggesting that ECR-V would be more likely to contain palate-specific control elements. Indeed, this was the case, since the sequences between -9.6kb and -6.1kb including ECR-V targeted reporter activity to the MEE/periderm (Fig. 4-3 and Fig. 4-6H, Y, Z), while ECR-VI and surrounding sequences (from -13.7kb to -9.7kb) did not (Fig. 4-3 and data not shown). To narrow down the regions within -9.7kb and -6.1kb that contained putative cis-regulatory modules, we next examined a 0.3-kb fragment that encompassed the highly conserved ECR-V (from -7.9kb to -7.6kb), and an adjacent conserved 0.8-kb region from -7.4kb to -6.6kb (Fig. 4-6A). Each region drove reporter expression in the tips of palatal shelves but relatively weakly (Fig. 4-3 and Fig. 4-6M, R) and with far less specifically than the larger (-

13.7 - -6.1kb) fragment. These results suggest that the 3.5-kb region in *Ift43* intron 2 contains two or more cis-regulatory elements independently able to direct the reporter activity in the MEE and adjacent periderm, but they are needed in combination to drive expression efficiently.
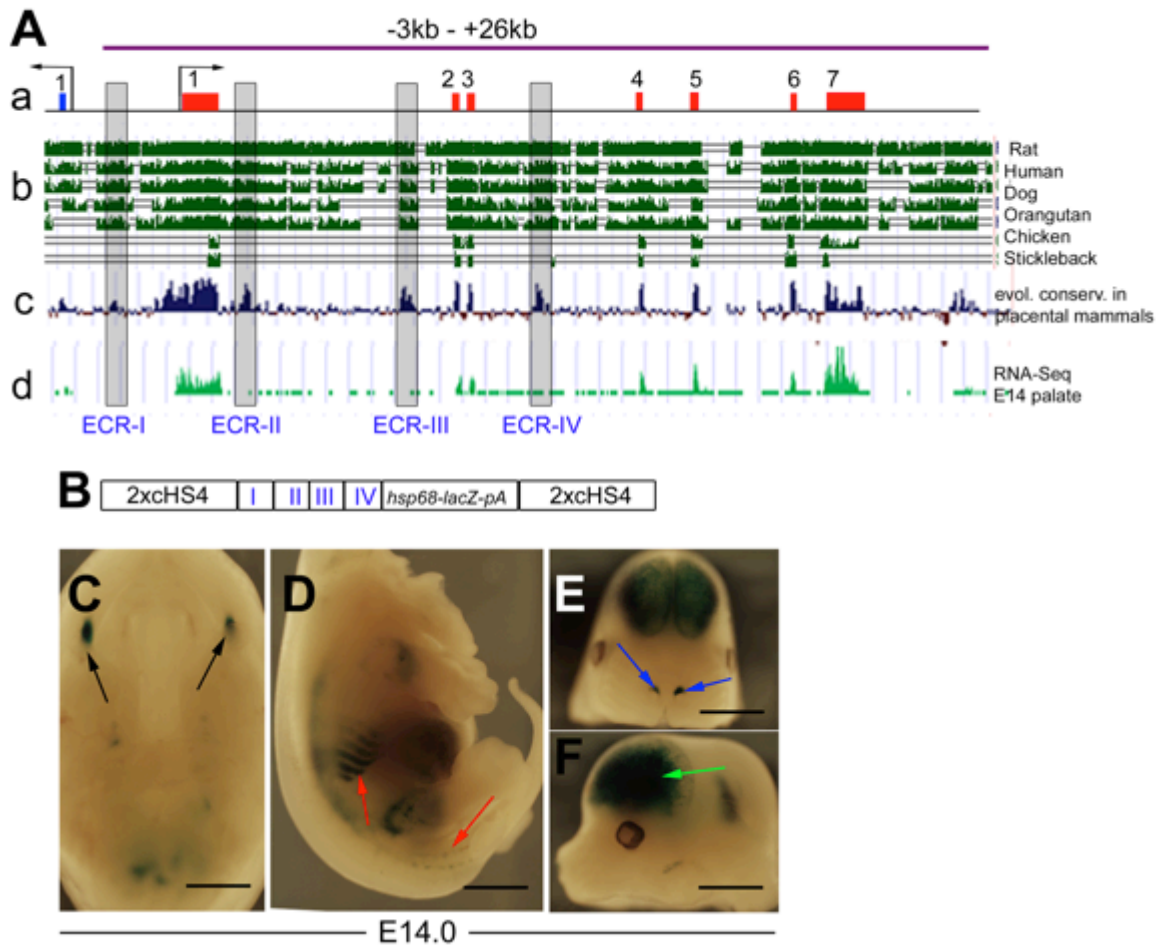
Figure 4-5. **Evolutionarily conserved regions within the *Tgfb3* gene do not direct reporter expression in palatal shelves.** A, Schematic representation (a) of the *Tgfb3* gene (red boxes depict *Tgfb3* exons 1-7; blue box depicts *Ift43* exon 1; black arrows show the TSSs for *Tgfb3* and *Ift43)* aligned with graphs of evolutionary sequence conservation among selected vertebrate species (b, UCSC genome browser), among placental mammals (c, UCSC genome browser) and RNA-seq profile in mouse palate at E14.5 (d, FaceBase Enhancer Project; A Visel)). Grey boxes indicate non-coding, evolutionarily conserved regions (ECRs I-IV). Purple line indicates the region present in the 29-kb *lacZ*-BAC. B, Schematic presentation of the reporter construct used to generate transgenic embryos shown in C-F. C-F, *ECR(1-IV)-hsp68-lacZ* embryos at E14 showing β-gal activity (blue staining) in molars (C, black arrows), ribs and lower spine (D, red arrows) and forebrain (F, green arrow). C, mouth roof at E14, inferior view, anterior on the top; D, torso at E14, right lateral view, E, head (mandible removed), frontal view; F, head (mandible removed), left lateral view. Scale bars in C, 700 μm; D, E, F, 1mm.
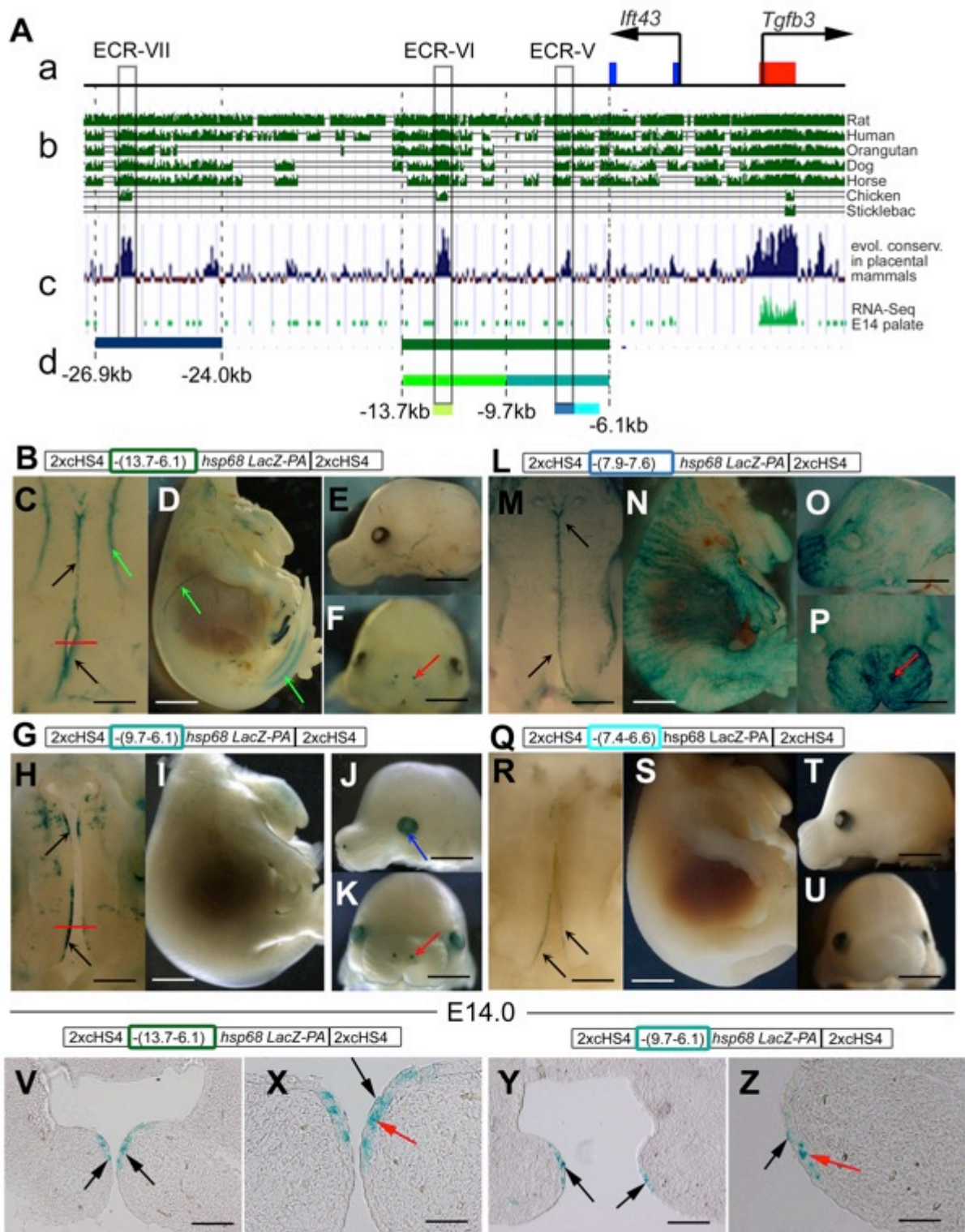
Figure 4-6. **Cis-regulatory elements targeting reporter activity to the MEE and adjacent periderm are located in intron 2 of the upstream *Ift43* gene.** A, a 28-kb sub-region of the 61-kb genomic fragment (a, see Fig. 4 and the main text) that includes *Tgfb3* exon 1 (red box) and exons 1 and 2 of the *Ift43* gene (blue boxes), (b) evolutionary sequence conservation among selected vertebrate species (UCSC genome browser), and (c) among placental mammals (UCSC genome browser), and (d) RNA-seq profile in mouse palate at E14.5 (FaceBase Enhancer Project; A Visel). Vertical rectangles depict the non-coding ECRs -V, -VI and -VII. Colored bars below (d) correspond to DNA fragments (see also Figure 3) examined by transient transgenic reporter assay in constructs shown schematically above images of the stained embryos generated (B-Y). C-F, Transgenic reporter embryos carrying a 7.6-kb DNA fragment from -13.7 to -6.1kb (green bar below (c) and green rectangle in construct schematic) showing β-gal activity (blue staining) in tips of palatal shelves (C, black arrows), blood vessels (C, D, green arrows) and nostrils (F, red arrow). H-K, Transgenic reporter embryos carrying a 3.6-kb DNA fragment from -9.7 to -6.1kb (-blue-green bar below (c) and blue-green rectangle in construct schematic) showing β-gal activity(blue staining) in tips of palatal shelves (H, black arrows), lens (J, blue arrow) and nostrils (K, red arrow). M-P, Transgenic reporter embryos carrying a 0.3-kb DNA fragment (ECR-V) from -7.9 to -7.6kb (light blue bar below (c) and light blue rectangle in construct schematic) showing β-gal activity (blue staining) in tips of palatal shelves (M, black arrows), apical ectoderm (N-P) and nostrils (P, red arrow). R-U, Transgenic reporter embryos carrying a 0.8-kb DNA fragment from -7.4 to -6.6kb (turquoise bar below (c) and rectangle in construct schematic) showing β-gal activity (blue staining) in tips of posterior palatal shelves (R, black arrows). V-X, Frontal sections of the X-Gal-stained 7.6-kb fragment transgenic embryo shown in C at the level of the posterior palate (indicated by the red line in C). Staining at the tips of palatal shelves (black arrows in V) is in both MEE cells (red arrow in X) and periderm cells (black arrow in X). Y-Z, Frontal sections of the X-Gal-stained 3.6-kb fragment transgenic embryo shown in H at the level of the posterior palate (indicated by the red line in H). Staining at the tips of palatal shelves (black arrows in Y) is in both in MEE cells (red arrow in Z) and periderm cells (black arrow in Z). Scale bars in C, H, M, R, 500µm; D, I, N, S, E, F, J, K, O, P, T, U, 1mm; V,Y, 100 µm; X, Z, 50µm.

4-4.5. An additional cis-regulatory region is located in a 5.3-kb fragment immediately upstream of *Tgfb3* exon 1

Since the overall conservation of the intergenic region between the *Ift43* and *Tgfb3* genes is relatively high, we examined whether this region could also contribute to MEE/periderm-specific expression. First we cloned the 9.8-kb region from -6.1kb to +3.7kb (i.e., *Ift43* intron 1, *Ift43* exon 1, intervening sequences between the *Ift43* and *Tgfb3* genes and *Tgfb3* exon 1) between concatamerized pairs of *cHS4* insulators, and inserted a *lacZ-PA* cassette in frame into the *Tgfb3* exon 1 (Fig. 4-7B). This construct, driven by the endogenous *Tgfb3* promoter, directed reporter activity specifically in the palatal midline region in transient transgenic embryos, although with a relatively low frequency (2/5) (Figs. 4-3B and 4-7C). To further define the important region within this 9.8kb fragment, we subcloned the 5.3-kb region from -6.1kb to -0.8kb into the 2xcHS4-*hsp68-lacZ-2xcHS4* vector, as it lacks the endogenous *Tgfb3* promoter (Fig. 4-7G). Two of the three resulting transgenic embryos showed reporter activity in the palatal midline (Fig. 4-7H) though also in several other tissues (Fig. 4-3 and 4-7I-K), suggesting that the shorter sequence lacked elements necessary for highly regionally specific regulation. Intron 1 of *Ift43* (from -6.1 to -3.7kb) alone, or the intervening sequence between *Ift43* and *Tgfb3* (from -3.7 to -0.8kb), did not direct β–galactosidase activity in the tips of palatal shelves (n=5 in each case) (Fig. 4-3B and data not shown). These data imply that a fragment from *Ift43* intron 1 to *Tgfb3* exon 1 contains a putative proximal MEE/periderm enhancer, which is dependent on DNA sequences separately located in smaller fragments.

A

Ift43   *Tgfb3*

Rat
Human
Orangutan
Dog
Horse
Chicken
Stickleback

evol. conserv. in placental mammals

RNA-Seq E14 palate

-6.1kb   -3.7kb   -0.8kb   +3.7kb
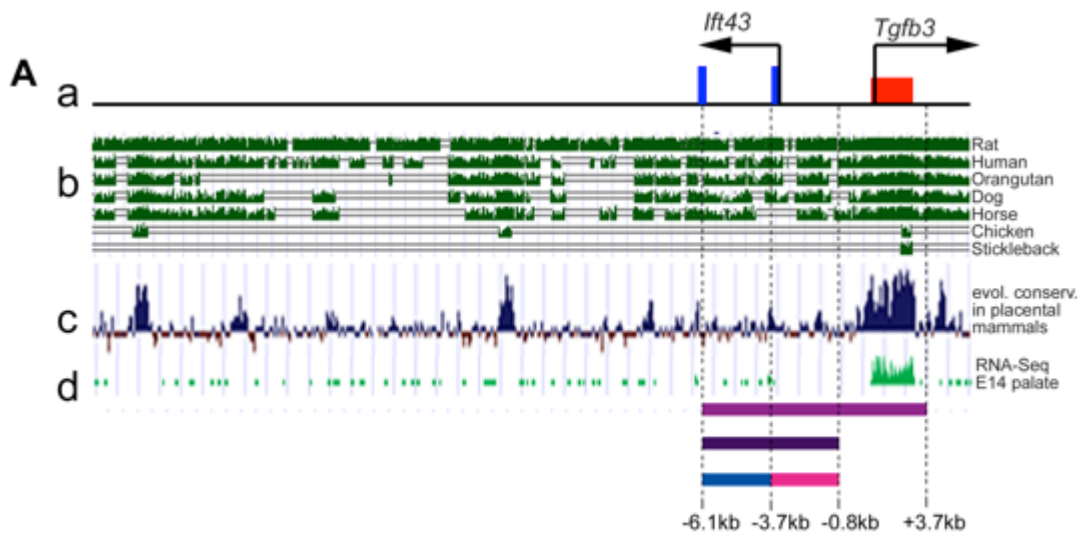
B | 2xcHS4 | -6.1 - +3.7 | *LacZ-PA* | 2xcHS4 |

G | 2xcHS4 | -(6.1-0.8) | *hsp68 LacZ-PA* | 2xcHS4 |

C **D** **E** **F**

H **I** **J** **K**
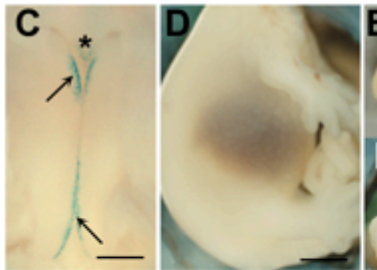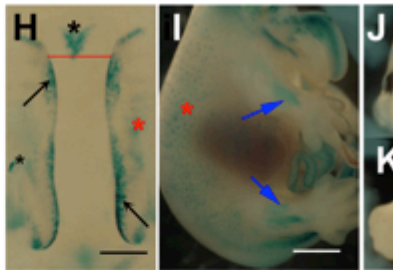
— E14.0 —

| 2xcHS4 | -(6.1-0.8) | *hsp68 LacZ-PA* | 2xcHS4 |

L **M** **N**

NS   PS   PS

PS   NS

139
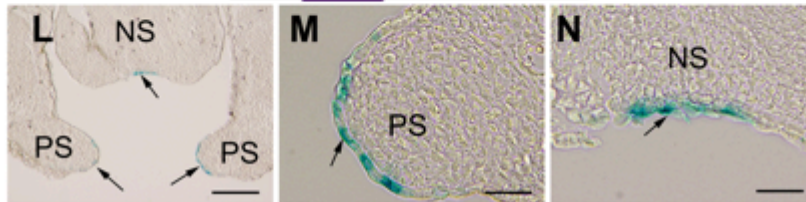
Fig. 4-7. **A putative proximal enhancer directing palatal expression lies in a 5.3-kb region upstream of the *Tgfb3* gene.** A, Schematic representation (a) of a 28-kb region upstream of *Tgfb3* exon 1 (red box) including *Ift43* exons 1 and 2 (blue boxes) aligned with (b) evolutionary conservation among selected vertebrate species (ucsc genome browser), (c) evolutionary conservation among the placental mammals (ucsc genome browser), (d) RNA-seq profile in mouse palate at E14.5. Colored bars below (d) correspond to DNA fragments examined using transient transgenic reporter assays (B-N). B, G, Schematic presentations of reporter constructs used to generate transgenic embryos (colored rectangles correspond to colored bars shown above (a)). C-F, Transgenic reporter embryo carrying the 9.8-kb DNA fragment from -6.1 to +3.7kb (magenta bar above (a) and magenta rectangle in B) showing β-gal activity (blue staining) in tips of palatal shelves (C, black arrows) and in the nasal septum (asterisk in C). No staining was seen in the torso (D) or head (E, F). H-K, Transgenic reporter embryo carrying the 5.3-kb DNA fragment from -6,1 to -0.8kb (dark purple bar above (a) and rectangle in G) showing β-gal activity (blue staining) in tips of palatal shelves (H, black arrows), in nasal septum (asterisk in H), in the ectoderm (red asterisks in H, I) and in skeletal structures (I, blue arrows) and olfactory bulbs (J, red arrows). L-N, Frontal sections of the X-Gal-stained 5.3-kb transgenic embryo shown in H at the level of the nasal septum (indicated by the red line in H). Staining can be seen at the tips of palatal shelves (black arrows in L, M) and in periderm cells of the nasal septum (black arrow in N). Scale bars in C, H, 500μm; D, I, E, F, J, K, 1mm; L, 200μm; M, N, 50μm.

4-5. Discussion

      Conditional Cre drivers are an invaluable tool for investigating the roles and timing of gene expression in processes involving several cell types such as palatogenesis. Key to this is knowledge of their recombination patterns and efficiency. Here we have shown that *K14*-Cre recombines efficiently in palatal medial edge epithelium (MEE) but it is not expressed in the overlying palatal periderm. This could explain the phenotypic differences between the germline *Tgfb3* mutants (in which no *Tgfb3* is expressed by MEE or periderm, periderm is inadequately shed and a complete cleft of the secondary palate occurs) and the epithelium-specific *Tgfb3:K14-Cre* mutants (in which genotypically normal periderm itself may be providing sufficient TGF-β3 signaling for some shedding, and thus a milder phenotype occurs). This proposed role for peridermal *Tgfb3* expression, and known peridermal responsiveness to TGF-β3-triggered signaling(Wu et al., 2013) combined with an inability of *K14-Cre* to recombine in peridermal cells could also explain why periderm behaves normally in *Tgfbr2:K14-Cre* mutants (Iwata et al., 2013). In contrast with these TGF-β3 signaling, *K14*-Cre conditional knock-outs, epithelium-specific β-catenin mutants (*Ctnn1b:K14-Cre*) lose *Tgfb3* expression in tips of palatal shelves but still develop total cleft of the secondary palate (He et al., 2011), raising the intriguing possibility that canonical Wnt signaling is specifically required in MEE for *Tgfb3* expression to occur in both the MEE and adjacent periderm. To test these and related hypotheses other conditional Cre drivers are required: to recombine only in palatal periderm, and to recombine in both MEE and the overlying periderm. It is not clear whether all other Cre-drivers currently used to delete genes in the palatal epithelium recombine in periderm as well, and many have additional limitations: *Pitx2-Cre* recombines predominantly in the posterior palatal epithelium (Xiong et al., 2009); recombination in the *Foxg1-Cre* line is highly background-dependent (Hebert and McConnell,

2000); and, as *Tgfb3* itself is expressed and required in several other tissues besides MEE and adjacent periderm during early embryogenesis, the *Tgfb3-Cre* knock-in line is of very limited use in studies of palatal epithelial fusion (Yang et al., 2008). As expression of *Tgfb3* in MEE and in periderm is so crucial to normal palatogenesis, occurs in precisely the regions where we would like to regulate the expression of other genes genetically, and its regulation poorly understood, we set out to identify the enhancer sequences responsible for this highly specific expression of *Tgfb3*. Using BAC deletion analysis we were able to identify a 61-kb region around the *Tgfb3* gene that could drive *lacZ* reporter expression specifically in the MEE and adjacent periderm. Expression of this reporter was much more specific to the MEE/periderm than that of the endogenous *Tgfb3* gene, and as this 61-kb region did not drive detectable expression before E12.5 it is a good candidate region for the development of novel palatal epithelium/periderm-specific Cre-driver lines.

In order to use enhancer sequence information to learn more about molecular regulation of *Tgfb3* expression we needed to identify the important sequences more precisely. Palatogenesis is an evolutionarily conserved developmental process in amniote animals (Bush and Jiang, 2012). Mammals and reptiles have a fused secondary palate, and although avians develop a beak and have a naturally cleft palate (Ferguson, 1988) fusion can be induced by exposing the appropriate stage avian palatal shelves (which do not express endogenous *cTgfb3*) to human recombinant TGF-β3 (Sun et al., 1998). Although it was therefore likely that enhancers directing palatal expression would be amongst non-coding highly conserved sequences amongst mammals, these are very numerous, and those that lay within the *Tgfb3* gene (ECRI-IV) turned out not to be palatal enhancers. The FaceBase project (www.facebase.org -A. Visel) to identify craniofacial transcriptional enhancers using ChIP-Seq (IP using anti-p300)

recently released a dataset obtained on E14 whole palates but this was not helpful for our specific

project; within the 61-kb region only a region around *Tgfb3* exon 1 was flagged as being a

putative enhancer; we could demonstrate only a putative vascular enhancer in the area of ECR-

VII (Fig. 4-3, Fig. 4-4 and data not shown) where the anti-p300 binding was above the

background level in ECR-VII (Fig. 4-4).

By directing our analysis outside the *Tgfb3* gene within the 61kb fragment, we were able

to identify a distal 3.5-kb region in *Ift43* intron 2 and a proximal 5.3-kb region encompassing

Ift43 intron 1 and most of the intergenic sequence between the *Ift43* and *Tgfb3* genes able to

target the reporter activity to the MEE and adjacent periderm. However, these smaller regions

directed less specific and weaker reporter activity than the 61kb fragment. While we were able

to break the distal 3.5-kb region down further into two smaller modules, which again showed

further reduced activity, our attempts to narrow down the 5.3-kb proximal region into even

shorter sequences were not successful, suggesting that palate-specific reporter activity seen in the

larger region was dependent on two or more regulatory elements separately located in the smaller

fragments. Although the same approach has yielded relatively short enhancers that drive very

precise and strong expression in other cases (Chandler et al., 2007; Dodou et al., 2004), it is

established that not all physically concise and robust expression is regulated in such a simple

manner(Evans et al., 2012). Genetic regulatory network studies in Drosophila first introduced

the concept of 'shadow' enhancers (Lagha et al., 2012). Perry et al reported that, in addition to

the proximal primary enhancer located just upstream of the promoter, the *snail* gene is regulated

by a distal enhancer located within the neighboring locus(Perry et al., 2010), which they

suggested be defined as a 'shadow' enhancer. Subsequent studies have suggested that secondary

enhancers are needed to obtain sufficient phenotypic robustness to drive tightly controlled

expression of important developmental genes (Frankel et al., 2010). Our findings of putative proximal (primary) enhancer(s) and two (or more) distal enhancers in the neighboring upstream gene that work precisely but only weakly in isolation are reminiscent of this mechanism. A 'lack of simplicity' may also extend to the organization of enhancers for other tissues and repressive elements controlling *Tgfb3* expression as we noticed that, unlike the 61-kb region which directed reporter activity specifically in the MEE/periderm, many of the smaller domains around the ECR-V also targeted the reporter activity to the vasculature including the palatal vessels. Similar vascular patterns were seen in embryos carrying either ECR-VI or ECR-VII (which were unable to direct expression in the MEE/periderm) suggesting that all three ECRs located in intron 2 of *Ift43* possess putative redundant vascular enhancer activities.

Very little is known about the molecular mechanisms regulating *Tgfb3* expression in the epithelial tips of pre-fusion palatal shelves. Venza et al recently reported that in *Foxe1* mutant embryos *Tgfb3* expression is dramatically reduced in the palatal epithelium, and that *Tgfb3* is a direct target of FoxE1 via FoxE1 binding sites in the *Tgfb3* promoter region (Venza et al., 2011). As outlined above, He et al reported that epithelium-specific mouse mutants lacking the gene encoding β-catenin also show a dramatic reduction in*Tgfb3* expression in the palatal epithelium suggesting that canonical Wnt signaling is involved in *Tgfb3* regulation (He et al., 2011). Whether these identified transcriptional regulators function purely by contributing to the core promoter activity or by also regulating *Tgfb3* expression via distal enhancers is not yet known. Nevertheless, even the smallest cis-regulatory region identified in this study (i.e., the 300-bp ECR-V located in the *Ift43* intron 2) contained three evolutionarily conserved TCF/LEF consensus binding sites and two FoxE1 binding sites (data not shown) implying that these factors may have the capacity to regulate *Tgfb3* in palatal shelf tissues by binding directly to the putative

144

enhancer elements. Thus our results are consistent with existing molecular regulation data, and suggest a model in which the MEE/periderm-specific *Tgfb3* expression is achieved via a complex regulatory landscape composed of a putative proximal (primary) enhancer(s) and two (or more) distal shadow enhancers i.e. some that lie in the neighboring upstream gene.

Chapter 5:

Conclusions

5.1. Summary of findings

Previous to work presented in this thesis, Smad-dependent TGF-β signaling within the palatal mesenchyme and epithelium was thought to be the key contributor to forming a functional palate. However, many of the studies that exist have been focused on conditional removal of Smad-dependent signaling components. Here, we show that Smad-independent signaling components Tak1 and Trim33 along with Smad4 play an under appreciated role in palatogenesis.

5.2. Tak1 signaling in the craniofacial neural crest

Our data demonstrate that Tak1 plays a larger role in craniofacial ectomesenchyme than just TGF-β and Bmp-induced activation of p38 Mapk (Smad-independent). Tak1 is responsible for agonist induced c-terminal and linker phosphorylation of Smad2 (Smad-dependent), which is needed for full transcriptional activation. In the absence of *Tak1* in the ectomesenchyme, palatal shelves fail to elevate and fuse. Previous to this study, the role of Tak1 in the mesenchyme was unknown; surprisingly Tak1 plays a role in both the Smad-independent and Smad-dependent TGF-β signaling pathway (Figure 5-2).

Tak1 phosphorylates the c-terminus of Smad2 in the mesenchyme during palatogenesis and when Tak1 is absent, Smad2 is not fully activated. This leads to a reduction of Smad2 in the

146

nucleus and therefor a reduction of Smad2 linker region phosphorylation. It has been shown that the linker region phosphorylation at Thr-220 is phosphorylated by CDKs and Mapks (JNK/ERK) phosphorylates Ser-250. When we inhibited CDKs in primary palatal mesenchymal cells, we saw that phosphorylation at both Thr-220 and Ser-250 was reduced. The next step would be to study the exact mechanism of phosphorylation by CDKs and the exact role Tak1 plays on the phosphorylation of the Smad2 linker region in the nucleus. In addition, it would be good to follow up on the "action turnover switch model" where the linker region phosphorylation is needed for full R-Smad activation and cessation of activation, which has never been examined in-vivo. In this model nuclear CDKs phosphorylate Thr-220 in Smad2 and create docking sites for transcriptional co-regulators, which then allows phosphorylation of Ser-250 in Smad2, which ultimately provides a docking site for ubiquitin ligases, which target Smad2 for proteasome-mediated degradation. How phosphorylation of Smad2 mediated by Tak1 provides docking sites for co-regulators and ubiquitin ligases and ultimately turns on and off Smad2 activity would add additional information on the role of the linker region phosphorylation in the larger signaling scheme.

The upstream components that lead to Tak1 activation during TGF-β signaling are not well known. Although, Tak1 is activated by TGF-β2 stimulation, the role of TGFβRI kinase activity on the activation of Tak1 has not been clearly examined. Additionally, there is a clear overlap between TGF-β-induced transcriptional responses dependent on both TGFβRI and Tak1 kinase activities. Our studies tested the role of TGFβRI protein lacking kinase activity with the use of the chemical inhibitor. Exactly how TGFβRI kinase activities or the presence of *TgfbrI* work to regulate downstream signaling events is an area for future research.

5.3. Tak1, Trim33 and Smad4 signaling in the pre-fusion palatal epithelium

Tak1 is expressed in the mesenchyme and in the epithelium of the developing palate. We show that when *Tak1* alone is removed from the palatal epithelium, there is no resulting palatal phenotype. Interestingly, we found that if *Smad4* is removed from the palatal epithelium, there is a subtle, but apparent defect in palatogenesis, which was not addressed in previous studies (Xu et al., 2006). However, if we remove *Tak1* and *Smad4* together, there is a resulting phenotype, which is more severe than removal of *Smad4* alone. We found that this defect resulted in a decrease in TGF-β3 signaling.

It is possible that phosphorylated Smad2 can partner with other transcriptional regulators to regulate target gene expression. We have shown that specific removal of *Trim33* alone in the palatal epithelium does not have a phenotype. However, when *Trim33* and *Smad4* are removed there is persistence of the midline epithelial seam.

Ultimately, Tak1, Trim33 and Smad4 play cooperative roles in MES removal and lead to a complete palate. We found that although the three genes play redundant roles, when two genes are removed (*Trim33 and Smad4*) along with an inhibitor against the third gene (*Tak1*), there is a more severe cleft of the secondary palate. (Figure 5-3)

Previously to this study, there has not been any research done on the mechanism by which p38 is activated within the palatal epithelium. We found *Tak1* is upstream of *p38* and that *Tak1* and *Smad4* work together to form a complete palate. We also found that when *Tak1* and *Smad4* are removed it does not result in the same phenotype as the *Tgfb3* global or *K14-Cre* conditional knockouts. This suggests that there are likely more genes involved in the removal of the midline epithelial seam. In the future, it is possible that TGF-β3 signaling along with another

pathway may work together to form the palate. What these molecules are is something that will need to be examined.

It is known that when Smad2 is activated through TGF-β3 dependent activation, it binds Smad4 and accumulates in the nucleus leading to target gene regulation. Although, there is advanced knowledge in signaling pathways, little is known about epigenetic alterations that allow the chromatin state to be coordinated with gene expression. Trim33 has been shown to be a histone-binding protein which complexes with Smad2 forming a Trim33-Smad2 chromatin reading complex (Xi et al., 2011). This reading complex recognizes and binds repressive marks on the histone tail, and increases acetylation, which allows Smad4 access to regulate target genes. However, if Trim33 is playing this role in the palatal epithelium is unknown. We have found in this study that Trim33 is needed along with Smad4 for *p21* expression leading to complete removal of the midline epithelial seam. Future studies could help to elucidate the exact mechanisms by which Trim33 plays a role in the nucleus leading to target gene expression resulting in removal of the midline epithelial seam.

5.4. *Tgfb3* expression in pre-fusion palatal epithelium

How does *Tgfb3* get specifically expressed within the MES? We know from previous studies that when *B-catenin* or *Foxe1* is removed from the palatal epithelium it leads to a complete cleft of the secondary palate and a reduction in *Tgfb3* expression (He et al., 2011; Venza et al., 2011). This study has shown for the first time the presence of multiple cis-regulatory elements that drive specific expression of *Tgfb3* in the palatal epithelium during palatogenesis (Figure 5-3).

Not much has been known about the upstream regulation of Tgfb3 expression. Amongst the cis-regulatory elements that we have found, we looked closely for the presence of downstream transcription factors that would bind and drive expression of *Tgfb3*, LEF1 and FOX transcription factor binding sites (Figure 5-1). A future experiment that could be done would be to use ChIP against the LEF1 and FOX sites and examine where they bound on the *Tgfb3* cis-regulatory elements that we have identified. We could then use these areas of binding to determine if they can drive expression and ultimately teach us about the upstream regulation of *Tgfb3*.

Finally, the next step in this research would be to make a transgenic mouse line using the cis-regulatory elements that we have found in this study. More specifically, we could use the 61kb fragment, which provided the most specific reporter activity. The mouse line would be useful to remove genes both in the palatal epithelium and periderm. We could then study the roles of genes in both the epithelium and overlying periderm during the exact times of adhesion and fusion.

5-5. TGF-β3 signaling during palatogenesis and health significance

The long-term goal of these studies is to understand the signaling mechanisms that are needed for proper palatogenesis. We can then prevent clefting in patients and remove the long-term nutritional and societal issues for these individuals.
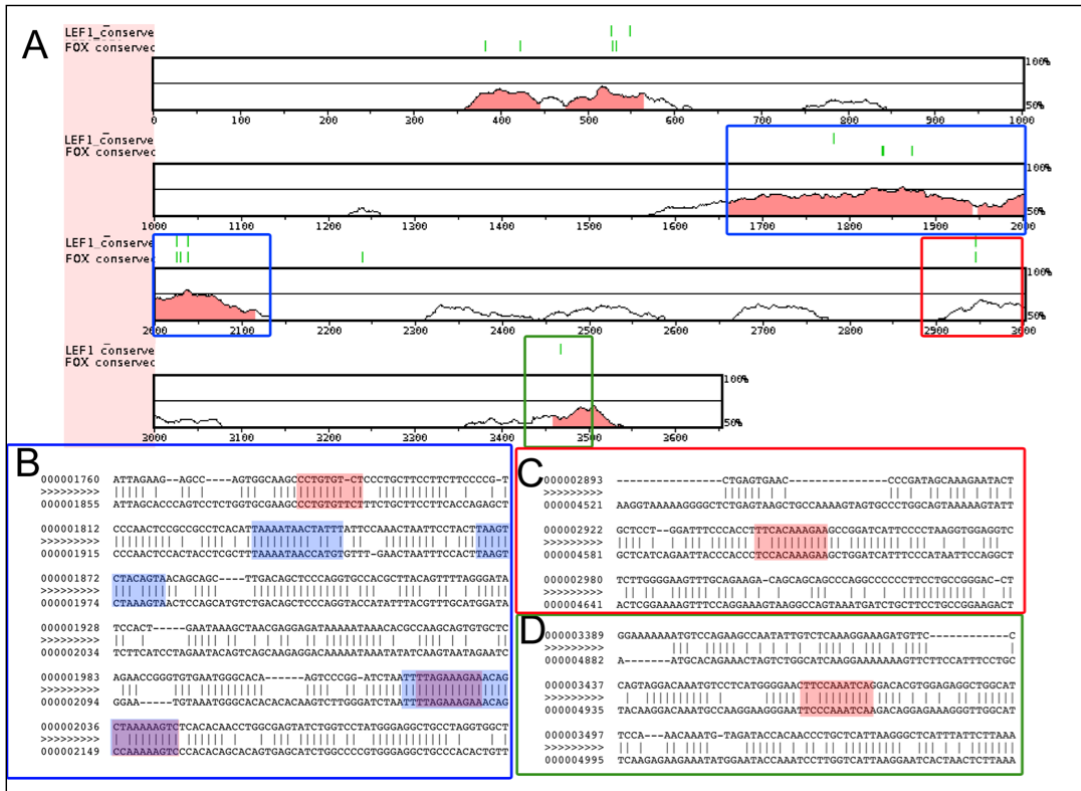
Figure 5-1. LEF1 and FOX sequence alignment to identified cis-regulatory elements of *Tgfb3.* A. Regions of the *Tgfb3* gene are shown with conservation between mouse and human. Above each area of conservation there are green lines that indicate the presence of either a LEF1 or FOX binding site. B. A larger detailed view of the blue-boxed region in A, where the upper sequence refers to mouse and the lower sequence refers to human. Pink highlighted regions indicate the presence of a LEF1 site and the blue highlighted regions indicate the presence of a FOX binding site. If both LEF1 and FOX binding sites are present, it is indicated in purple. C. A larger detailed view of the red-boxed region in A. The presence of one LEF1 site is indicated. D. A larger detailed view of the green-boxed region in A. The presence of one LEF1 site is indicated.
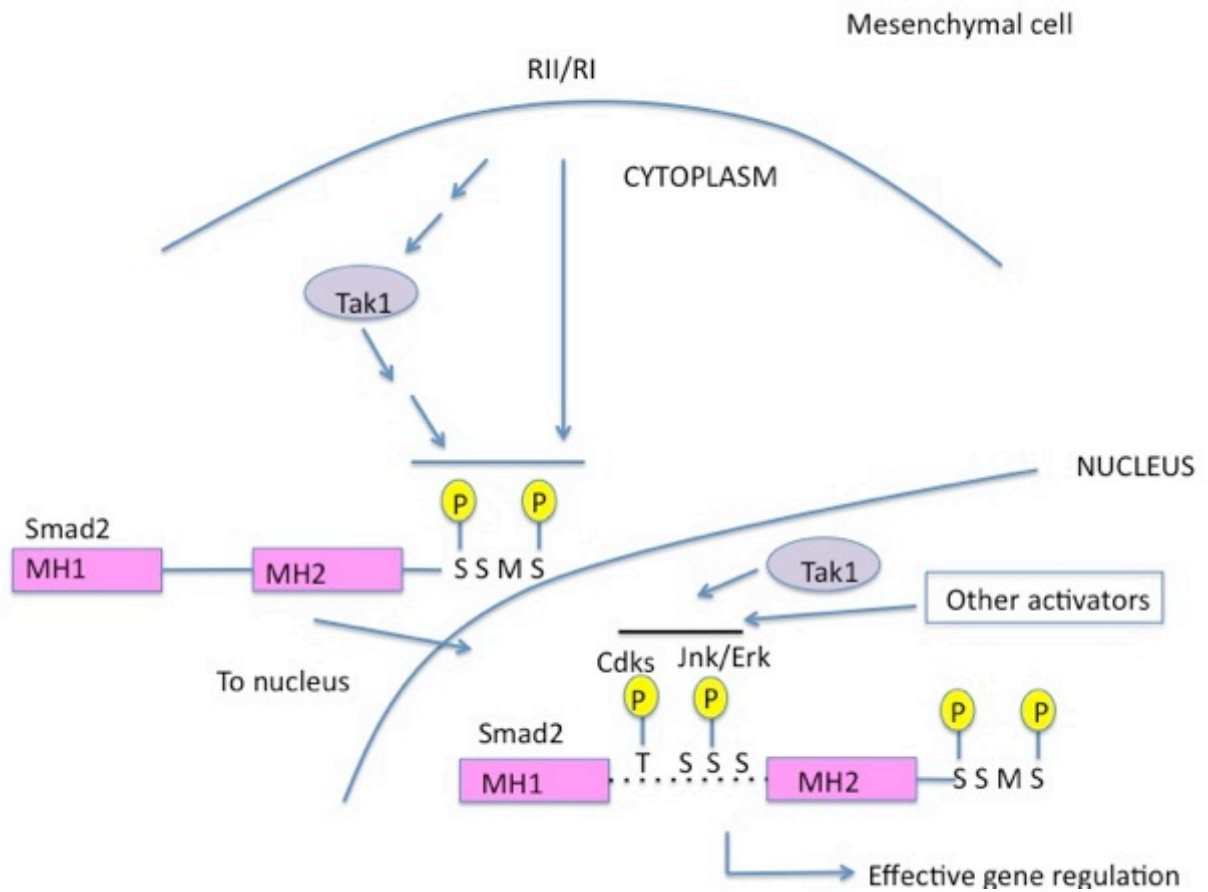
Figure 5-2. Schematic representation of mesenchymal Smad2 activation via Tak1.

Upon TGF-β activation, Smad2 C-terminal phosphorylation is increased in the presence of Tak1. Cdk-dependent phosphorylation of Threonine-220 occurs in the nucleus along with Jnk/ERK dependent phosphorylation of Serine-250.
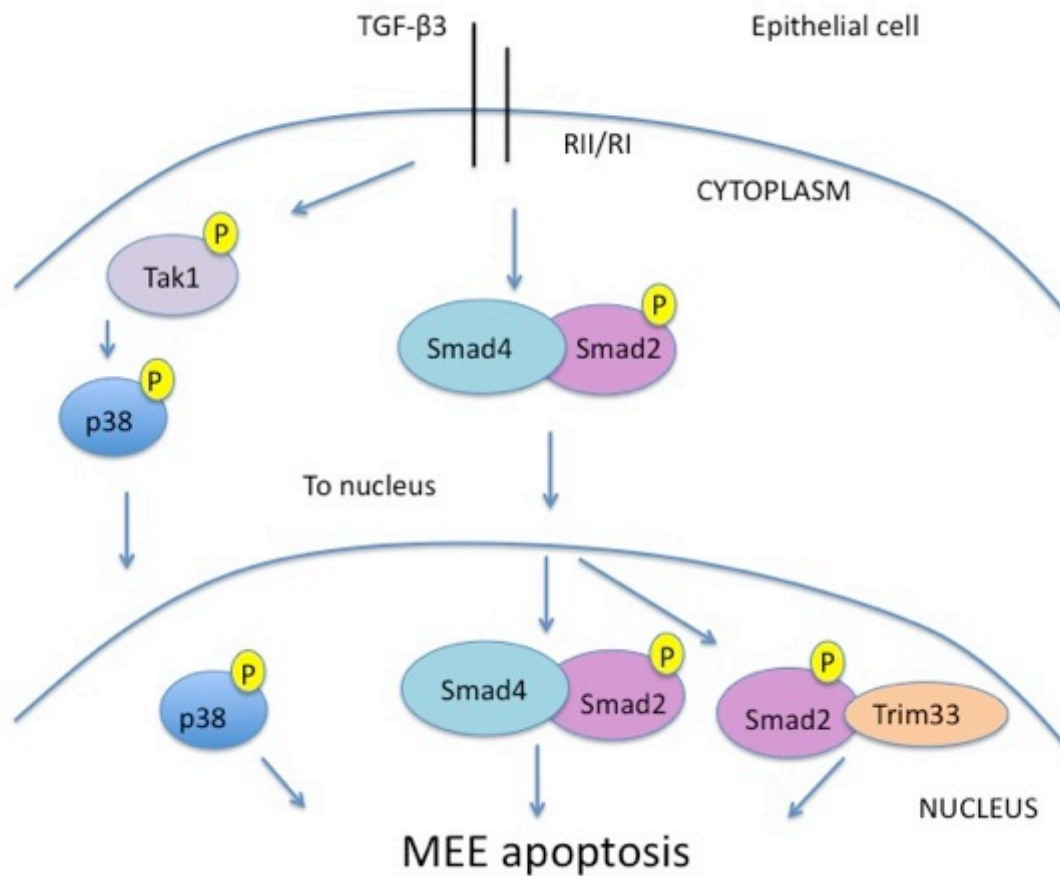
Figure 5-3. Schematic representation of Tak1, Smad4 and Trim33 redundant functions during palatal epithelial fusion.

Tak1 and Smad2 are activated upon TGF-β3 activation. Tak1 activates p38 where is performs a redundant role in leading to medial edge epithelium (MEE) apoptosis. Activated Smad2 binds to the common co-mediator, Smad4 where Smad2/Smad4 accumulate in the nucleus and play a redundant role in MEE apoptosis. Some nuclear activated Smad2 binds to Trim33 in the nucleus and also plays a role in MEE apoptosis.
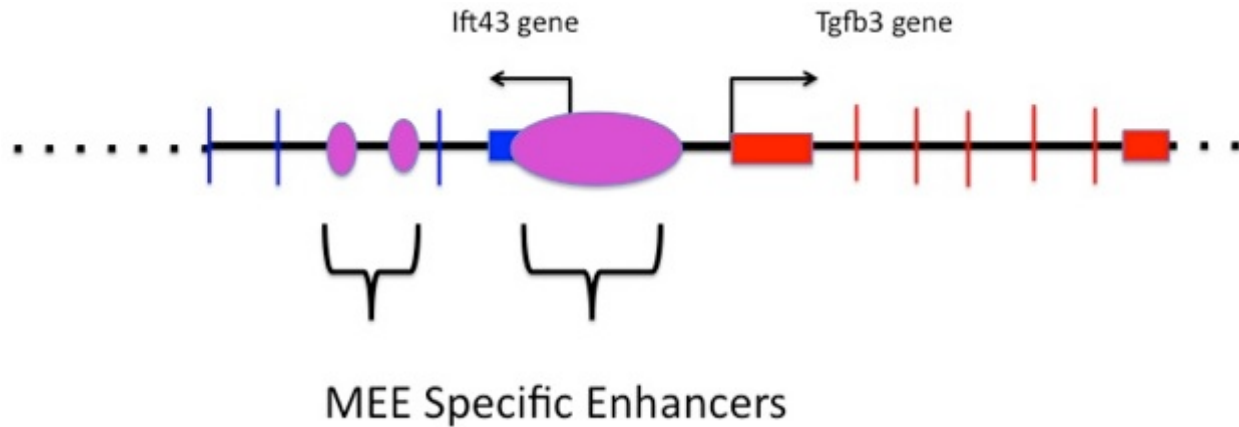
Figure 5-4. Schematic representation of medial edge epithelium (MEE) specific cis-regulatory elements.

Three cis-regulatory elements were identified; one in the intergenic region between the *Ift43* and *Tgfb3* genes, and two small, non-coding, evolutionarily conserved regions in intron 2 of the *Ift43* gene.

Bibliography

.

Agricola, E., Randall, R.A., Gaarenstroom, T., Dupont, S., Hill, C.S., 2011. Recruitment of TIF1gamma to chromatin via its PHD finger-bromodomain activates its ubiquitin ligase and transcriptional repressor activities. Molecular cell 43, 85-96.

Ahmed, S., Liu, C.C., Nawshad, A., 2007. Mechanisms of palatal epithelial seam disintegration by transforming growth factor (TGF) beta3. Developmental biology 309, 193-207.

Alappat, S.R., Zhang, Z., Suzuki, K., Zhang, X., Liu, H., Jiang, R., Yamada, G., Chen, Y., 2005. The cellular and molecular etiology of the cleft secondary palate in Fgf10 mutant mice. Dev.Biol. 277, 102-113.

Alarcon, C., Zaromytidou, A.I., Xi, Q., Gao, S., Yu, J., Fujisawa, S., Barlas, A., Miller, A.N., Manova-Todorova, K., Macias, M.J., Sapkota, G., Pan, D., Massague, J., 2009. Nuclear CDKs drive Smad transcriptional activation and turnover in BMP and TGF-beta pathways. Cell 139, 757-769.

Andl, T., Ahn, K., Kairo, A., Chu, E.Y., Wine-Lee, L., Reddy, S.T., Croft, N.J., Cebra-Thomas, J.A., Metzger, D., Chambon, P., Lyons, K.M., Mishina, Y., Seykora, J.T., Crenshaw, E.B., 3rd, Millar, S.E., 2004. Epithelial Bmpr1a regulates differentiation and proliferation in postnatal hair follicles and is essential for tooth development. Development 131, 2257-2268.

Aragon, E., Goerner, N., Zaromytidou, A.I., Xi, Q., Escobedo, A., Massague, J., Macias, M.J., 2011. A Smad action turnover switch operated by WW domain readers of a phosphoserine code. Genes & development 25, 1275-1288.

Baek, J.A., Lan, Y., Liu, H., Maltby, K.M., Mishina, Y., Jiang, R., 2011. Bmpr1a signaling plays critical roles in palatal shelf growth and palatal bone formation. Developmental biology 350, 520-531.

Behringer, A.N.M.G.K.V.R., 2003. Manipulating the mouse embryo - a laboratory manual, Third ed. Academic Press, New York.

Bellusci, S., Furuta, Y., Rush, M.G., Henderson, R., Winnier, G., Hogan, B.L., 1997. Involvement of Sonic hedgehog (Shh) in mouse embryonic lung growth and morphogenesis. Development 124, 53-63.

Blobe, G.C., Schiemann, W.P., Lodish, H.F., 2000. Role of transforming growth factor beta in human disease. The New England journal of medicine 342, 1350-1358.

Block, S.R., Watkins, S.M., Salemi, J.L., Rutkowski, R., Tanner, J.P., Correia, J.A., Kirby, R.S., 2013. Maternal pre-pregnancy body mass index and risk of selected birth defects: evidence of a dose-response relationship. Paediatric and perinatal epidemiology 27, 521-531.

Bush, J.O., Jiang, R., 2012. Palatogenesis: morphogenetic and molecular mechanisms of secondary palate development. Development 139, 231-243.

Bush, J.O., Lan, Y., Maltby, K.M., Jiang, R., 2002. Isolation and developmental expression analysis of Tbx22, the mouse homolog of the human X-linked cleft palate gene. Developmental dynamics : an official publication of the American Association of Anatomists 225, 322-326.

Capecchi, M.R., 2005. Gene targeting in mice: functional analysis of the mammalian genome for the twenty-first century. Nature reviews. Genetics 6, 507-512.

Cardoso, S., Robertson, S.P., Daniel, P.B., 2012. TGFBR1 mutations associated with Loeys-Dietz syndrome are inactivating. J Recept Signal Transduct Res 32, 150-155.

Carinci, F., Scapoli, L., Palmieri, A., Zollino, I., Pezzetti, F., 2007. Human genetic factors in nonsyndromic cleft lip and palate: an update. Int J Pediatr Otorhinolaryngol 71, 1509-1519.

Carver, E.A., Stubbs, L., 1997. Zooming in on the human-mouse comparative map: genome conservation re-examined on a high-resolution scale. Genome research 7, 1123-1137.

Casey, L.M., Lan, Y., Cho, E.S., Maltby, K.M., Gridley, T., Jiang, R., 2006. Jag2-Notch1 signaling regulates oral epithelial differentiation and palate development. Dev.Dyn. 235, 1830-1844.

Chai, Y., Jiang, X., Ito, Y., Bringas, P., Jr., Han, J., Rowitch, D.H., Soriano, P., McMahon, A.P., Sucov, H.M., 2000. Fate of the mammalian cranial neural crest during tooth and mandibular morphogenesis. Development 127, 1671-1679.

Chai, Y., Maxson, R.E., Jr., 2006. Recent advances in craniofacial morphogenesis. Dev.Dyn. 235, 2353-2375.

Chandler, R.L., Chandler, K.J., McFarland, K.A., Mortlock, D.P., 2007. Bmp2 transcription in osteoblast progenitors is regulated by a distant 3' enhancer located 156.3 kilobases from the promoter. Molecular and cellular biology 27, 2934-2951.

Cohen-Solal, K.A., Merrigan, K.T., Chan, J.L., Goydos, J.S., Chen, W., Foran, D.J., Liu, F., Lasfar, A., Reiss, M., 2011. Constitutive Smad linker phosphorylation in melanoma: a mechanism of resistance to transforming growth factor-beta-mediated growth inhibition. Pigment Cell Melanoma Res 24, 512-524.

Daly, A.C., Randall, R.A., Hill, C.S., 2008. Transforming growth factor beta-induced Smad1/5 phosphorylation in epithelial cells is mediated by novel receptor complexes and is essential for anchorage-independent growth. Molecular and cellular biology 28, 6889-6902.

Danielian, P.S., Muccino, D., Rowitch, D.H., Michael, S.K., McMahon, A.P., 1998. Modification of gene activity in mouse embryos in utero by a tamoxifen- inducible form of Cre recombinase. Curr.Biol. 8, 1323-1326.

Derynck, R., Zhang, Y., Feng, X.H., 1998. Smads: transcriptional activators of TGF-beta responses. Cell 95, 737-740.

Derynck, R., Zhang, Y.E., 2003. Smad-dependent and Smad-independent pathways in TGF-beta family signalling. Nature 425, 577-584.

Descargues, P., Sil, A.K., Sano, Y., Korchynskyi, O., Han, G., Owens, P., Wang, X.J., Karin, M., 2008. IKKalpha is a critical coregulator of a Smad4-independent TGFbeta-Smad2/3 signaling pathway that controls keratinocyte differentiation. Proceedings of the National Academy of Sciences of the United States of America 105, 2487-2492.

Dixon, M.J., Marazita, M.L., Beaty, T.H., Murray, J.C., 2011. Cleft lip and palate: understanding genetic and environmental influences. Nature reviews. Genetics 12, 167-178.

Dodou, E., Verzi, M.P., Anderson, J.P., Xu, S.M., Black, B.L., 2004. Mef2c is a direct transcriptional target of ISL1 and GATA factors in the anterior heart field during mouse embryonic development. Development 131, 3931-3942.

Doetschman, T., Georgieva, T., Li, H., Reed, T.D., Grisham, C., Friel, J., Estabrook, M.A., Gard, C., Sanford, L.P., Azhar, M., 2012. Generation of mice with a conditional allele for the transforming growth factor beta3 gene. Genesis 50, 59-66.

Dudas, M., Kaartinen, V., 2005. Tgf-beta superfamily and mouse craniofacial development: interplay of morphogenetic proteins and receptor signaling controls normal formation of the face. Curr.Top.Dev.Biol. 66:65-133., 65-133.

Dudas, M., Kim, J., Li, W.Y., Nagy, A., Larsson, J., Karlsson, S., Chai, Y., Kaartinen, V., 2006. Epithelial and ectomesenchymal role of the type I TGF-beta receptor ALK5 during facial morphogenesis and palatal fusion. Dev.Biol. 296, 298-314.

Dudas, M., Li, W.Y., Kim, J., Yang, A., Kaartinen, V., 2007. Palatal fusion - Where do the midline cells go? A review on cleft palate, a major human birth defect. Acta Histochem. 109, 1-14.

Dudas, M., Nagy, A., Laping, N.J., Moustakas, A., Kaartinen, V., 2004. Tgf-beta3-induced palatal fusion is mediated by Alk-5/Smad pathway. Dev.Biol. 266, 96-108.

Economou, A.D., Ohazama, A., Porntaveetus, T., Sharpe, P.T., Kondo, S., Basson, M.A., Gritli-Linde, A., Cobourne, M.T., Green, J.B., 2012. Periodic stripe formation by a Turing mechanism operating at growth zones in the mammalian palate. Nature genetics 44, 348-351.

Evans, M., 2011. Discovering pluripotency: 30 years of mouse embryonic stem cells. Nature reviews. Molecular cell biology 12, 680-686.

Evans, M.J., Kaufman, M.H., 1981. Establishment in culture of pluripotential cells from mouse embryos. Nature 292, 154-156.

Evans, N.C., Swanson, C.I., Barolo, S., 2012. Sparkling insights into enhancer structure, function, and evolution. Current topics in developmental biology 98, 97-120.

Falk, S., Joosten, E., Kaartinen, V., Sommer, L., 2013. Smad4 and Trim33/Tif1gamma Redundantly Regulate Neural Stem Cells in the Developing Cortex. Cerebral cortex.

Feil, S., Valtcheva, N., Feil, R., 2009. Inducible Cre mice. Methods in molecular biology 530, 343-363.

Ferguson, M.W., 1987. Palate development: mechanisms and malformations. Ir.J.Med.Sci. 156, 309-315.

Ferguson, M.W., 1988. Palate development. Development 103 Suppl, 41-60.

Fitzpatrick, D.R., Denhez, F., Kondaiah, P., Akhurst, R.J., 1990. Differential expression of TGF beta isoforms in murine palatogenesis. Development 109, 585-595.

Frankel, N., Davis, G.K., Vargas, D., Wang, S., Payre, F., Stern, D.L., 2010. Phenotypic robustness conferred by apparently redundant transcriptional enhancers. Nature 466, 490-493.

Fraser, F.C., Walker, B.E., Trasler, D.G., 1957. Experimental production of congenital cleft palate: genetic and environmental factors. Pediatrics 19, 782-787.

Friedel, R.H., Wurst, W., Wefers, B., Kuhn, R., 2011. Generating conditional knockout mice. Methods in molecular biology 693, 205-231.

Funato, N., Nakamura, M., Richardson, J.A., Srivastava, D., Yanagisawa, H., 2012. Tbx1 regulates oral epithelial adhesion and palatal development. Human molecular genetics 21, 2524-2537.

Gao, S., Alarcon, C., Sapkota, G., Rahman, S., Chen, P.Y., Goerner, N., Macias, M.J., Erdjument-Bromage, H., Tempst, P., Massague, J., 2009. Ubiquitin ligase Nedd4L targets activated Smad2/3 to limit TGF-beta signaling. Molecular cell 36, 457-468.

Gingery, A., Bradley, E.W., Pederson, L., Ruan, M., Horwood, N.J., Oursler, M.J., 2008. TGF-beta coordinately activates TAK1/MEK/AKT/NFkB and SMAD pathways to promote osteoclast survival. Experimental cell research 314, 2725-2738.

Goudy, S., Law, A., Sanchez, G., Baldwin, H.S., Brown, C., 2010. Tbx1 is necessary for palatal elongation and elevation. Mechanisms of development 127, 292-300.

Grainge, I., Pathania, S., Vologodskii, A., Harshey, R.M., Jayaram, M., 2002. Symmetric DNA sites are functionally asymmetric within Flp and Cre site-specific DNA recombination synapses. Journal of molecular biology 320, 515-527.

Gregory, S.G., Sekhon, M., Schein, J., Zhao, S., Osoegawa, K., Scott, C.E., Evans, R.S., Burridge, P.W., Cox, T.V., Fox, C.A., Hutton, R.D., Mullenger, I.R., Phillips, K.J., Smith, J., Stalker, J., Threadgold, G.J., Birney, E., Wylie, K., Chinwalla, A., Wallis, J., Hillier, L., Carter, J., Gaige, T., Jaeger, S., Kremitzki, C., Layman, D., Maas, J., McGrane, R., Mead, K., Walker, R., Jones, S., Smith, M., Asano, J., Bosdet, I., Chan, S., Chittaranjan, S., Chiu, R., Fjell, C., Fuhrmann, D., Girn, N., Gray, C., Guin, R., Hsiao, L., Krzywinski, M., Kutsche, R., Lee, S.S., Mathewson, C., McLeavy, C., Messervier, S., Ness, S., Pandoh, P., Prabhu, A.L., Saeedi, P., Smailus, D., Spence, L., Stott, J., Taylor, S., Terpstra, W., Tsai, M., Vardy, J., Wye, N., Yang, G., Shatsman, S., Ayodeji, B., Geer, K., Tsegaye, G., Shvartsbeyn, A., Gebregeorgis, E., Krol, M., Russell, D., Overton, L., Malek, J.A., Holmes, M., Heaney, M., Shetty, J., Feldblyum, T., Nierman, W.C., Catanese, J.J., Hubbard, T., Waterston, R.H., Rogers, J., de Jong, P.J., Fraser, C.M., Marra, M., McPherson, J.D., Bentley, D.R., 2002. A physical map of the mouse genome. Nature 418, 743-750.

Griswold, S.L., Sajja, K.C., Jang, C.W., Behringer, R.R., 2011. Generation and characterization of iUBC-KikGR photoconvertible transgenic mice for live time-lapse imaging during development. Genesis 49, 591-598.

Gritli-Linde, A., 2007. Molecular control of secondary palate development. Dev.Biol. 301, 309-326.

Han, J., Mayo, J., Xu, X., Li, J., Bringas, P., Jr., Maas, R.L., Rubenstein, J.L., Chai, Y., 2009. Indirect modulation of Shh signaling by Dlx5 affects the oral-nasal patterning of palate and rescues cleft palate in Msx1-null mice. Development 136, 4225-4233.

Harlow, E., Lane, D., 1988. Antibodies. A Laboratory Manual. CSH Press, New York.

Hashmi, S.S., Waller, D.K., Langlois, P., Canfield, M., Hecht, J.T., 2005. Prevalence of nonsyndromic oral clefts in Texas: 1995-1999. American journal of medical genetics. Part A 134, 368-372.

He, F., Xiong, W., Wang, Y., Li, L., Liu, C., Yamagami, T., Taketo, M.M., Zhou, C., Chen, Y., 2011. Epithelial Wnt/beta-catenin signaling regulates palatal shelf fusion through regulation of Tgfbeta3 expression. Developmental biology 350, 511-519.

He, W., Dorn, D.C., Erdjument-Bromage, H., Tempst, P., Moore, M.A., Massague, J., 2006. Hematopoiesis controlled by distinct TIF1gamma and Smad4 branches of the TGFbeta pathway. Cell. 125, 929-941.

Hebert, J.M., McConnell, S.K., 2000. Targeting of cre to the Foxg1 (BF-1) locus mediates loxP recombination in the telencephalon and other developing head structures. Developmental biology 222, 296-306.

Hilliard, S.A., Yu, L., Gu, S., Zhang, Z., Chen, Y.P., 2005. Regional regulation of palatal growth and patterning along the anterior-posterior axis in mice. J.Anat. 207, 655-667.

Hoffmann, A., Preobrazhenska, O., Wodarczyk, C., Medler, Y., Winkel, A., Shahab, S., Huylebroeck, D., Gross, G., Verschueren, K., 2005. Transforming growth factor-beta-activated kinase-1 (TAK1), a MAP3K, interacts with Smad proteins and interferes with osteogenesis in murine mesenchymal progenitors. The Journal of biological chemistry 280, 27271-27283.

Holm, T.M., Habashi, J.P., Doyle, J.J., Bedja, D., Chen, Y., van Erp, C., Lindsay, M.E., Kim, D., Schoenhoff, F., Cohn, R.D., Loeys, B.L., Thomas, C.J., Patnaik, S., Marugan, J.J., Judge, D.P., Dietz, H.C., 2011. Noncanonical TGFbeta signaling contributes to aortic aneurysm progression in Marfan syndrome mice. Science 332, 358-361.

Hough, C., Radu, M., Dore, J.J., 2012. Tgf-Beta induced erk phosphorylation of smad linker region regulates smad signaling. PloS one 7, e42513.

Humphreys, R., Zheng, W., Prince, L.S., Qu, X., Brown, C., Loomes, K., Huppert, S.S., Baldwin, S., Goudy, S., 2012. Cranial neural crest ablation of Jagged1 recapitulates the craniofacial phenotype of Alagille syndrome patients. Human molecular genetics 21, 1374-1383.

Ingraham, C.R., Kinoshita, A., Kondo, S., Yang, B., Sajan, S., Trout, K.J., Malik, M.I., Dunnwald, M., Goudy, S.L., Lovett, M., Murray, J.C., Schutte, B.C., 2006. Abnormal skin, limb and craniofacial morphogenesis in mice deficient for interferon regulatory factor 6 (Irf6). Nature genetics 38, 1335-1340.

Ishii, M., Arias, A.C., Liu, L., Chen, Y.B., Bronner, M.E., Maxson, R.E., 2012. A stable cranial neural crest cell line from mouse. Stem Cells Dev 21, 3069-3080.

Ito, Y., Yeo, J.Y., Chytil, A., Han, J., Bringas, P., Jr., Nakajima, A., Shuler, C.F., Moses, H.L., Chai, Y., 2003. Conditional inactivation of Tgfbr2 in cranial neural crest causes cleft palate and calvaria defects. Development 130, 5269-5280.

Iwata, J., Hacia, J.G., Suzuki, A., Sanchez-Lara, P.A., Urata, M., Chai, Y., 2012a. Modulation of noncanonical TGF-beta signaling prevents cleft palate in Tgfbr2 mutant mice. The Journal of clinical investigation 122, 873-885.

Iwata, J., Suzuki, A., Pelikan, R.C., Ho, T.V., Sanchez-Lara, P.A., Urata, M., Dixon, M.J., Chai, Y., 2013. Smad4-Irf6 genetic interaction and TGFbeta-mediated IRF6 signaling cascade are crucial for palatal fusion in mice. Development 140, 1220-1230.

Iwata, J., Tung, L., Urata, M., Hacia, J.G., Pelikan, R., Suzuki, A., Ramenzoni, L., Chaudhry, O., Parada, C., Sanchez-Lara, P.A., Chai, Y., 2012b. Fibroblast Growth Factor 9 (FGF9)-Pituitary Homeobox 2 (PITX2) Pathway Mediates Transforming Growth Factor beta (TGFbeta) Signaling to Regulate Cell Proliferation in Palatal Mesenchyme during Mouse Palatogenesis. The Journal of biological chemistry 287, 2353-2363.

Kaartinen, V., Cui, X.M., Heisterkamp, N., Groffen, J., Shuler, C.F., 1997. Transforming growth factor-beta3 regulates transdifferentiation of medial edge epithelium during palatal fusion and associated degradation of the basement membrane. Dev.Dyn. 209, 255-260.

Kaartinen, V., Voncken, J.W., Shuler, C., Warburton, D., Bu, D., Heisterkamp, N., Groffen, J., 1995. Abnormal lung development and cleft palate in mice lacking TGF-beta 3 indicates defects of epithelial-mesenchymal interaction. Nat.Genet. 11, 415-421.

Kim, J., Kaartinen, V., 2008. Generation of mice with a conditional allele for Trim33. Genesis 46, 329-333.

Kleinsmith, L.J., Pierce, G.B., Jr., 1964. Multipotentiality of Single Embryonal Carcinoma Cells. Cancer research 24, 1544-1551.

Kretzschmar, M., Liu, F., Hata, A., Doody, J., Massague, J., 1997. The TGF-beta family mediator Smad1 is phosphorylated directly and activated functionally by the BMP receptor kinase. Genes Dev. 11, 984-995.

Lagha, M., Bothma, J.P., Levine, M., 2012. Mechanisms of transcriptional precision in animal development. Trends in genetics : TIG 28, 409-416.

Lan, Y., Jiang, R., 2009. Sonic hedgehog signaling regulates reciprocal epithelial-mesenchymal interactions controlling palatal outgrowth. Development 136, 1387-1396.

Lan, Y., Ovitt, C.E., Cho, E.S., Maltby, K.M., Wang, Q., Jiang, R., 2004. Odd-skipped related 2 (Osr2) encodes a key intrinsic regulator of secondary palate growth and morphogenesis. Development 131, 3207-3216.

Lan, Y., Wang, Q., Ovitt, C.E., Jiang, R., 2007. A unique mouse strain expressing Cre recombinase for tissue-specific analysis of gene function in palate and kidney development. Genesis 45, 618-624.

Lane, J., Kaartinen, V., 2014. Signaling networks in palate development. Wiley interdisciplinary reviews. Systems biology and medicine 6, 271-278.

Lane, J., Yumoto, K., Pisano, J., Azhar, M., Thomas, P.S., Kaartinen, V., 2014. Control elements targeting Tgfb3 expression to the palatal epithelium are located intergenically and in introns of the upstream Ift43 gene. Frontiers in physiology 5, 258.

Larsson, J., Goumans, M.J., Sjostrand, L.J., van Rooijen, M.A., Ward, D., Leveen, P., Xu, X., ten Dijke, P., Mummery, C.L., Karlsson, S., 2001. Abnormal angiogenesis but intact hematopoietic potential in TGF-beta type I receptor-deficient mice. EMBO J. 20, 1663-1673.

Leslie, E.J., Marazita, M.L., 2013. Genetics of cleft lip and cleft palate. American journal of medical genetics. Part C, Seminars in medical genetics 163C, 246-258.

Li, L., Lin, M., Wang, Y., Cserjesi, P., Chen, Z., Chen, Y., 2011. BmprIa is required in mesenchymal tissue and has limited redundant function with BmprIb in tooth and palate development. Developmental biology 349, 451-461.

Li, Q., Ding, J., 2007. Gene expression analysis reveals that formation of the mouse anterior secondary palate involves recruitment of cells from the posterior side. The International journal of developmental biology 51, 167-172.

Lidral, A.C., Romitti, P.A., Basart, A.M., Doetschman, T., Leysens, N.J., Daack-Hirsch, S., Semina, E.V., Johnson, L.R., Machida, J., Burds, A., Parnell, T.J., Rubenstein, J.L., Murray, J.C., 1998. Association of MSX1 and TGFB3 with nonsyndromic clefting in humans. Am.J.Hum.Genet. 63, 557-568.

Lieff, S., Olshan, A.F., Werler, M., Strauss, R.P., Smith, J., Mitchell, A., 1999. Maternal cigarette smoking during pregnancy and risk of oral clefts in newborns. American journal of epidemiology 150, 683-694.

Liu, W., Lan, Y., Pauws, E., Meester-Smoor, M.A., Stanier, P., Zwarthoff, E.C., Jiang, R., 2008. The Mn1 transcription factor acts upstream of Tbx22 and preferentially regulates posterior palate growth in mice. Development 135, 3959-3968.

Liu, W., Sun, X., Braut, A., Mishina, Y., Behringer, R.R., Mina, M., Martin, J.F., 2005. Distinct functions for Bmp signaling in lip and palate fusion in mice. Development 132, 1453-1461.

Loeys, B.L., Chen, J., Neptune, E.R., Judge, D.P., Podowski, M., Holm, T., Meyers, J., Leitch, C.C., Katsanis, N., Sharifi, N., Xu, F.L., Myers, L.A., Spevak, P.J., Cameron, D.E., De, B.J., Hellemans, J., Chen, Y., Davis, E.C., Webb, C.L., Kress, W., Coucke, P., Rifkin, D.B., De Paepe, A.M., Dietz, H.C., 2005. A syndrome of altered cardiovascular, craniofacial, neurocognitive and skeletal development caused by mutations in TGFBR1 or TGFBR2. Nat.Genet. 37, 275-281.

Mansour, S.L., Thomas, K.R., Capecchi, M.R., 1988. Disruption of the proto-oncogene int-2 in mouse embryo-derived stem cells: a general strategy for targeting mutations to non-selectable genes. Nature 336, 348-352.

Massague, J., 1998. TGF-beta signal transduction. Annu.Rev.Biochem. 67, 753-791.

Massague, J., Seoane, J., Wotton, D., 2005. Smad transcription factors. Genes & development 19, 2783-2810.

Matsuzaki, K., Kitano, C., Murata, M., Sekimoto, G., Yoshida, K., Uemura, Y., Seki, T., Taketani, S., Fujisawa, J., Okazaki, K., 2009. Smad2 and Smad3 phosphorylated at both linker and COOH-terminal regions transmit malignant TGF-beta signal in later stages of human colorectal cancer. Cancer research 69, 5321-5330.

Millan, F.A., Denhez, F., Kondaiah, P., Akhurst, R.J., 1991. Embryonic gene expression patterns of TGF beta 1, beta 2 and beta 3 suggest different developmental functions in vivo. Development 111, 131-143.

Moorman, A.F., Houweling, A.C., de Boer, P.A., Christoffels, V.M., 2001. Sensitive nonradioactive detection of mRNA in tissue sections: novel application of the whole-mount in situ hybridization protocol. J.Histochem.Cytochem. 49, 1-8.

Novak, A., Guo, C., Yang, W., Nagy, A., Lobe, C.G., 2000. Z/EG, a double reporter mouse line that expresses enhanced green fluorescent protein upon Cre-mediated excision. Genesis. 28, 147-155.

Paulson, G.W., Paulson, R.B., 1981. Teratogenic effects of anticonvulsants. Archives of neurology 38, 140-143.

Pauws, E., Moore, G.E., Stanier, P., 2009. A functional haplotype variant in the TBX22 promoter is associated with cleft palate and ankyloglossia. Journal of medical genetics 46, 555-561.

Pelton, R.W., Dickinson, M.E., Moses, H.L., Hogan, B.L., 1990. In situ hybridization analysis of TGF beta 3 RNA expression during mouse development: comparative studies with TGF beta 1 and beta 2. Development 110, 609-620.

Perry, M.W., Boettiger, A.N., Bothma, J.P., Levine, M., 2010. Shadow enhancers foster robustness of Drosophila gastrulation. Current biology : CB 20, 1562-1567.

Proetzel, G., Pawlowski, S.A., Wiles, M.V., Yin, M., Boivin, G.P., Howles, P.N., Ding, J., Ferguson, M.W., Doetschman, T., 1995. Transforming growth factor-beta 3 is required for secondary palate fusion. Nat.Genet. 11, 409-414.

Rajewsky, K., Gu, H., Kuhn, R., Betz, U.A., Muller, W., Roes, J., Schwenk, F., 1996. Conditional gene targeting. J.Clin.Invest 98, 600-603.

Ray, H.J., Niswander, L., 2012. Mechanisms of tissue fusion during development. Development 139, 1701-1711.

Rice, R., Spencer-Dene, B., Connor, E.C., Gritli-Linde, A., McMahon, A.P., Dickson, C., Thesleff, I., Rice, D.P., 2004. Disruption of Fgf10/Fgfr2b-coordinated epithelial-mesenchymal interactions causes cleft palate. The Journal of clinical investigation 113, 1692-1700.

Richardson, R.J., Dixon, J., Jiang, R., Dixon, M.J., 2009. Integration of IRF6 and Jagged2 signalling is essential for controlling palatal adhesion and fusion competence. Human molecular genetics 18, 2632-2642.

Rienhoff, H.Y., Jr., Yeo, C.Y., Morissette, R., Khrebtukova, I., Melnick, J., Luo, S., Leng, N., Kim, Y.J., Schroth, G., Westwick, J., Vogel, H., McDonnell, N., Hall, J.G., Whitman, M., 2013. A mutation in TGFB3 associated with a syndrome of low muscle mass, growth retardation,

distal arthrogryposis and clinical features overlapping with Marfan and Loeys-Dietz syndrome. American journal of medical genetics. Part A 161A, 2040-2046.

Rot-Nikcevic, I., Reddy, T., Downing, K.J., Belliveau, A.C., Hallgrimsson, B., Hall, B.K., Kablar, B., 2006. Myf5-/- :MyoD-/- amyogenic fetuses reveal the importance of early contraction and static loading by striated muscle in mouse skeletogenesis. Development genes and evolution 216, 1-9.

Rowitch, D.H., Echelard, Y., Danielian, P.S., Gellner, K., Brenner, S., McMahon, A.P., 1998. Identification of an evolutionarily conserved 110 base-pair cis-acting regulatory sequence that governs Wnt-1 expression in the murine neural plate. Development 125, 2735-2746.

Sadowski, P.D., 1995. The Flp recombinase of the 2-microns plasmid of Saccharomyces cerevisiae. Progress in nucleic acid research and molecular biology 51, 53-91.

Sauer, B., 1998. Inducible gene targeting in mice using the Cre/lox system. Methods 14, 381-392.

Schutte, B.C., Murray, J.C., 1999. The many faces and factors of orofacial clefts. Hum.Mol.Genet. 8, 1853-1859.

Shaw, G.M., Lammer, E.J., 1999. Maternal periconceptional alcohol consumption and risk for orofacial clefts. The Journal of pediatrics 134, 298-303.

Shi, Y., Massague, J., 2003. Mechanisms of TGF-beta signaling from cell membrane to the nucleus. Cell 113, 685-700.

Shim, J.H., Greenblatt, M.B., Xie, M., Schneider, M.D., Zou, W., Zhai, B., Gygi, S., Glimcher, L.H., 2009. TAK1 is an essential regulator of BMP signalling in cartilage. The EMBO journal 28, 2028-2041.

Smithies, O., Gregg, R.G., Boggs, S.S., Koralewski, M.A., Kucherlapati, R.S., 1985. Insertion of DNA sequences into the human chromosomal beta-globin locus by homologous recombination. Nature 317, 230-234.

Song, Z., Liu, C., Iwata, J., Gu, S., Suzuki, A., Sun, C., He, W., Shu, R., Li, L., Chai, Y., Chen, Y., 2013. Mice with Tak1 deficiency in neural crest lineage exhibit cleft palate associated with abnormal tongue development. The Journal of biological chemistry 288, 10440-10450.

Soriano, P., 1999. Generalized lacZ expression with the ROSA26 Cre reporter strain. Nat.Genet. 21, 70-71.

Sorrentino, A., Thakur, N., Grimsby, S., Marcusson, A., von Bulow, V., Schuster, N., Zhang, S., Heldin, C.H., Landstrom, M., 2008. The type I TGF-beta receptor engages TRAF6 to activate TAK1 in a receptor kinase-independent manner. Nat Cell Biol 10, 1199-1207.

Sun, D., Vanderburg, C.R., Odierna, G.S., Hay, E.D., 1998. TGFbeta3 promotes transformation of chicken palate medial edge epithelium to mesenchyme in vitro. Development 125, 95-105.

Taya, Y., O'Kane, S., Ferguson, M.W., 1999. Pathogenesis of cleft palate in TGF-beta3 knockout mice. Development 126, 3869-3879.

Thomas, K.R., Capecchi, M.R., 1987. Site-directed mutagenesis by gene targeting in mouse embryo-derived stem cells. Cell 51, 503-512.

Thomas, P.S., Kim, J., Nunez, S., Glogauer, M., Kaartinen, V., 2010. Neural crest cell-specific deletion of Rac1 results in defective cell-matrix interactions and severe craniofacial and cardiovascular malformations. Developmental biology 340, 613-625.

Tolarova, M.M., Cervenka, J., 1998. Classification and birth prevalence of orofacial clefts. American journal of medical genetics 75, 126-137.

Vaziri Sani, F., Hallberg, K., Harfe, B.D., McMahon, A.P., Linde, A., Gritli-Linde, A., 2005. Fate-mapping of the epithelial seam during palatal fusion rules out epithelial-mesenchymal transformation. Developmental biology 285, 490-495.

Venza, I., Visalli, M., Parrillo, L., De Felice, M., Teti, D., Venza, M., 2011. MSX1 and TGF-beta3 are novel target genes functionally regulated by FOXE1. Human molecular genetics 20, 1016-1025.

Wang, C., Deng, L., Hong, M., Akkaraju, G.R., Inoue, J., Chen, Z.J., 2001. TAK1 is a ubiquitin-dependent kinase of MKK and IKK. Nature 412, 346-351.

Wang, G., Matsuura, I., He, D., Liu, F., 2009. Transforming growth factor-{beta}-inducible phosphorylation of Smad3. The Journal of biological chemistry 284, 9663-9673.

Warming, S., Costantino, N., Court, D.L., Jenkins, N.A., Copeland, N.G., 2005. Simple and highly efficient BAC recombineering using galK selection. Nucleic acids research 33, e36.

Wrighton, K.H., Feng, X.H., 2008. To (TGF)beta or not to (TGF)beta: fine-tuning of Smad signaling via post-translational modifications. Cell Signal 20, 1579-1591.

Wu, C., Endo, M., Yang, B.H., Radecki, M.A., Davis, P.F., Zoltick, P.W., Spivak, R.M., Flake, A.W., Kirschner, R.E., Nah, H.D., 2013. Intra-amniotic transient transduction of the periderm with a viral vector encoding TGFbeta3 prevents cleft palate in Tgfbeta3(-/-) mouse embryos. Molecular therapy : the journal of the American Society of Gene Therapy 21, 8-17.

Wu, T., Schwender, H., Ruczinski, I., Murray, J.C., Marazita, M.L., Munger, R.G., Hetmanski, J.B., Parker, M.M., Wang, P., Murray, T., Taub, M., Li, S., Redett, R.J., Fallin, M.D., Liang, K.Y., Wu-Chou, Y.H., Chong, S.S., Yeow, V., Ye, X., Wang, H., Huang, S., Jabs, E.W., Shi, B., Wilcox, A.J., Jee, S.H., Scott, A.F., Beaty, T.H., 2014. Evidence of gene-environment interaction for two genes on chromosome 4 and environmental tobacco smoke in controlling the risk of nonsyndromic cleft palate. PloS one 9, e88088.

Xi, Q., Wang, Z., Zaromytidou, A.I., Zhang, X.H., Chow-Tsang, L.F., Liu, J.X., Kim, H., Barlas, A., Manova-Todorova, K., Kaartinen, V., Studer, L., Mark, W., Patel, D.J., Massague, J., 2011. A poised chromatin platform for TGF-beta access to master regulators. Cell 147, 1511-1524.

Xiong, W., He, F., Morikawa, Y., Yu, X., Zhang, Z., Lan, Y., Jiang, R., Cserjesi, P., Chen, Y., 2009. Hand2 is required in the epithelium for palatogenesis in mice. Developmental biology 330, 131-141.

Xu, X., Han, J., Ito, Y., Bringas, P., Jr., Deng, C., Chai, Y., 2008. Ectodermal Smad4 and p38 MAPK are functionally redundant in mediating TGF-beta/BMP signaling during tooth and palate development. Developmental cell 15, 322-329.

Xu, X., Han, J., Ito, Y., Bringas, P., Jr., Urata, M.M., Chai, Y., 2006. Cell autonomous requirement for Tgfbr2 in the disappearance of medial edge epithelium during palatal fusion. Dev.Biol. 297, 238-248.

Yamaguchi, K., Shirakabe, K., Shibuya, H., Irie, K., Oishi, I., Ueno, N., Taniguchi, T., Nishida, E., Matsumoto, K., 1995. Identification of a member of the MAPKKK family as a potential mediator of TGF-beta signal transduction. Science 270, 2008-2011.

Yamashita, M., Fatyol, K., Jin, C., Wang, X., Liu, Z., Zhang, Y.E., 2008. TRAF6 mediates Smad-independent activation of JNK and p38 by TGF-beta. Molecular cell 31, 918-924.

Yang, L.T., Kaartinen, V., 2007. Tgfb1 expressed in the Tgfb3 locus partially rescues the cleft palate phenotype of Tgfb3 null mutants. Dev.Biol. 312, 384-395.

Yang, L.T., Li, W.Y., Kaartinen, V., 2008. Tissue-specific expression of Cre recombinase from the Tgfb3 locus. Genesis 46, 112-118.

Yang, X., Li, C., Herrera, P.L., Deng, C.X., 2002. Generation of Smad4/Dpc4 conditional knockout mice. Genesis 32, 80-81.

Yoshida, M., Shimono, Y., Togashi, H., Matsuzaki, K., Miyoshi, J., Mizoguchi, A., Komori, T., Takai, Y., 2012. Periderm cells covering palatal shelves have tight junctions and their desquamation reduces the polarity of palatal shelf epithelial cells in palatogenesis. Genes to cells : devoted to molecular & cellular mechanisms 17, 455-472.

Yu, K., Ornitz, D.M., 2011. Histomorphological study of palatal shelf elevation during murine secondary palate formation. Developmental dynamics : an official publication of the American Association of Anatomists 240, 1737-1744.

Yu, L., Gu, S., Alappat, S., Song, Y., Yan, M., Zhang, X., Zhang, G., Jiang, Y., Zhang, Z., Zhang, Y., Chen, Y., 2005. Shox2-deficient mice exhibit a rare type of incomplete clefting of the secondary palate. Development. 132, 4397-4406.

Zhang, L., Yoshimura, Y., Hatta, T., Otani, H., 1999. Myogenic determination and differentiation of the mouse palatal muscle in relation to the developing mandibular nerve. Journal of dental research 78, 1417-1425.

Zhang, Z., Song, Y., Zhao, X., Zhang, X., Fermin, C., Chen, Y., 2002. Rescue of cleft palate in Msx1-deficient mice by transgenic Bmp4 reveals a network of BMP and Shh signaling in the regulation of mammalian palatogenesis. Development 129, 4135-4146.

Zhou, J., Gao, Y., Lan, Y., Jia, S., Jiang, R., 2013. Pax9 regulates a molecular network involving Bmp4, Fgf10, Shh signaling and the Osr2 transcription factor to control palate morphogenesis. Development 140, 4709-4718.